



**HAL**  
open science

## The sensitivity of sub-seasonal to seasonal streamflow forecasts to meteorological forcing quality, modelled hydrology and the initial hydrological conditions

Louise Arnal, Hannah L Cloke, Linus Magnusson, Bastian Klein, Dennis Meissner, Alberto de Tomas, Johannes Hunink, Ilias Pechlivanidis, Louise Crochemore, Sara Suarez, et al.

### ► To cite this version:

Louise Arnal, Hannah L Cloke, Linus Magnusson, Bastian Klein, Dennis Meissner, et al.. The sensitivity of sub-seasonal to seasonal streamflow forecasts to meteorological forcing quality, modelled hydrology and the initial hydrological conditions. [Research Report] IRSTEA. 2019. hal-03350525

**HAL Id: hal-03350525**

**<https://hal.inrae.fr/hal-03350525>**

Submitted on 21 Sep 2021

**HAL** is a multi-disciplinary open access archive for the deposit and dissemination of scientific research documents, whether they are published or not. The documents may come from teaching and research institutions in France or abroad, or from public or private research centers.

L'archive ouverte pluridisciplinaire **HAL**, est destinée au dépôt et à la diffusion de documents scientifiques de niveau recherche, publiés ou non, émanant des établissements d'enseignement et de recherche français ou étrangers, des laboratoires publics ou privés.



# IMPROVING PREDICTIONS AND MANAGEMENT OF HYDROLOGICAL EXTREMES



 @imprex\_eu



Funded by  
the Horizon 2020  
Framework Programme  
of the European Union

Grant agreement No. 641811



<b>Deliverable</b>	<b>The sensitivity of sub-seasonal to seasonal streamflow forecasts to meteorological forcing quality, modelled hydrology and the initial hydrological conditions</b>
Related Work Package:	WP4: Improved predictability of hydrological extremes
Deliverable lead:	University of Reading
Author(s):	Louise Arnal, Hannah L. Cloke, Linus Magnusson, Bastian Klein, Dennis Meissner, Alberto de Tomas, Johannes Hunink, Ilias Pechlivanidis, Louise Crochemore, Sara Suarez, Abel Solera, Joaquin Andreu, Jeff Knight, Felicity Liggins, Albrecht Weerts, Maria-Helena Ramos, Guillaume Thirel
Contact for queries	Louise.arnal@ecmwf.int
Grant Agreement Number:	n° 641811
Instrument:	HORIZON 2020
Start date of the project:	01.10.2015
Duration of the project:	48 months
Website:	www.IMPRES.eu
Abstract	This report presents the sensitivity of seasonal discharge forecasting to meteorological forcing quality, modelled hydrology and initial hydrological conditions and the dependency of the skill to the basin characteristics. The analyses are focused on key sectoral applications of IMPRES.

Dissemination level of this document



X	PU	Public
	PP	Restricted to other programme participants (including the Commission Services)
	RE	Restricted to a group specified by the consortium (including the European Commission Services)
	CO	Confidential, only for members of the consortium (including the European Commission Services)

### Versioning and Contribution History

Version	Date	Modified by	Modification reasons
v.01	02/02/2017	L. Arnal	First draft submission
	08/02/2017		Review by Bart vd Hurk
v.02	31/03/2017	L. Arnal	Revised version submission
	04/04/2017		Review by Bart vd Hurk
v.03	07/04/2017	L. Arnal	Modification of the introduction



## Table of Contents

Executive summary .....	6
Glossary.....	10
1 Introduction .....	11
2 Sub-seasonal to seasonal streamflow forecasting: background, applications and limitations.....	13
2.1 An overview of sub-seasonal to seasonal streamflow forecasting.....	13
2.2 Sectoral applications.....	14
2.2.1 Flood forecasting - University of Reading.....	14
2.2.2 Navigation - BfG.....	15
2.2.3 Agriculture - FutureWater .....	17
2.2.4 Hydropower - SMHI.....	18
2.2.5 Reservoir management - UPV.....	18
2.2.6 Flood & low flow forecasting - Deltares.....	20
2.3 Sensitivity analyses as a tool to diagnose seasonal streamflow forecasting uncertainties.....	21
2.4 Comparative analysis in large sample hydrology.....	22
3 Data and methods.....	24
3.1 The forecasting systems.....	24
3.2 The forecasting systems intercomparison .....	29
3.3 The EPB sensitivity analysis.....	38
3.4 Seasonal hydrological forecasts - Clustering of the skill .....	41
4 Results .....	44
4.1 The forecasting systems intercomparison .....	44
4.1.1 Central European Rivers.....	44
4.1.2 The Thames River Basin .....	56
4.1.3 The Segura and Tagus River Basins.....	63
4.1.4 The Jucar River Basin.....	68
4.1.5 Swedish Rivers.....	77
4.2 The EPB sensitivity analysis.....	81



4.3	Comparative analysis.....	87
5	Lessons learnt .....	91
6	References .....	95
7	Annex A – Tabulated overview on hydrological model features .....	98



## Executive summary

Information about streamflow for the coming months (sub-seasonal time-scale) to seasons is needed for decision-making in many sectors of society. Examples are in a reservoir management context, for applications such as hydropower generation, water allocation for drinking water and agriculture, navigation, flood and drought mitigation. Here, sub-seasonal and seasonal forecasts can be a valuable tool. Compared to short range forecasts, these forecasts allow for an increased operational margin for early warning and maximised benefits. However, the potential skill on the longer time-scales are limited due to a low inherent predictability (of the atmosphere and hydrosphere) and limited quality of models and observations.

In order to meet these needs and tackle those challenges, IMPREX will (1) analyse the current skill of state-of-the-art sub-seasonal to seasonal streamflow forecasts over Europe and (2) improve their capabilities, with a focus on extreme events (i.e., high and low flows) and variables, aggregation periods, seasons and lead times of interest to the users of the forecasts involved in IMPREX (which cover the water sectors mentioned above).

This deliverable consists of three parts. The first part is a technical intercomparison of the performance of five different sub-seasonal to seasonal streamflow forecasting systems, operated by partners of IMPREX: ECMWF, SMHI, FW, BfG, UPV and Deltares. This is to be done for key locations in Europe, selected based on the case studies of the project. They include Central European River and Swedish River stations and the Thames, Segura, Tagus, and Jucar River basins. The forecasting systems investigated in this deliverable all use the same meteorological forecasting system, ECMWF's System 4 (with or without applying a bias correction method to the latter) and a variety of hydrological models. This intercomparison therefore enables us to identify the contribution of hydrological model structure and the presence of a bias correction of the meteorological forecasts to the streamflow forecasting skill on sub-seasonal to seasonal time scales and for an array of diverse locations, seasons and extreme events in Europe. This first part has revealed several major differences between the seasonal streamflow forecasting systems and their



impacts on the relevant water sectors. Notably, the BfG seasonal streamflow forecasts tend to underestimate the observed streamflow for the Central European River stations, which could be a problem for the navigation sector, dependent on accurate low flow forecasts in the summer. The ECMWF seasonal streamflow forecasts appear to systematically overestimate the spring flow and to underestimate the winter flow for the Central European River stations and the Thames River basin. The latter could be an issue for the flood protection sector as the forecasts would be prone to missing or underestimating the magnitude of flood events. The ECMWF forecasts are however very accurate for summer flow forecasting in the Segura and Tagus River Basins. This could be highly beneficial for the agricultural sector in this region. Both the ECMWF and the SMHI seasonal streamflow forecasts underestimate the May flow for Swedish River stations, which could be a challenge for the hydropower generation sector, relying on accurate spring flow predictions. The SMHI forecasts seem to generally overestimate the winter flow for the Central European River stations and the Thames River basin, which could once again be a problem for the flood protection sector as the forecasts would potentially lead to false alarms. The FW seasonal streamflow forecasts tend to overestimate largely the early spring-spring flow for the Tagus River Basin and to underestimate slightly the flow during all year for the Segura River Basin. Both biases could be challenging for the agricultural sector.

This first technical intercomparison forms a benchmark, to which improved systems from other IMPREX tasks can be compared. The intercomparison can moreover be enriched during the course of IMPREX, with more stations and scores.

The second part of the deliverable consists in a sensitivity analysis, specifically designed to diagnose the relative contributions of errors in the initial hydrological conditions (IHC) and in the meteorological forecasts (MF, sometimes called seasonal climate forecasts [SCF]) on sub-seasonal to seasonal streamflow forecasting uncertainty. This sensitivity analysis was carried out using the ECMWF and the BfG seasonal streamflow forecasts and highlighted several significant results. The analysis indicates that improving the IHC would yield a higher improvement of the



seasonal streamflow forecasts for the first month of lead time, after which the SCF become rapidly more influential on the skill of the streamflow forecasts. This signal is however contrasted in space and time, highlighting geographical and seasonal variations of the flow generating mechanisms in Europe. For example for streamflow forecasts made in the summer (May-July) and with one month of lead time, there appears to be a larger number of regions in Europe where the IHC dominate the quality of the streamflow forecasts, compared to forecasts made in the winter with the same lead time. This is probably due to the lower rainfall over Europe during the summer months, leading to groundwater dominated streamflow. For most leeward regions in Scandinavia, the IHC dominate the quality of the forecasts made in the winter, with one to three months of lead time. This is potentially due to precipitation falling as snow in the winter, leading to groundwater dominated streamflow in the winter and snowmelt driven flow in the following spring. For most regions of the Iberian Peninsula, the IHC seem relatively more important for streamflow forecasts made in the summer (June-September), with one to three months of lead time. This is probably due to groundwater dominated streamflow in the summer in those regions and a land surface memory spanning several months. Over the eastern part of central Europe, streamflow forecasts made in the spring seem to be more sensitive to the IHC, which might translate snowmelt driven spring flow.

The third part of this deliverable is devoted to the identification of the key drivers (beyond IHC and SCF) that control and influence the hydrological forecasting skill. For this, an alternative sensitivity analysis was designed based on the results from about 35000 European basins, which allows linking the seasonal hydrological forecasting skill (from the SMHI forecasts) to the regional physiographic-hydro-climatic characteristics. This analysis showed that seasonal hydrological forecasting skill is mainly dependent on the basin's hydrological regime. Other factors, such as the elevation and the remaining bias in temperature, were also identified to be important aspects (i.e., dependence of response of mountainous basins to temperature). Another significant result is that seasonal hydrological forecasting skill



seems to be limited for relatively flashy basins, experiencing strong flow dynamics over the year (i.e., less memory in the system).

The results of this deliverable will guide future research in IMPREX, indicating where improvements should be made in the forecasting chain (improvements to the IHC, the SCF) in order to improve the seasonal streamflow forecasts over Europe.



## Glossary

**Bias correction:** Process aiming at removing systematic errors in the output of a model. Methods include: linear scaling, distribution-based Scaling, quantile mapping, to cite a few.

**Lead time:** The time between the initiation and completion of a forecast.

**Discharge:** River discharge is the volume of water flowing through a river channel at any given point and is measured in cubic metres per second (m<sup>3</sup>/s).

**Target month or target season:** The season or month for which the forecast is made.

**Forecast quality:** How well a forecast compares against a corresponding observation of what actually occurred, or some good estimate of the true outcome.

**Sensitivity analysis:** The study of how the uncertainty in the output of a model or system can be apportioned to different sources of uncertainty in its inputs.

**Skill elasticity:** A measure of the sensitivity of the seasonal discharge forecasting skill to changes in the skill of its two main predictability sources: the initial hydrological conditions or the seasonal climate forcing.

**Initial hydrological conditions (IHC):** The hydrological states (soil moisture, snow cover, water already in the river, among others) at or close to the start of the forecast run.

**Seasonal climate forcing (SCF):** The seasonal meteorological forecast used as input to a hydrological model.



## 1 Introduction

Information about streamflow during the coming month (sub-seasonal time-scale) and season is needed for decision-making in many sectors. Examples are in a reservoir management context, for applications such as hydropower generation, water allocation for drinking water and agriculture, navigation, flood and drought mitigation. Here, sub-seasonal and seasonal forecast can be a valuable tool. Compared to short range forecasts, these forecasts allow for an increased operational margin for early warning and maximised benefits. However, the potential skill on the longer time-scales are limited due to a low inherent predictability and limited quality of models and observations.

In order to meet these needs, IMPREX will (1) analyse the current skill of state-of-the-art sub-seasonal to seasonal streamflow forecasts over Europe and (2) improve their capabilities, with a focus on extreme events (i.e., high and low flows) and variables, aggregation periods, seasons and lead times of interest to the users of the forecasts involved in IMPREX (which cover the water sectors mentioned above).

This deliverable consists of three parts. The first part will use the verification scoreboard designed in WP4 (deliverable 4.1) to analyse and compare the skill of multiple sub-seasonal to seasonal streamflow forecasting systems, operated by partners of IMPREX. This will be done for key locations selected based on the case studies of the project. Since the forecasting systems investigated here all use the same meteorological forecasting system (with or without applying a bias correction method) and a variety of hydrological models, this work will enable us to identify the contribution of (hydrological) model structure and the presence of a bias correction of the seasonal meteorological forecasts to the streamflow forecasting skill on sub-seasonal to seasonal time scales and for an array of diverse locations, seasons and extreme events in Europe. This first technical intercomparison will form a benchmark, to which more stations, scores and improved systems from other IMPREX tasks can be added and compared. The main aim of this part is to highlight major differences and similarities between the performance of the seasonal



streamflow forecasting systems and the potential impacts of those performances on the sectoral applications at stake in the case study areas. This technical part will also inform later tasks of the IMPREX project, such as the multi-modelling and the data assimilation exercises.

The second part of this deliverable will inform future IMPREX work through a sensitivity analysis, specifically designed to diagnose the relative contributions of initial hydrological conditions (IHC) and errors of the meteorological forecast (MF, sometimes called seasonal climate forecast [SCF]) on sub-seasonal to seasonal streamflow forecasting quality. This will indicate the potential achievable improvements in sub-seasonal to seasonal streamflow forecasting skill through the improvement in either one of the two error (or predictability) sources.

The third part of this deliverable is devoted to the identification of the key drivers (beyond IHC and SCF) that control and influence the hydrological forecasting skill. For this an alternative sensitivity analysis was designed based on the results from about 35000 European basins, which allows linking the skill to the regional physiographic-hydro-climatic characteristics.

The aim of this work is to produce a 'hydrological sensitivity chart', providing information about the state-of-the-art in terms of sub-seasonal to seasonal streamflow forecasting, as well as about potential targeted improvements on which IMPREX should focus. An overview of sub-seasonal to seasonal streamflow forecasting and the use of sensitivity analyses to diagnose its uncertainties are given in Section 2. Section 3 introduces the methodology, with an overview of the forecasting systems, the data and the methods used for the analyses. The results are subsequently presented in Section 4 and finally discussed in Section 5. Section 5 additionally states the lessons learnt and recommendations for future work.



## 2 Sub-seasonal to seasonal streamflow forecasting: background, applications and limitations

### 2.1 An overview of sub-seasonal to seasonal streamflow forecasting

The first seasonal streamflow forecasting methods were statistical methods, regression-based, using antecedent hydrological conditions (i.e., snowpack measurements, soil moisture, among others) to give an indication of the streamflow for the following months (Church, 1935; Wood and Lettenmaier, 2006). With the understanding of hydrological processes and the advances in computer technologies, the first numerical hydrological models were created (Helms et al. 2008). In the 1970s, one of the first dynamical forecasting system was constructed using a hydrological model, initialising it with observed hydrological conditions (IHC) and forcing it with historical time series of observed precipitation and temperature from all the previous years of recorded meteorological observations. This method was introduced by the National Weather Service (NWS) in the United States and was termed the Extended Streamflow Prediction (ESP) system (Twedt et al., 1974; Day, 1985). The ESP nowadays stands for Ensemble Streamflow Prediction and describes the same forecasting process.

Despite its strength, the ESP is limited by the fact that it is based on the assumption that the historical weather can give an accurate indication of the future weather. In the 1950s, the use of seasonal meteorological forecasts for seasonal streamflow forecasting for water management was first investigated but its skill was judged too poor for operational purposes (Pagano and Garen, 2005). The 1970s were a milestone for seasonal meteorological forecasting, due to the understanding of atmosphere-ocean-land interactions and the importance of teleconnections forecasting on seasonal time scales (such as the ENSO, NAO, etc; Pagano and Garen, 2005). It is however not until the late 1990s that seasonal meteorological forecasts were used for operational purposes, as a result of the very strong El-Niño of 1997-98 (Pagano and Garen, 2005).



Statistical forecasting techniques are still widely used, sometimes based on complex regression methods, harnessing the teleconnection indicators (Wang et al, 2011). It is only recently that dynamical seasonal streamflow forecasting (based on forcing a hydrological model with meteorological seasonal forecasts to obtain seasonal hydrological forecasts) has become a real potential to surpass statistical seasonal streamflow forecast skill (Easy et al. 2006). Statistical-dynamical hybrid systems also exist, for instance the use of teleconnection indicators to resample the historical observed meteorological years, removing anti-analogues, to force a hydrological model (Schaake, 1978; Pagano and Garen, 2005; Bierkens and van Beek, 2009).

## 2.2 Sectoral applications

Sub-seasonal to seasonal streamflow forecasts are valuable for many applications of the water sector, including reservoir management for hydropower generation and water allocation for drinking water and agriculture, navigation and flood and drought mitigation. These applications are diverse in terms of their needs and operational use of the forecasts. For example, the flood protection sector is more vulnerable to high river flow, while the navigation, agriculture, hydropower and reservoir management sectors are more vulnerable to low flows. Additionally, the flood protection sector requires accuracy in the timing and the intensity of an event, while the hydropower sector requires information on the flow accumulations for the spring. The various sectors and their individual needs and current operational practices are described below.

### 2.2.1 Flood forecasting - University of Reading

Flood forecasting is currently done successfully at short to medium time scales (up to a month ahead). Beyond this lead time, the capacity of the forecasts to indicate the potential for an extreme event to happen is still limited, let alone the exact day or even week when this event might happen and the exact location of this event. This is the main reason for which the Environment Agency (EA) does not currently use any sub-seasonal to seasonal forecasts for their decision-making. The main need for decision-making in a flood context is the probability of an event happening, an indication of how extreme the event will be and the estimate date of



the event. The EA bases their decisions on a very low threshold (i.e., allowing a high false alarm ratio), as the loss for not taking any action is much larger than the cost of taking action. Their strategies could be categorised as risk-averse, as the consequences of a false alarm are lower than for a miss. There is nonetheless the potential to integrate sub-seasonal to seasonal information in their current system. Information for the longer time scale could give an indication of the trend in discharge for the following months and flag areas to watch for these coming months, following a "ready-set-go" approach (Goddard et al. 2014). The EA has expressed interest in this kind of information.

### 2.2.2 Navigation - BfG

Monthly to seasonal forecasts are required for Inland Waterway Transport (IWT) for the the medium- to long-term planning and enhancement of the water bound logistic chain (stock management, adjustment of the industrial production chain, modal split planning). Information about the future evolution of flow and water levels in the large rivers is especially required by the stakeholders before and within the typical low flow seasons when transport capacity on rivers is limited. The required forecast lead time depends on the specific waterway user and the decisions to be taken. It ranges from weeks, for example to shift cargo from shipping to another means of transportation, to months, to adapt the fleet / usable transport capacity (see Klein and Meissner, 2016). Despite the great demand and interest of the IWT sector, no operational forecasts with lead times exceeding 8 days are available at the moment for the Rivers Rhine (max. lead time 4 days), Elbe (max. published lead time 2- 8 days depending on the gauge) and Upper Danube (max. published lead time 2-4 days depending on the gauge), mainly due to the large uncertainties and the limited skill on monthly and seasonal time scales.

In order to provide stakeholders with monthly to seasonal forecast information, a prototype is being developed in the context of IMPREX. To model the water balance and the flow in rivers the hydrological model LARSIM-ME is applied. The hydrological model was set up for the large rivers in Germany including their



international parts (model acronym LARSIM-M(iddle)E(urope)) and covers the catchments of the River Rhine, River Elbe, River Weser/Ems, River Odra and River Danube up to gauge Nagymaros in Hungary. The total catchment size simulated by the model is approx. 800 000 km<sup>2</sup>. The spatial resolution is 5km x 5 km. As meteorological forcings resampled observed climatology (ESP) and seasonal forecasts from ECMWF Seasonal Forecast System 4 are used. 2-m temperature of the past 24 hours and daily total precipitation of System4 are interpolated to a common 50km x 50km grid (multiple of the 5km x 5km raster). Both variables were bias corrected on the 50km x 50km grid using linear scaling with the meteorological observation dataset set used for the baseline simulation (also aggregated to the 50km x 50km grid as reference data). As seasonal forecasts tend to drift towards their own model climate with increasing lead time, giving rise to model bias, separate bias correction factors have been estimated for each forecast initialisation date (starting on the first day of each calendar month) and monthly lead times (first month, second month, etc, to sixth month). In total 12 x 6 = 72 scaling factors for precipitation and 72 additive terms for temperature were calculated for each 50km x 50km raster to correct the model drift of ECMWF's System 4. In the next step temperature and precipitation are downscaled to the 5km x 5km model grid. In future versions of the navigation related seasonal forecasting prototype NavSEAS-ME seasonal forecasts from GloSea5 from UK Metoffice will be included in addition.

To analyse the potential skill of ECMWF-System4 for navigation related seasonal forecasting, the reforecast data set 01.01.1981 - 01.04.2011 as well as the pre-operational and operational forecasts of the period 01.04.2011 - 31.12.2015 are applied. In the reforecast, the number of ensemble members is limited to 15 for the initialisation months January, March, June, July, September, October, and December. The number of ensemble members is extended to 51 for the initialisation months February, May, August and November. From April 2011 onwards, the (operational) ensemble size is 51 for all initialisation months. For verification the ensemble size of the operational forecasts was reduced to the ensemble size of the reforecast (15 members) for the initialisation months January, March, June, July, September,



October, and December. The hydrological re-forecasts with LARSIM-ME are evaluated for relevant low- and medium flow indicators.

### 2.2.3 Agriculture - FutureWater

Irrigated agriculture is the main economic activity of Campo de Cartagena in the Segura River basin, Spain. However, water scarcity compromises such activity, which is mainly dependant on the water input it receives from the connected Tagus River basin. Mitigation measures of droughts in Spain are based on a number of drought indicators that are derived from the available water in the storage reservoirs. In order to anticipate drought episodes, decision-makers need to forecast the corresponding reservoir inflows. In the case of the Segura River, forecasts are currently estimated from simple regressions of river discharges from the preceding 6 months, leading to updated management plans twice a year.

In order to provide stakeholders in the basin with a more robust forecasting system that would allow them to better anticipate drought episodes and put into practice more effective allocation and mitigation practices, a prototype of a hydrological seasonal forecasting system is presented. The prototype uses the Spatial Processes in HYdrology model (SPHY) forced with the ECMWF's System 4 (15 ensembles) seasonal meteorological forecasts to predict monthly river inflows at the reservoirs of the upper basins of the Segura and Tagus Rivers. The model was first calibrated for the 1980-2000 period (using 1979 as a warm-up year) against discharge observations at three stations located at the major storage reservoirs: Entrepeñas and Buendía in the Tagus basin and Fuensanta in the Segura basin (see Figure 1). The Cenajo station in the Segura basin was not included in the calibration due to data availability on water transfers between catchments in the Segura basin, but it was included in the simulation runs.

The system focuses on four major periods (initialisation months) relevant for the regional climatology (January, April, July and October), with a forecasting lead time of three months, aiming at finding the most suitable period(s) to take decisions.



#### 2.2.4 Hydropower - SMHI

The regulated mountainous basins are commonly highly influenced by snowmelt runoff and volumes in hydropower production, particularly when a multi-reservoir system is present. In the case study of the Umeälven River (Sweden), seasonal forecasts of snowmelt runoff volumes, together with ground based and remote sensing snow cover monitoring, are key inputs to the decision models of the hydropower companies when planning the production for the current and next winter seasons. It is very common that the operational seasonal forecasts are based on an ESP. Reservoir operators are interested in accumulated forecasts of inflows over the spring flood period (April to July). Forecasts for the April-July accumulated runoff are issued once a month from January until the start of the melt season in April. An important driver is the reservoir level at the end of summer, where a trade-off between water usage for power production during the spring period and the desire to have high water levels at the end of the summer is present. Unnecessary release of water that cannot be used for production is recognised as spill and loss of potential production which can be translated into an economical value. Spill of water may happen when the remaining spring flood volumes were underestimated and reservoirs filled up too early. Therefore, score metrics that are based on volume errors are appropriate measures to describe the improvements in forecasting skill.

#### 2.2.5 Reservoir management - UPV

In the Júcar River Basin, an important characteristic is the semi-aridity of the climate that leads to high hydrological variability, resulting in recurrent periods of drought lasting several years (more than 4 years in some instances). In order to decrease the vulnerability of the water resources system, large reservoirs were built and conjunctive use of surface and groundwater is a regular practice, also integrating wastewater reclamation and reuse. Therefore, integrated and improved management of the water resources system is essential. In addition, proactive drought management requires continuous monitoring and assessment of risk in order to anticipate measures. For this purpose, reliable seasonal forecasts of climate



variables (i.e., precipitation and temperature) and hydrological forecasts (river flows) are needed for the management of the system, which in this case is based on the risk of failure in the supply for all uses, mainly water allocation for drinking water and agriculture.

The analysis must be performed in an integrated way for all elements of the water resources system of the entire basin. Otherwise, physical connections between elements (rivers, aquifers, returns from irrigation and urban uses, etc.) and implications of any decisions in the rest of the system (even from downstream to upstream), would be ignored and results would not be realistic.

For reservoir management, the key is to be able to use the decision support system (DSS) to estimate the risk of failure in the supply of water to all users, as well the risk of failure in the compliance with the established ecological flows, during the next 12 to 24 months (anticipation period). If the risk is considered to be too high, then measures must be proposed and their efficacy be tested with the DSS. A key result is also the forecast of the volume of water remaining in the reservoirs system at the end of the irrigation season. Deterministic and probabilistic forecasts will allow management measures that optimize farmer yields, maintaining high reliability of supplies to the cities, and with an adequate degree of environmental protection

Currently, the analysis is performed using flow forecasts in several places of the basin (we will focus on 5) obtained by multivariate synthetic flow forecasts generation conditioned to the present time state of the system and to past flows. The objective would be to improve the flow forecasts by incorporating short term and seasonal meteorological forecasts as forcing inputs.

For this case study, at UPV we have compared river flow data, obtained from the hydrological model E-HYPE, with regional river flow observations. Hydrological model data were provided by SMHI, corresponding to the continentally calibrated E-HYPE model for the period 1980-2010 and for five sub-basins of the Júcar River basin. Regional observations are naturalized river flows (NRF) for these sub-basins. This comparison has the purpose of testing the reliability of the E-HYPE model and to evaluate the need for a bias correction.



### 2.2.6 Flood & low flow forecasting - Deltares

In the Netherlands, salt intrusion occurs when the river flows of the Rhine and Meuse are low and coincidentally, wind storms push sea water into the river mouth. As a result, water boards cannot take in water to flush their polders, as these could suffer from saline seepage. This problem is a prerequisite for accurate and reliable forecasts of river flows, water levels, tide and surge, water demand and availability in the polder areas, salt concentrations and intrusion. Rijkswaterstaat (the Ministry of Infrastructure and the Environment) is currently predicting river flows up to 10-15 days for the main rivers Rhine and Meuse.

For drought forecasting in the Netherlands, the National Hydrological Model (LHM) was operationalised to support water management (e.g., lakes, surface water, etc) between April and November (Berendrecht et al., 2011). This system is forced with measured and forecasted river flows at the boundary and areal precipitation and potential evaporation (250x250m). Timely information about low flow conditions at the monthly to seasonal scale (1-3 months) can help to take measures such as raising the level of Lake IJssel. This might also have consequences for the flood risk (e.g., due to windstorms causing surge on Lake IJssel) and flow forecasts for the Rhine and Meuse should therefore be accurate and reliable.



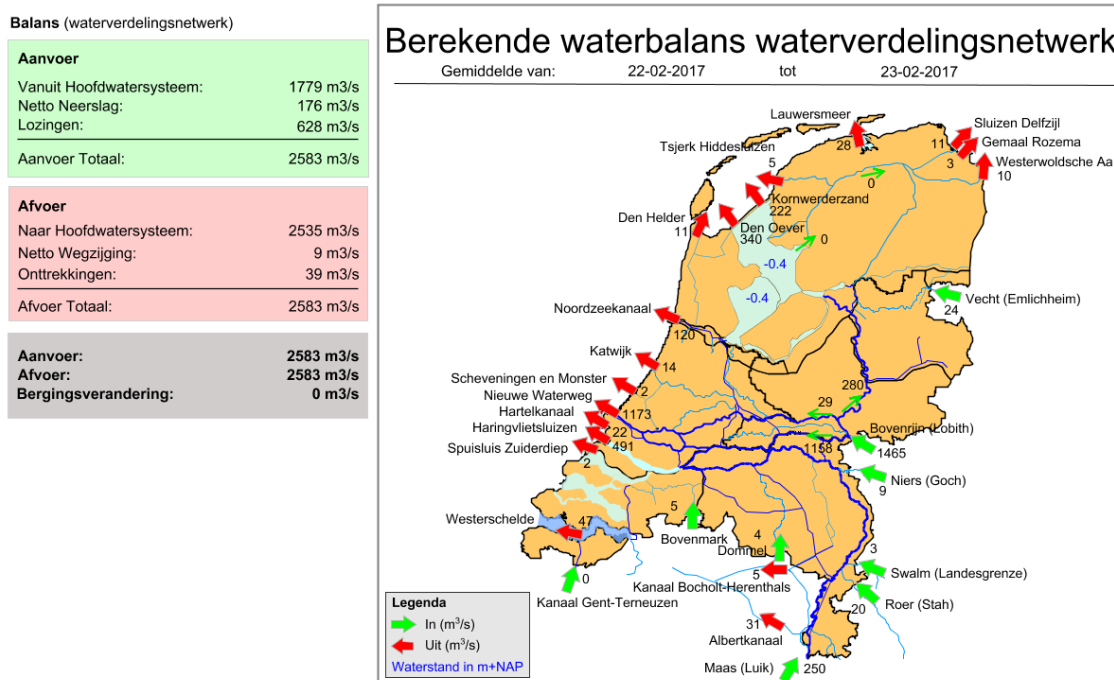


Figure 1 Example display of the operational water management system for the Netherlands, showing a daily computed or forecasted water balance for the surface water network for the Netherlands.

### 2.3 Sensitivity analyses as a tool to diagnose seasonal streamflow forecasting uncertainties

Despite great advances in sub-seasonal to seasonal streamflow forecasting in the last decade, the forecasting skill in Europe is still limited. This is due to a combination of errors, such as the poor seasonal meteorological forecasting skill in the extra-tropics (Arribas et al., 2010), errors in the IHC, hydrological model and downscaling errors.

Sensitivity analyses are a useful tool to diagnose the sensitivity of the model output (here hydrological variables such as discharge) to the model inputs (SCF, IHC and model parameters; Saltelli et al., 2004; 2008). They can be used for a variety of motivations, ranging from research prioritisation (improving solely certain aspects of the forecasting chain) to model simplification (Saltelli et al., 2008). To this end,



forecasting systems intercomparison can help disentangle the sources of uncertainty and/or corroborate skill both in time and space.

Another sensitivity analysis method widely used in seasonal streamflow forecasting is based on the ESP and the reverse-ESP and was first introduced by Wood and Lettenmaier (2003; 2008). The reverse-ESP can only be run in hindcast and is produced by forcing the hydrological model with a single meteorological trace (the meteorological observations for that specific time of the year). The hydrological model is initialised with an ensemble of historical IHCs (resampled from that same initialisation month for all the previous years). Contrary, the ESP is started from a single set of current IHC and forced with an ensemble of historical meteorological observations (resampled from the past meteorological observations available for all previous years and for the same time of the year as the one for which the ESP forecast is run). The ESP can be run as a forecast or in hindcast.. Whereas the uncertainty in the ESP is given by the SCF, the uncertainty in the reverse-ESP is given by the IHC. By comparing the ESP and reverse-ESP skill for a catchment-season-lead time combination, it is possible to tell which component of the forecast mainly leads the uncertainty (i.e., the SCF or the IHC). Recently, this method was extended by Wood et al. (2016) to a method called VESPA (Variational Ensemble Streamflow Prediction Assessment). The VESPA method aims at assessing intermediate uncertainty points between the climatological and 'perfect' (i.e., current observed meteorological data) skill present in the reverse-ESP and the ESP. This method allows the calculation of a metric called 'skill elasticity', a measure of the potential to increase the seasonal streamflow forecasting skill as a result of increasing the SCF or the IHC skill. In this deliverable we will use an alternative method to the VESPA method, a description of which is given in Section 3.3.

## 2.4 Comparative analysis in large sample hydrology

Large-scale (i.e. continental) multi-basin modelling can complement the "deep" knowledge from basin-based modelling and enhance process understanding, increase robustness of generalisations, facilitate classification of basin behaviour and



prediction, support better understanding of prediction uncertainty, and go beyond sensitivities related to IHC and SCF (Pechlivanidis and Arheimer, 2015). This type of modelling has the potential to cross regional and international boundaries whilst the analysis over a number of basins allows the consideration of different geophysical and climatic zones (Gupta et al., 2014); hence it can provide a deeper understanding of the underlying sensitivities in the forecasting skill. Such modelling type can also advance hydrological science since it finds a numerical background for comparative hydrology (Blöschl et al., 2013). The use of a large sample of stations, particularly when analyses are conducted at the continental scale (i.e., as in Europe), can also allow for exploration of emerging patterns and facilitate comparative hydrology, allowing to test sensitivities for many catchments with a wide range of environmental conditions (Blöschl et al., 2013).

However, understanding processes in large systems is challenging, given that physical properties (e.g., vegetation and soil type) generally exhibit high spatial variability, which consequently results in significant differences in system behaviour and predictability. As expected, this spatial heterogeneity introduces further high uncertainty on the categorisation of important drivers that influence the predictive hydrological skill. In addition, large river basins are often strongly influenced by human activities (e.g., irrigation, hydropower production, groundwater use) for which information is rarely available and therefore rarely described in hydrological model processes; hence introducing additional uncertainty regarding process understanding and description. Although such modelling type has limitations which vary in space, in here we make the step forward to gain insights in spatial patterns of hydrological skill at the large scale, and link this to the characteristics of the basin system.



## 3 Data and methods

### 3.1 The forecasting systems

All the partners of this deliverable use dynamical ensemble seasonal forecasting systems. These systems all use the same seasonal meteorological forecasts but are diverse in terms of the hydrological models and the presence or not of a bias correction method for the seasonal meteorological forcing. This was done in order to obtain insights into the seasonal discharge forecast sensitivity to the hydrological model type. An overview of the various systems and their characteristics is given in Table 1. For more details on the hydrological models used, see Annex A.



Table 1 Dynamical ensemble seasonal hydrological forecasting systems.

Partner	Meteorological forecasts	Interpolation method	Bias correction of the meteorological forecasts	Hydrological model	# of ensemble members	Hindcasts period for which scores calculated	Forecast starting dates	Lead time and time step	Spatial domain
ECMWF	System 4	Inverse distance weighting. Temperature was first corrected using the elevation	None	LISFLOOD (5x5km)	15, extended to 51 every three months	1990 - 2010	On the first of every month	Up to 7 months, daily values	Europe
BfG	System 4	Precipitation Voronoi	Linear scaling, Separate	LARSIM-ME (5x5km)	15, extended to	1990 - 2010	On the first of	Up to 6 months	Catchments of the Rivers



		tessellation Temperature constant lapse rate and inverse distance weighting	scaling factors are derived in dependence of initialization month and monthly lead time		51 every three months		every month		Rhine, Elbe, Weser/Ems, Odra and Danube up to gauge Nagymaros in Hungary
SMHI	System 4		Distribution- Based Scaling (DBS) approach	E-HYPE (215 km <sup>2</sup> )	15	1990 - 2010	On the first of every month	Up to 7 months	Europe
FW	System 4		Bias correction using Spain02 observation data (Herrera et al. 2016)	SPHY (5x5km - Tagus; 2x2km Segura)	15	1990 - 2010	On the first of: January, April, July and October	Up to 3 months	Tagus and Segura River basins



UPV	System 4		None	EVALHID (semi-distributed application at sub-basin scale)	15	1990 - 2015	On the first of every month	Up to 7 months, daily values	Jucar River basin
DELTA S*	System 4	Precipitation HYRAS data set extended with emulated HYRAS  Temperature HYRAS data set extended with a constant	None	wflow_hbv (1.44 km <sup>2</sup> )	15, extended to 51 every three months	1980 - 2015	On the first of every month	Up to 3 months, daily values	Rhine



		lapse rate based on DEM and inverse distance weighting							
	System 4	EFAS forcing dataset (See ECMWF)	None	W3RA (0.5 km <sup>2</sup> and 0.05 km <sup>2</sup> )	15, extended to 51 every three months	1990 - 2014	On the first of every month	Up to 3 months, daily values	Europe

\*As the seasonal forecast runs from Deltares were not ready at the time of this deliverable, results of discharge simulations from the two models shown above for Deltares, as well as discharge simulations produced from the HBV96 model will be shown in the results. The W3RA was run with EFAS historical forcing data from 1991-2014, while the lumped HBV96 and distributed wflow\_hbv models were run using HYRAS data from 1991-2006.



### 3.2 The forecasting systems intercomparison

The first part of this deliverable compares the performance of the dynamical sub-seasonal to seasonal hydrological forecasting systems listed above (see Table 1). For the intercomparison, a common set of stations was selected, based on data available to the partners of this deliverable (see Figure 2 and Table 2). Observed discharge data was distributed for the corresponding stations by a few partners to all partners involved in WP4, in order to have a consistent verification across partners.

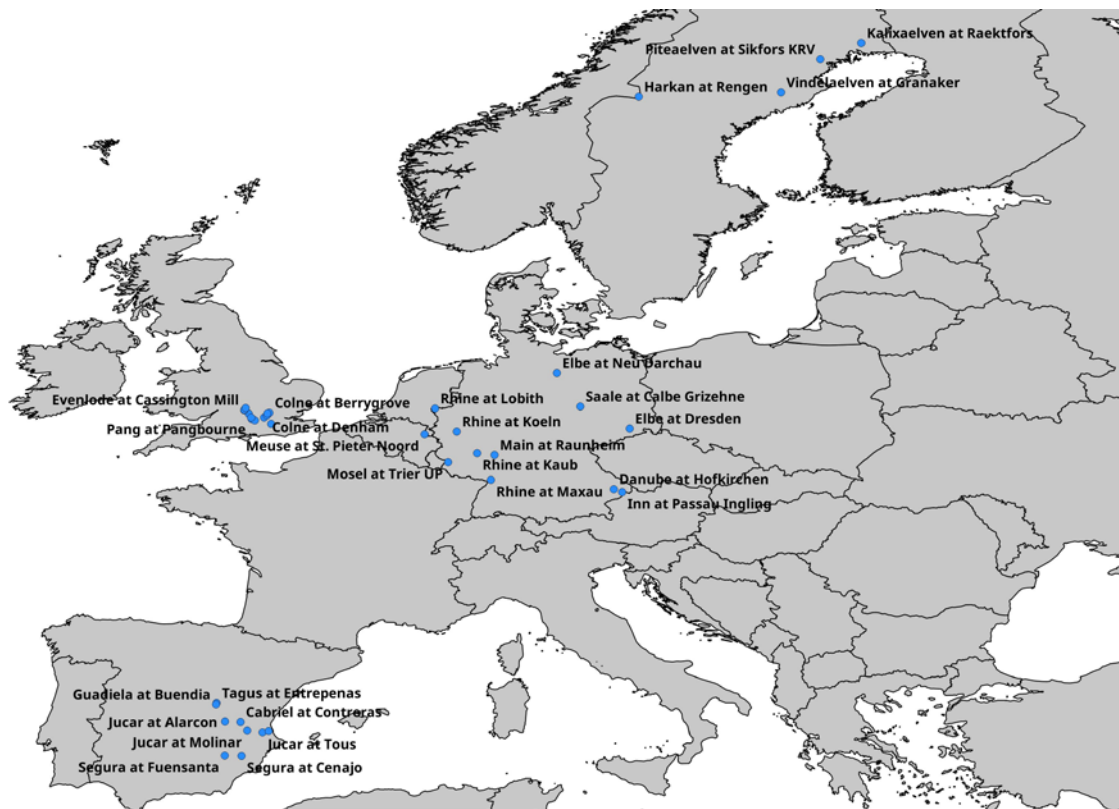


Figure 2 Map of the stations used for the analysis.



Table 2 Observed discharge data for the selected stations.

Case study	Data source	Station code	Station name	Station coordinates (lat, lon)	Drainage area (km <sup>2</sup> )	Elevation (m)	River (country)
<b>The Thames River Basin</b>	Observed discharge from the NRFA (National River Flow Archive)	UOR39088	Rickmansworth	51.64199826, -0.461235789	105	47.1	Chess (UK)
		UOR39072	Royal Windsor Park	51.48562525, -0.589407615	7046	13.5	Thames (UK)
		UOR39068	Castle Mill	51.23842724, -0.31118153	316	39.2	Mole (UK)
		UOR39034	Cassington Mill	51.786274, -1.351677333	430	60.2	Evenlode (UK)
		UOR39027	Pangbourne	51.48462376, -1.08759943	170.9	39.6	Pang (UK)
		UOR39021	Enslow Mill	51.86135121, -1.301356378	551.7	65	Cherwell (UK)
		UOR39016	Theale	51.43274011, -	1033.4	43.4	Kennet (UK)



				1.066925886			
		UOR39013	Berrygrove	51.67066472, - 0.380218207	352.2	54.7	Colne (UK)
		UOR39010	Denham	51.56631768, - 0.483890807	743	34.1	Colne (UK)
		UOR39008	Eynsham	51.77524074, - 1.356429965	1616.2	59.7	Thames (UK)
		UOR39007	Swallowfield	51.37737889, - 0.951223862	354.8	42.3	Blackwater (UK)
		UOR39002	Days Weir	51.63852061, - 1.179455188	3444.7	45.8	Thames (UK)
<b>Central European Rivers</b>	The Global Runoff Data centre, 56068 Koblenz, Germany	GRDC634030 0	Calbe Grizehne	51.916608,11.8099 82	23719	49.36	Saale (Germany)
		GRDC634012 0	Dresden	51.054456,13.7388 29	53096	102.68	Elbe (Germany)
		GRDC634280	Hofkirchen	48.67657,13.11427	47496	299.6	Danube



		0		9			(Germany)
		GRDC633510	Kaub	50.085613,7.76500	103488	67.66	Rhine (Germany)
		0		8			
		GRDC633506	Koeln	50.937359,6.96322	144232	34.97	Rhine (Germany)
		0		5			
		GRDC633520	Maxau	49.038933,8.30553	50196	97.76	Rhine (Germany)
		0		5			
		GRDC634011	Neu Darchau	53.232337,10.8887	131950	5.68	Elbe (Germany)
		0		73			
		GRDC634390	Passau Ingling	48.5629,13.443071	26063	289.19	Inn (Germany)
		0					
		BFG2409530	Raunheim	50.016067,8.44824	27142	82.9	Main (Germany)
		2		8			
		GRDC633650	Trier UP	49.732655,6.624	23857	121	Mosel (Germany)
		0					
	Observed discharge from	GRDC643506	Lobith	51.84, 6.11	160800	8.53	Rhine (The Netherlands)
		0					



	RWS	GRDC6421101	St Pieter Noord	50.83, 5.71	21300	44	Meuse (The Netherlands)
<b>The Segura and Tagus River Basins</b>	Reservoir inflows	FWUT_1	Entrepenas	40.2938,-2.4456	3825.5	636	Tagus (Spain)
		FWUT_2	Buendia	40.236,-2.4657	3355.7	636	Guadiela (Spain)
		FWSG_1	Fuensanta	38.2333,-2.1224	1210.1	524	Segura (Spain)
		FWSG_2	Cenajo	38.22,-1.4629	1394.4	335	Segura (Cenajo)
<b>The Jucar River Basin</b>	Reservoir inflows and Spain02	UPV8001	Alarcon	39.564597,-2.112084	2937	831	Jucar (Spain)
		UPV8009	Contreras	39.543559,-1.502849	3266	1030	Cabriel (Spain)
		UPV8026	El Molinar	39.207931,-1.239957	7912	690	Jucar (Spain)



		UPV8030	Tous	39.132927,- 0.650729	17821	64	Jucar (Spain)
		UPV8089	Sueca	38.939532,- 0.478048	21497	18	Jucar (Spain)
<b>Swedish Rivers</b>	The Global Runoff Data centre, 56068 Koblenz, Germany	GRDC6233510	Granaker	64.239979,19.66624	11850.5	NA	Vindaelven (Sweden)
		GRDC6233710	Sikfors KRV	65.532833,21.20877 8	10816.1	NA	Piteaelven (Sweden)
		GRDC6233850	Raectfors	66.170645,22.81577 5	23102.9	NA	Kalixaelven (Sweden)
		GRDC6233470	Rengen	64.069902,14.09551 9	1110.1	NA	Harkan (Sweden)



In order to compare the performance of the different ensemble seasonal hydrological forecasting systems, several scores were chosen including both deterministic and probabilistic scores and covering the main attributes of ensemble forecasting relevant for sectoral applications (see Section 3b). These scores include:

- Deterministic scores:
  - o **The Mean Absolute Error (MAE)** (cawcr, 2015):

$$MAE = \frac{1}{N} \sum_{i=1}^N |F_i - O_i|$$

The MAE ranges from 0 to an upper boundary defined by the system's variability, with a perfect score of 0, and indicates the average magnitude of the forecast errors. Where  $F_i$  is the ensemble mean and  $O_i$  is the observed discharge for the same time.  $N$  is the sample size, it is the total number of forecasts made for the same target month and with the same lead time and temporal aggregation type. This score does not indicate the direction of the forecast deviations, which will be calculated using the Mean Error (ME).

- o **The Mean Error (ME)** (cawcr, 2015):

$$ME = \frac{1}{N} \sum_{i=1}^N (F_i - O_i)$$

The  $ME$  ranges from  $-\infty$  to  $+\infty$ , with a perfect score of 0, and is a measure of the average forecast error, considering the ensemble mean. It indicates the forecast average additive bias (i.e., its tendency to underestimate or overestimate observed discharge). Note, a good ME score does not guarantee that the forecast is perfect as overestimations and underestimations made by the latter can compensate each other.

- o The **normalised volumetric term of the Kling-Gupta Efficiency ( $\beta$ )** (Gupta et al., 2009):

$$\beta = 1 - \sqrt{(\beta - 1)^2}$$

$\beta$  is defined as the ratio of the monthly mean of the forecasts (the output of the model forced by meteorological forecasts) over the monthly mean of the





perfect forecasts (the output of the model forced by the reference forcing dataset); note that the range of the values for each term varies between  $-\infty$  and 1 with 1 being the optimum.

- Probabilistic scores:
  - o **The Continuous Ranked Probability Score (CRPS)** (Hersbach, 2000):

$$CRPS(P, x_a) = \int_{-\infty}^{\infty} [P(x) - P_a(x)]^2 dx$$

Where  $P$  is the ensemble forecast cumulative distribution function (cdf) and  $P_a$  is the observation cdf and is defined by:

$$P_a(x) = H(x - x_a)$$

For the observed discharge  $x_a$ , with  $H(x)$  the Heaviside function:

$$H(x) = \begin{cases} 0 & \text{for } x < 0 \\ 1 & \text{for } x \geq 0 \end{cases}$$

The CRPS ranges from 0 to  $+\infty$ , with a perfect score of 0, and is a measure of the difference between the forecast and the observation cdfs. A perfect score of 0 is achieved in the case of a perfect deterministic forecast. The CRPS is a measure of the forecast accuracy and sharpness. It can be further decomposed into reliability, resolution and uncertainty components, according to:

$$CRPS = \text{reliability} + CRPS_{\text{potential}}$$

Where the potential CRPS is the CRPS value that a forecast with perfect reliability (reliability=0) would have, expressed as:

$$CRPS_{\text{potential}} = \text{uncertainty} - \text{resolution}$$

The reliability is a measure of the bias and the spread of the system. The uncertainty is the variability of the observations and the resolution is the



ability of the forecast to distinguish situations with distinctly different frequencies of occurrence. The components all range from 0 to  $+\infty$ , with a perfect score of 0. The CRPS and its components were averaged over all the forecasts made for the same forecast initialisation date and with the same lead time and temporal aggregation (monthly averages here).

o **The Brier score (BS)** (cawcr, 2015):

$$BS = \frac{1}{N} \sum_{i=1}^N (p_i - o_i)^2 = \frac{1}{N} \sum_{k=1}^K n_k (p_k - \bar{o}_k)^2 - \frac{1}{N} \sum_{k=1}^K n_k (\bar{o}_k - \bar{o})^2 + \bar{o}(1 - \bar{o})$$

Where  $N$  is the sample size, the total number of forecasts made for the same target season and with the same lead time, temporal aggregation type and for the same event.  $o_i$  is a binary observation, it is 1 if a predefined event happened and 0 if it did not.  $p_i$  is the forecast probability of the event happening. The BS ranges from 0 to 1, with a perfect score of 0 and is a measure of the mean squared error of the probability forecasts over the verification sample. The events selected to calculate the Brier score are the upper and the lower terciles of the observed discharge for the specific season for which the score is calculated. These thresholds were chosen in order to have a large enough sample as this score is sensitive to the climatological frequency of the event: the rarer an event is, the easier it will be to obtain a good BS without necessarily having any real skill. The BS can be further decomposed into a (1) reliability, (2) resolution and (3) uncertainty part. The BS and its three parts were averaged over all the forecasts made for the same target season and with the same lead time, temporal aggregation (monthly averages here) and for the same event (upper or lower terciles).

o **The skill scores:** the forecast skill was also calculated for the CRPS and the BS using the following equation:

$$Skillscore = 1 - \frac{score_{forecast}}{score_{reference}}$$





For the reference, two benchmarks were selected. The first benchmark is the climatology of observed discharge and the corresponding skill scores of the CRPS and the BS are called the CRPSS\_CLI and the BSS\_CLI, respectively. The climatology covers the same period as is covered by each forecasting system (excluding the year analysed) and is the climatology of a given target month (or season for the Brier Score). The second benchmark is the ESP corresponding to each system, for the same forecast initialisation date, lead time and temporal aggregation (monthly averages here). The corresponding skill scores of the CRPS and the BS are called the CRPSS\_ESP and the BSS\_ESP, respectively

The analysis will present scores measured for the discharge forecasted from various forecast starting dates or target seasons (for the BS), lead times, monthly aggregations and several stations in Europe. This intercomparison will provide a spatio-temporal overview of the performance of the seasonal hydrological forecasting systems overall as well as for extreme events (high and low flows).

### 3.3 The EPB sensitivity analysis

The VESPA method is a sensitivity analysis method in the sense that it measures the response of the model output (discharge in our case) to a known variation in the model input(s) (here the SCF and the IHC). It was designed and tested on 424 catchments in the contiguous United States (CONUS), for which it successfully exposed the relative contributions of the two sources of errors (SCF and IHC) on seasonal streamflow forecasting uncertainty. Moreover, the 'skill elasticity' produced by the VESPA method indicates the potential to improve the seasonal streamflow forecasting skill by improving the SCF and/or the IHC skill. This information is valuable for guiding resources in seasonal forecasting system development towards useful improvements. One drawback of the VESPA method however is that it is computationally expensive to run as it is based on a very large number of simulations. Recently, an alternative and cheaper method called EPB (End Point Blending) was designed and tested on 18 catchments of the CONUS for which it gave almost identical results to the VESPA method (Arnal et al. 2017). Because the EPB sensitivity analysis is a



reliable and computationally cheap method which can give insightful results in the context of seasonal streamflow forecasting improvements, it will be used in this deliverable.

The EPB is constructed by combining four sources of data (also called end points): the ESP, the reverse-ESP, the climatology and the 'perfect' forecast. The term 'perfect' refers to current observed meteorological data and the term climatological refers to the whole distribution of historical meteorological observed data. Each end point corresponds to a combination of IHC and SCF weights ( $w_{IHC}$  and  $w_{SCF}$  respectively; the axes on Figure 3). A weight of 0 is the 'perfect' knowledge (upper right corner on Figure 3) whereas a weight of 1 is the climatological knowledge of either of the two predictability sources (bottom left corner on Figure 3). A 'perfect' forecast (forecast generated by starting a hydrological model with the current IHC and forcing it with the current observed meteorological data) has a  $w_{IHC}$  and a  $w_{SCF}$  of 0. The climatological forecast ('climo' on Figure 3; forecast generated by starting a hydrological model with all historical IHC and forcing it with all historical observed meteorological data) has a  $w_{IHC}$  and a  $w_{SCF}$  of 1 by definition. The reverse-ESP is forced with a single meteorological trace, the meteorological observations for that specific time of the year ( $w_{SCF}$  of 0) and the model is initialised with a range of historical IHC ( $w_{IHC}$  of 1). The ESP is forced with historical observed meteorological data ( $w_{SCF}$  of 1) and the current IHC ( $w_{IHC}$  of 0).

The EPB combines these four end points for each intermediate SCF and IHC weights ( $w = 0, 0.05, 0.10, 0.25, 0.50, 0.75, 0.90, 0.95, 1.0$ ), as shown on Figure 3 below. Those intermediate weights were chosen in order to coincide with the VESPA method (Wood et al. 2016). For each  $w_{SCF}$ - $w_{IHC}$  combination (each cross on Figure 3 below), a new 100-member hindcast is generated by a weighted averaging of the forecasts carried out for the four end points. The percentage of each end point used, EP [%] (i.e., the number of members randomly selected from each end point), is given for each combination point by the following equation:

$$EP[\%] = (1 - |x_{EP} - w_{IHC}|) \times (1 - |y_{EP} - w_{SCF}|)$$





Where  $x_{EP}$  and  $y_{EP}$  are the  $w_{IHC}$  and  $w_{SCF}$  values of the end point for which the percentage is calculated, respectively. For example, if the  $w_{IHC}$  and  $w_{SCF}$  match the end point values, 100 percent of the EPB hindcast members are resampled from that end point (i.e., the end point skill is reproduced). This was done for each forecast initialisation date for a given location.

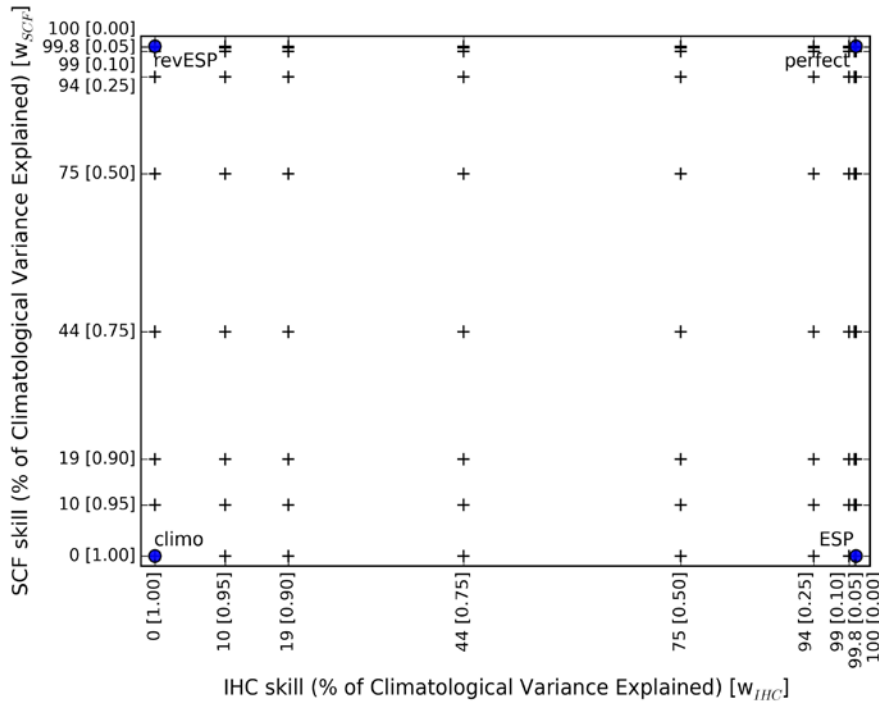


Figure 3 Resampling surface for the EPB sensitivity analysis method (taken from Arnal et al. 2017).

Once the new EPB hindcasts have been generated, their quality can be calculated for each combination point. A plot of the forecast quality as a function of IHC and SCF skill can then be drawn and is called skill surface plot in Wood et al. (2016). Finally, for each response surface (i.e., skill elasticity plot) skill elasticities for the IHC and the SCF ( $E_{IHC}$  and  $E_{SCF}$  respectively) can be measured from the scores from the following equations:

$$E_{IHC} = 100 \times \left\{ \frac{S(F[75,19]) - S(F[19,19])}{75\% - 19\%} + \frac{S(F[75,44]) - S(F[19,44])}{75\% - 19\%} + \frac{S(F[75,75]) - S(F[19,75])}{75\% - 19\%} \right\} / 3$$

$$E_{SCF} = 100 \times \left\{ \frac{S(F[19,75]) - S(F[19,19])}{75\% - 19\%} + \frac{S(F[44,75]) - S(F[44,19])}{75\% - 19\%} + \frac{S(F[75,75]) - S(F[75,19])}{75\% - 19\%} \right\} / 3$$



The numerators, expressed as  $S(F[-]) - S(F[-])$ , are the streamflow forecast skill gradients between IHC skill (or SCF skill) values of 75% and 19% (the denominator). The values in the square brackets of the numerator are the IHC skill followed by the SCF skill values, indicating a wSCF - wIHC combination point in the example skill surface plot (i.e., Figure 3). In the denominator, the IHC and SCF skill gradients are gradients in the percentage of the climatological variance explained in the respective predictability source. The skill elasticities ( $E_{IHC}$  and  $E_{SCF}$ ) are positively oriented; where a skill elasticity of zero is obtained when the predictability source has no influence on the skill of the streamflow forecast, while positive (negative) elasticities mean that an improvement in the predictability source will lead to higher (lower) streamflow forecast skill.

For this deliverable, we calculated the IHC and SCF skill elasticities for the ECMWF seasonal discharge forecasts described in Table 1, for each initialisation date (the first of each month), monthly forecast aggregations from 1 to 7 months of lead time and over 74 geoclimatological regions in Europe. These 74 regions were selected as they are the same regions for which the ECMWF seasonal streamflow forecast is currently operational in EFAS (European Flood Awareness System). The skill elasticities are based on the CRPSS, calculated against the climatological forecast. This analysis assumes that the model is perfect as the CRPS is calculated against the 'perfect' forecast (i.e., discharge simulation) and not actual discharge observations. Additionally, skill elasticities were calculated for the BfG seasonal discharge forecasts described in Table 1, for each initialisation date (the first of each month), monthly forecast aggregations from 1 to 6 months of lead time and for the stations shared by the BfG and presented in Table 2.

### 3.4 Seasonal hydrological forecasts - Clustering of the skill

To better understand the potential factors influencing the skill of a model and to identify regions of similarity, we apply classification and regression trees (CART). Here, we explored the spatial runoff patterns across the entire subcontinent by analysing the skill in all 35408 catchments modelled by the E-HYPE model. CART is a recursive-partitioning algorithm that





classifies the space defined by the input variables/descriptors (i.e. physiographic-hydrologic-climatic characteristics, and remaining climatic biases) based on the output variable (i.e. beta skill for lead month 2 and month March). The tree consists of a series of nodes, where each node is a logical expression based on a similarity metric in the input space (physiographic-hydro-climatic characteristics etc.). CART also provides information on the probabilities of different output groups at each leaf node. In this case, beta (see section 3.2) is divided into five groups - bad ( $\beta < 0.2$ ), poor ( $0.2 < \beta < 0.4$ ), medium ( $0.4 < \beta < 0.6$ ), good ( $0.6 < \beta < 0.8$ ) and very good ( $\beta > 0.8$ ), which are termed C0, C1, C2, C3 and C4 respectively. A terminal leaf exists at the end of each branch of the tree, where the probability of belonging to any of the three output groups can be inspected. Here we summarised the basin characteristics into climatic, topographic, human impacts, biases in forcing input and hydrologic bias (Table 3). We next calculate the predictors' importance (and rank them) by summing changes in the risk due to splits on every predictor and dividing the sum by the number of branch nodes.

It is important to note that in order to avoid the high dimensionality in the CART analysis, the hydrologic signatures were firstly clustered into 11 groups with each group receiving an ID (named FlowID). We applied a k-means clustering approach within the 12-dimensional space (consisting of the 12 calculated flow signatures in Table 3) to categorise the subbasins based on their combined similarity in flow signatures. Through the mapping of the spatial pattern we gained insight into the similarities of catchment functioning and could identify the dominant flow generating processes for specific regions.

Table 3 Basin characteristics used in the clustering analysis.

<b>Climatology characteristics</b>	<b>(7)</b>	<b>Topography</b>	<b>Human impact</b>	<b>Forcing</b>	<b>biases</b>	<b>Hydrologic signatures (12)</b>
		<b>(4)</b>	<b>(1)</b>	<b>(2)</b>		
Precipitation (mm/month); Prec.		Area (km <sup>2</sup> ); Area	Degree of regulation (%); DoR	Precipitation (%); BiasPrec.		Mean annual specific runoff; Qm
Temperature (°C); Temp.		Elevation (m); Elev.		Temperature (%); BiasTemp.		Normalised high flow; q05
Snow depth (cm/month); Snow		Relief ratio (-); Relief				Normalised low flow; q95
Actual evaporation (mm/month); AET		Slope (%); Slope				Normalised relatively low flow; q70



Potential evaporation (mm/month); P				Slope of flow duration curve; mFDC
Dryness index (-); P/Prec.				Range of Parde coefficient; DPar
Evaporative index (-); AET/P				Coefficient of variation; CV
				Flashiness; Flash
				Normalised peak distribution; PD
				Rising limb density; RLD
				Declining limb density; DLD
				Baseflow index; BFI





## 4 Results

### 4.1 The forecasting systems intercomparison

A set of scores was added from each forecasting system (from the ECMWF, SMHI, BfG and FW) into the scoreboard for the selected stations shown in Table 2. This allows to have a first view of the similarities as well as differences between the forecasting systems' performances and highlights common forecasts' behaviours across river basins.

The seasonal discharge forecasts' quality depends on the target month, the lead time and the station for which the forecast is made. We will split the results according to the geographical location of the river basins, as there are some noticeable similar characteristics in terms of forecast performance for stations in a given area of Europe.

#### 4.1.1 Central European Rivers

For stations of the Central European Rivers case study, scores were calculated from the SMHI, the BfG and the ECMWF forecasting systems. From this set of stations, there appears to be two types of forecast performance behaviours. For the most western Central European Rivers stations included in this deliverable (the Main at Raunheim, the Rhine at Koeln, Kaub and Maxau and the Mosel at Trier UP), all forecasts show similar CRPS values, with larger errors from November-April. Figure 4 is an example of the CRPS for the three systems for the Rhine at Koeln.

For the most eastern Central European Rivers stations included in this deliverable (the Elbe at Neu Darchau and Dresden and the Saale at Calbe Grizehne), the SMHI forecasts display larger CRPS values than the two other systems, especially from December-April. Figure 5 is an example of the CRPS for the three systems for the Elbe at Dresden.

In general however, the BfG and the ECMWF seasonal discharge forecasts have a lower CRPS than the SMHI forecasts for the first forecast month.



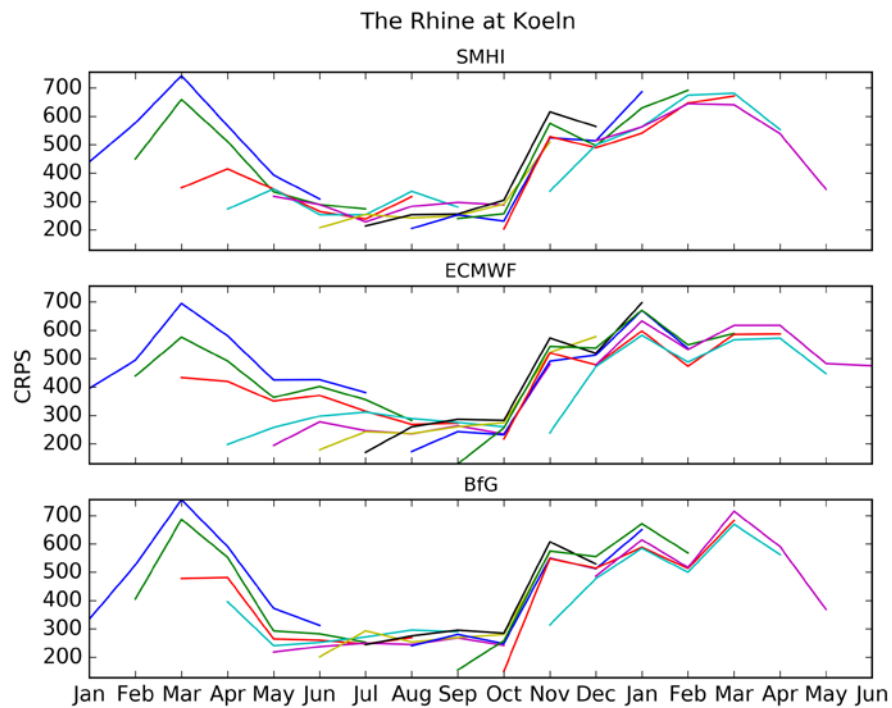


Figure 4 Continuous Ranked Probability Score (CRPS) for the Rhine at Koeln for (top) the SMHI forecasts, (middle) the ECMWF forecasts and (bottom) the BfG forecasts. CRPS = 0 denotes a perfect forecast. The CRPS is given for each forecast initialisation date (on the first of each month, different colours) and for 6 months of lead time (for the SMHI and the BfG forecasts) or 7 months of lead time (for the ECMWF forecasts).



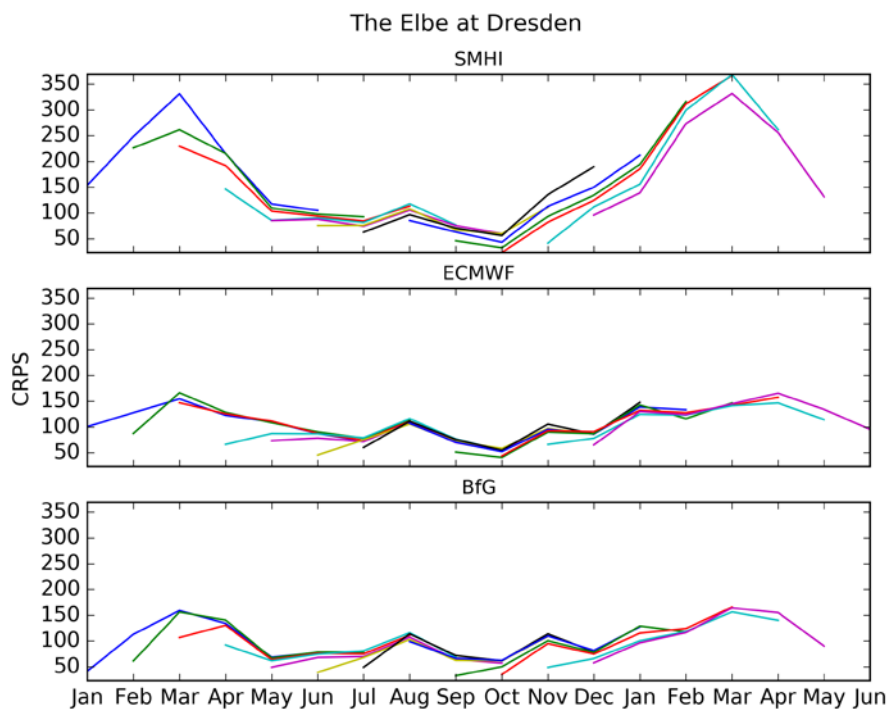


Figure 5 Same as Figure 4 but for the Elbe at Dresden.

While the seasonal forecasts with the W3RA model are not available at this time, results are shown from the simulation run (spanning 1990-2014, with one year of spin up) obtained from the W3RA model from Deltares for the Elbe at Dresden. The results, presented on Figure 6, are plotted as monthly values of the mean absolute error (MAE; comparable with the CRPS as shown above for the SMHI, ECMWF and BfG models). From these results, it appears that the W3RA model has the largest errors from October-May. This is similar to the pattern of the CRPS observed on Figure 5 for the SMHI forecasts for the same station.



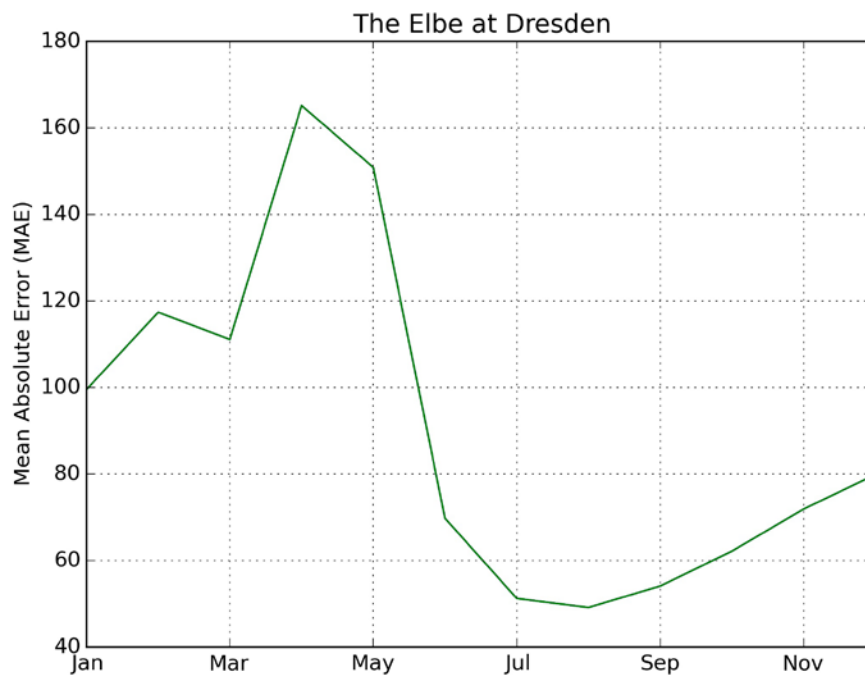


Figure 6 Mean Absolute Error (MAE) for the Elbe at Dresden (at lead time 0) for the W3RA model for the period 1991-2014.

For the Rhine at Lobith, the results are also plotted as monthly values of the mean absolute error for the W3RA model, the lumped HBV96 model and the distributed wflow\_hbv model (Figure 7). Note that W3RA was run with EFAS historical forcing data, while the lumped HBV96 and distributed wflow\_hbv models were run using HYRAS data (details given in Table 1). From Figure 7, it appears that the W3RA model displays larger errors than the two other models almost all year long, especially in summer. This could be an indication that the EFAS historical forcing data has large uncertainties for this station. It could furthermore be due to a misrepresentation of essential discharge generating mechanisms in this region by the W3RA model.



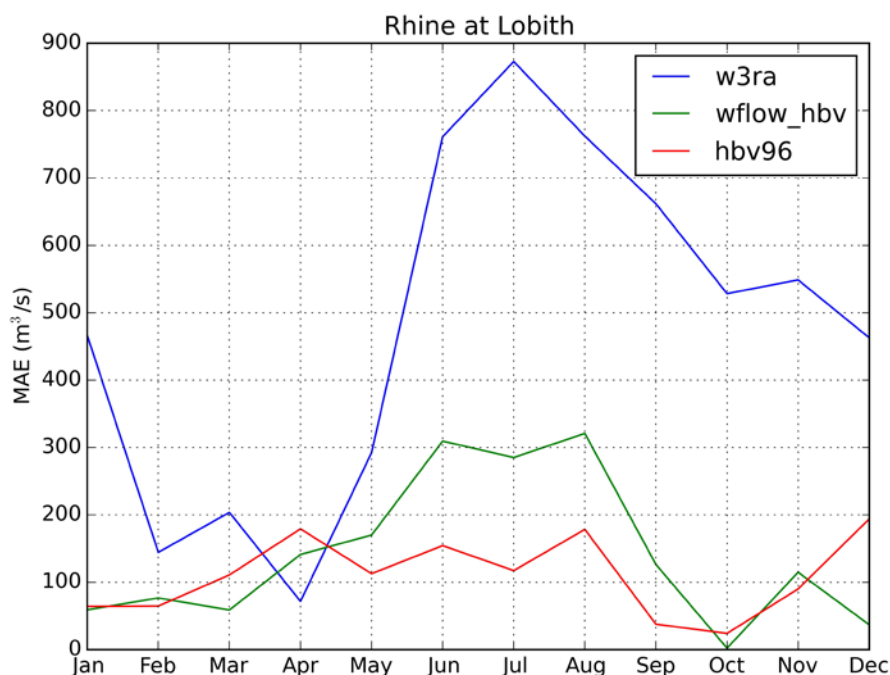


Figure 7 MAE for the Rhine at Lobith (at lead time 0) for the W3RA (1991-2014), the lumped HBV96 and the distributed wflow\_hbv models (both for the period 1991-2006).

Figures 8 and 9 show the bias (i.e., the ME) for all forecast initialisation dates and all lead times for the Rhine at Koeln and the Elbe at Dresden, respectively. For most Central European Rivers stations included in this analysis, the SMHI forecasts overestimate the observed discharge in the winter to spring months. This is both the case for the Rhine at Koeln (Figure 8) and the Elbe at Dresden (Figure 9). This positive bias could be due to a hydrological model error, where the model releases more water as river flow than is observed because it cannot store enough water as groundwater. For the Rhine at Koeln (and a few other stations of the most western Central European Rivers stations, not shown), the SMHI forecasts additionally present a negative bias for the rest of the year.

The ECMWF forecasts overall overestimate the observed discharge during the spring months (more largely at longer lead times) while underestimating the winter discharge. This is both true for the Rhine at Koeln and the Elbe at Dresden (see Figures 8 and 9). This positive bias extends into the early summer months for some stations. These biases could be due to meteorological forecast error as the input meteorological forecasts used to produce the ECMWF seasonal discharge forecasts was not bias corrected, contrary to the BfG and the



SMHI forecasts. It seems that ECMWF generates too much of the precipitation falling as snow in winter, leading to underestimated discharge in those months and a snowmelt compensation in spring.

The BfG forecasts underestimate the observed discharge for winter and early spring months or all target months, depending on the station (see Figures 8 and 9). This behaviour could either be due to the bias correction of the meteorological forecasts input to the hydrological model, which produces too dry conditions compared to the observed amount, or to the hydrological model which stores too much incoming water as groundwater.

These are general characteristics of the SMHI, BfG and ECMWF forecasts and the magnitude of the bias depend on the station, target month and lead time for which the forecasts were made.

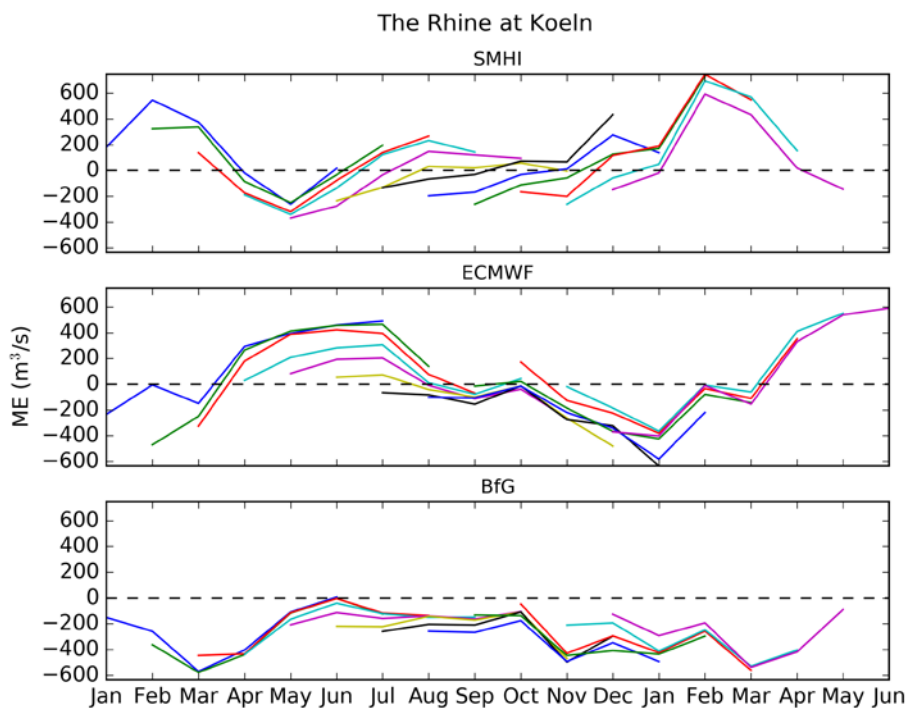


Figure 8 Mean Error (ME) for the Rhine at Koeln for (top) the SMHI forecasts, (middle) the ECMWF forecasts and (bottom) the BfG forecasts. ME = 0 denotes no bias, while ME > 0 denotes a positive forecast bias and the ME < 0 a negative forecast bias. The ME is given for each forecast initialisation date (on the first of each month, different





colours) and for 6 months of lead time (for the SMHI and the BfG forecasts) or 7 months of lead time (for the ECMWF forecasts).

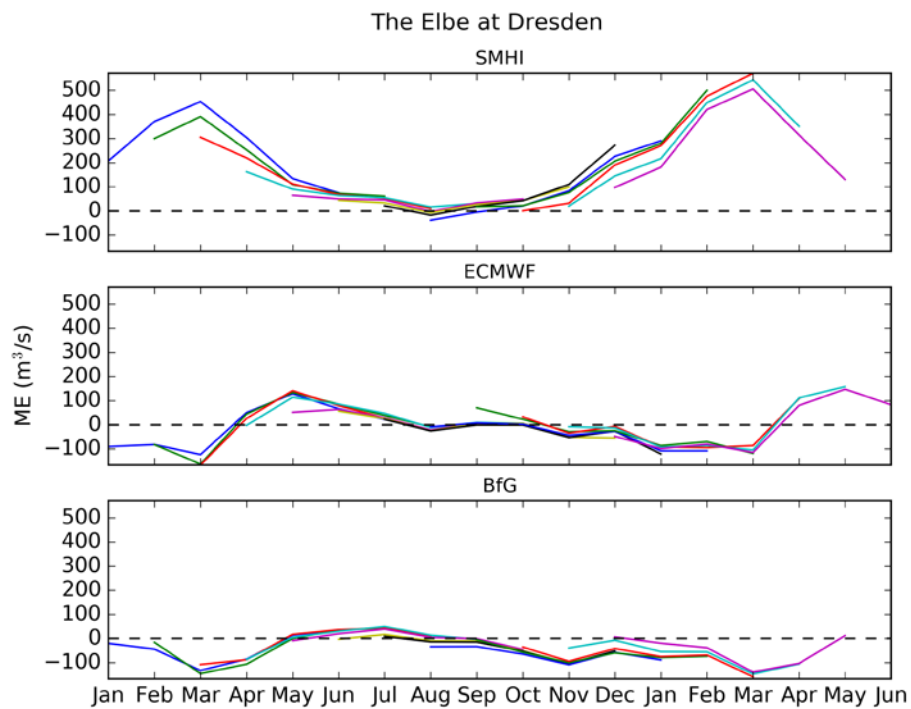


Figure 9 Same as Figure 8 but for the Elbe at Dresden.

Figure 10 shows the bias (i.e., the ME) for the W3RA model simulation for the Elbe at Dresden. From this figure, it can be seen that the W3RA underestimates the discharge for all months of the year, especially in April.



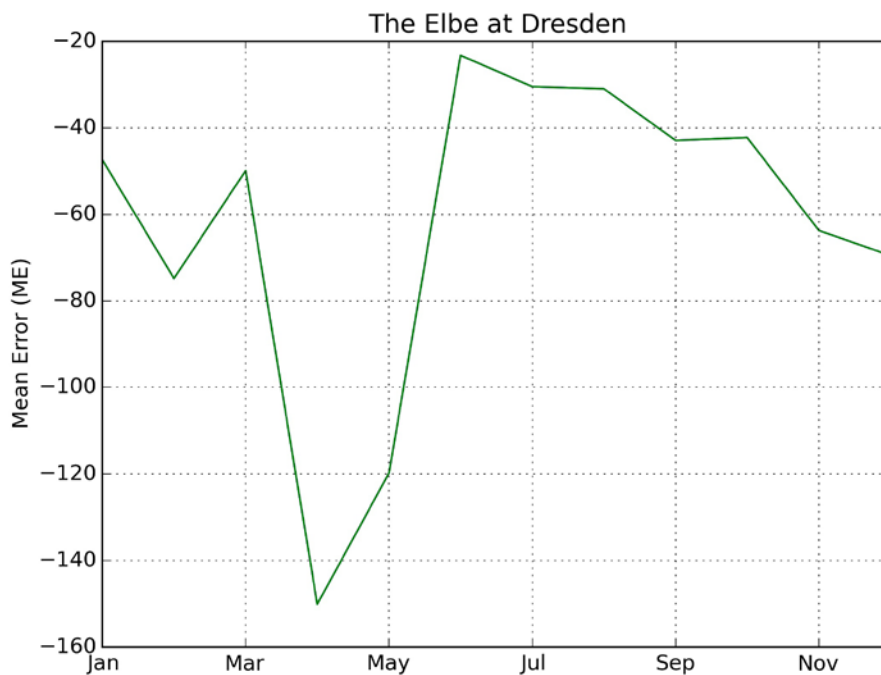


Figure 10 ME for the Elbe at Dresden (at lead time 0) for the W3RA model for the period 1991-2014.

Figure 11 displays the Mean Error (ME) for the Rhine at Lobith for the W3RA, the lumped HBV96 and the distributed wflow\_HBV models. For this station, the W3RA model largely overestimates the discharge for all months. The wflow\_hbv model overestimates the observed discharge mostly in the summer, while it underestimates it slightly in November and January-February. The HBV96 model underestimates the observed discharge for October-November and overestimates it for the rest of the year.



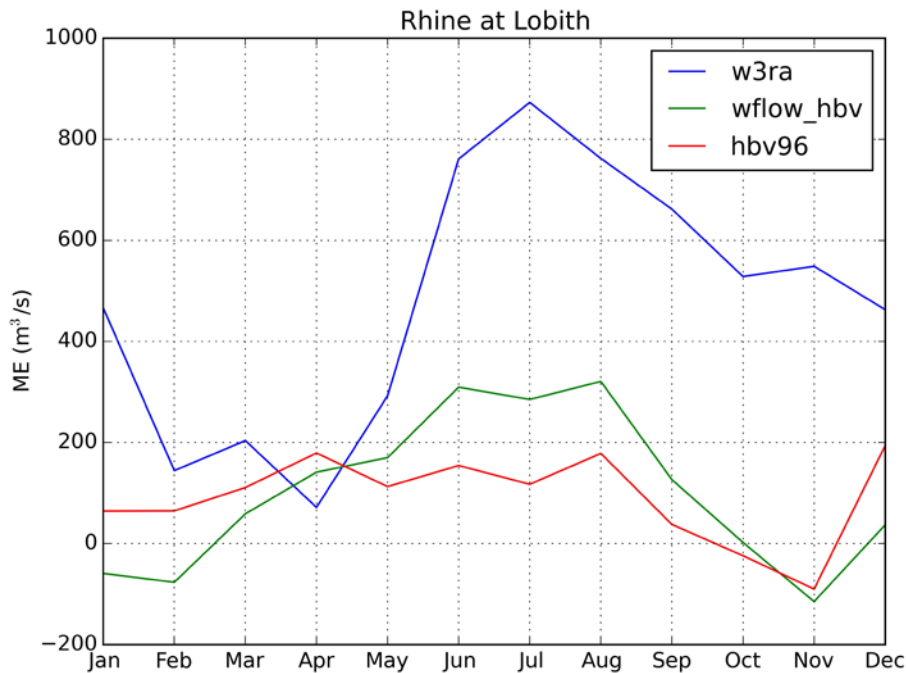


Figure 11 ME for the Rhine at Lobith (at lead time 0) for the W3RA (1991-2014), the lumped HBV96 and the distributed wflow\_hbv models (both for the period 1991-2006).

In terms of the reliability of the forecasts (i.e., CRPS reliability), the results are contrasted and vary from station to station. For the most western Central European Rivers stations, the CRPS reliability appears highly influenced by the forecast lead time as well as the event which is being forecasted. Figure 12 is an example of the CRPS reliability for the three systems for the Rhine at Koeln. For this station, the SMHI forecasts are less reliable from February-March and May at 1 month lead time. The ECMWF forecasts are less reliable from May-July and January. The BfG forecasts are less reliable from March-April.

For the most eastern Central European Rivers stations, the CRPS reliability, the ECMWF and the BfG forecasts display a better reliability than the SMHI forecasts, especially for December-April. Figure 13 is an example of the CRPS reliability for the three systems for the Elbe at Dresden.



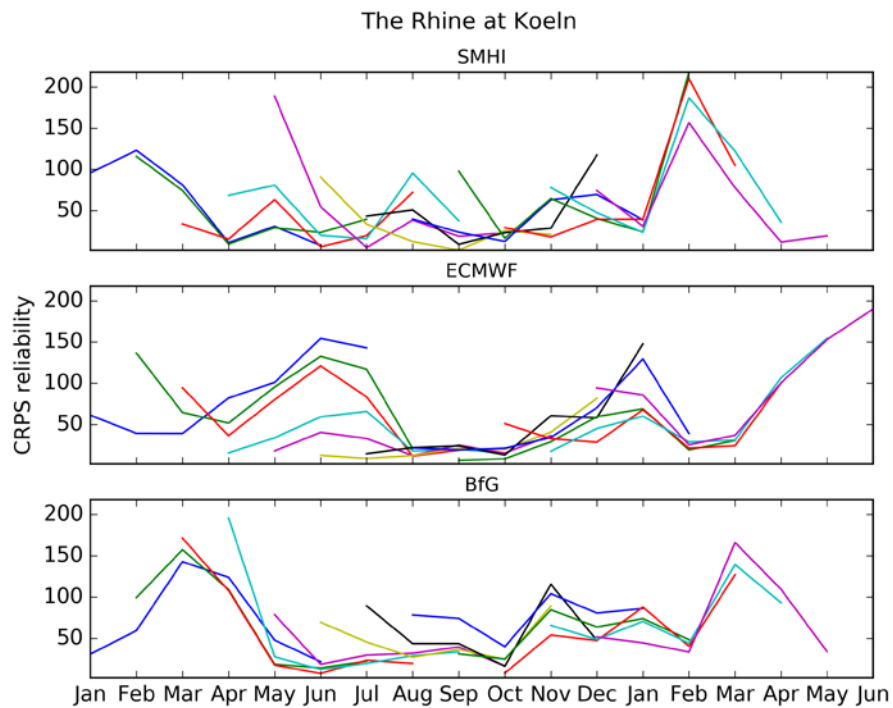


Figure 12 CRPS reliability for the Rhine at Koeln for (top) the SMHI forecasts, (middle) the ECMWF forecasts and (bottom) the BfG forecasts. CRPS reliability = 0 denotes a perfect forecast reliability. The CRPS reliability is given for each forecast initialisation date (on the first of each month, different colours) and for 6 months of lead time (for the SMHI and the BfG forecasts) or 7 months of lead time (for the ECMWF forecasts).



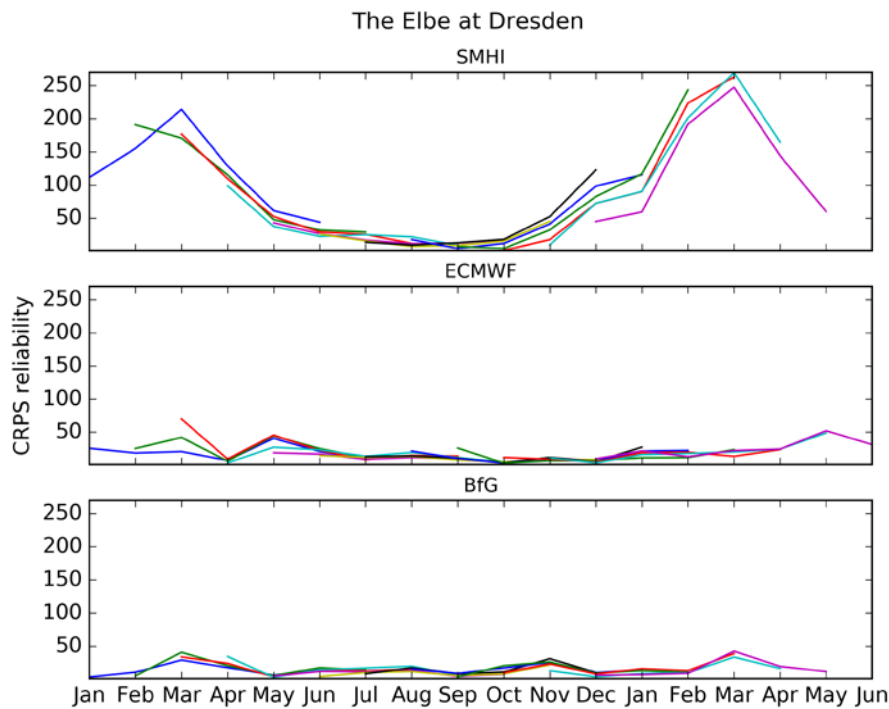


Figure 13 Same as Figure 12 but for the Elbe at Dresden.

If we look at the seasonal discharge forecasts skill, when compared to the observed discharge climatology (CRPSS\_CLI), it appears that the seasonal discharge forecasts produced by the three systems are more accurate and sharp than the observed discharge climatology for the first month to two months of lead time, depending on the station and the event forecasted. In some cases however, the seasonal discharge forecasts show a lower performance than the observed discharge climatology, for all lead times. In general, the ECMWF and the BfG forecasts are more skilful than the SMHI forecasts for the first month of lead time. Figures 14 and 15 are examples of the CRPSS\_CLI for the three systems for the Rhine at Koeln and the Elbe at Dresden, respectively.



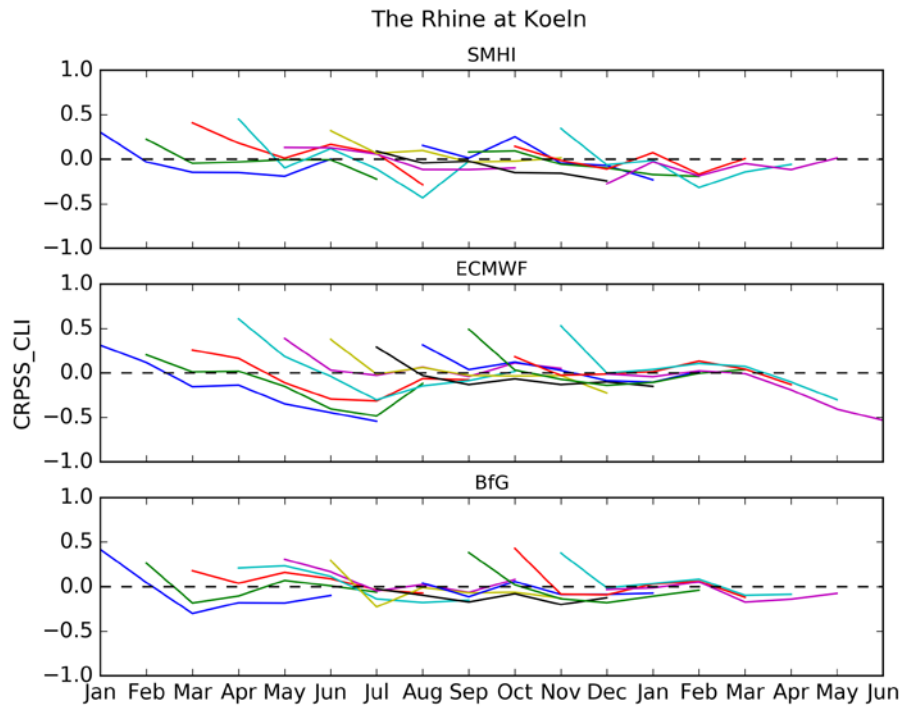


Figure 14 Continuous Ranked Probability Skill Score (CRPSS) of the seasonal discharge forecast against the observed discharge climatology for the Rhine at Koeln for (top) the SMHI forecasts, (middle) the ECMWF forecasts and (bottom) the BfG forecasts. CRPSS = 1 denotes a perfect forecast skill. The CRPSS is given for each forecast initialisation date (on the first of each month, different colours) and for 6 months of lead time (for the SMHI and the BfG forecasts) or 7 months of lead time (for the ECMWF forecasts).



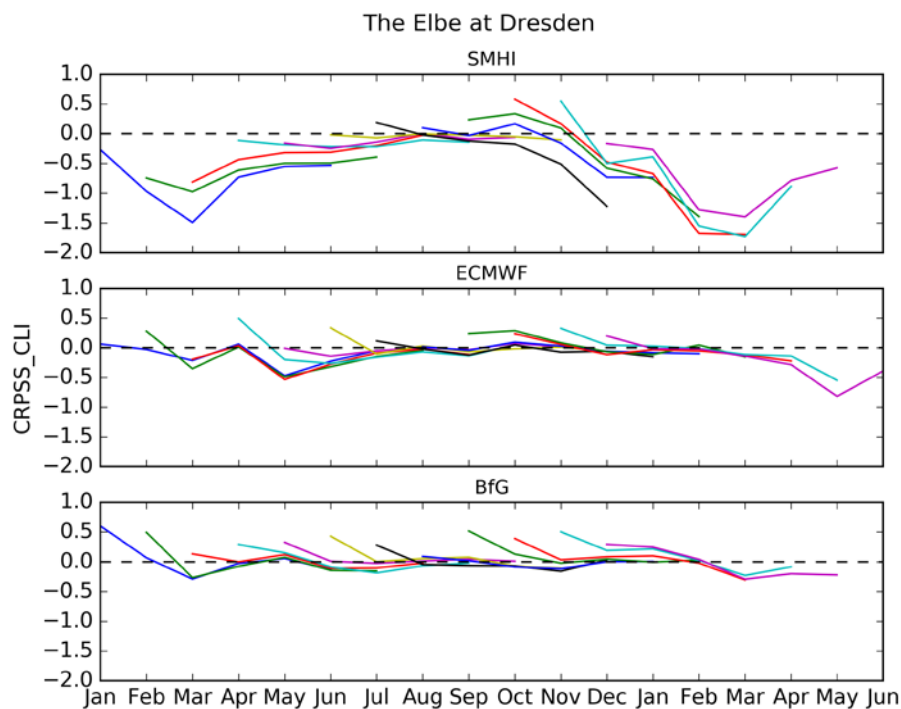


Figure 15 Same as Figure 14 but for the Elbe at Dresden.

For the upper and the lower terciles of the observed discharge, all forecasts show a very similar accuracy (Brier score of 0.2-0.3 on average over all lead times and all target seasons). There are however slight differences for single stations, for which the SMHI forecasts have a lower performance than the other forecasts for the summer target season for the lower tercile (BS33) and for the summer and the winter target season for the upper tercile (BS66; not shown).

#### 4.1.2 The Thames River Basin

For stations for the Thames River Basin case study, scores were calculated from the SMHI and the ECMWF forecasting systems. From this set of stations, there are several observable forecast performance behaviours. For several stations, both the SMHI and the ECMWF forecasts appear overall less accurate and sharp (in terms of the CRPS) from October-April. Figure 16 is an example of such a behaviour and shows the CRPS for the Thames at Royal Windsor Park for both systems.



For several other stations, the SMHI forecasts are less accurate and sharp than the ECMWF forecasts throughout the year, especially from November-April. This can be seen on Figure 17 of the CRPS for the Pang at Pangbourne for both systems.



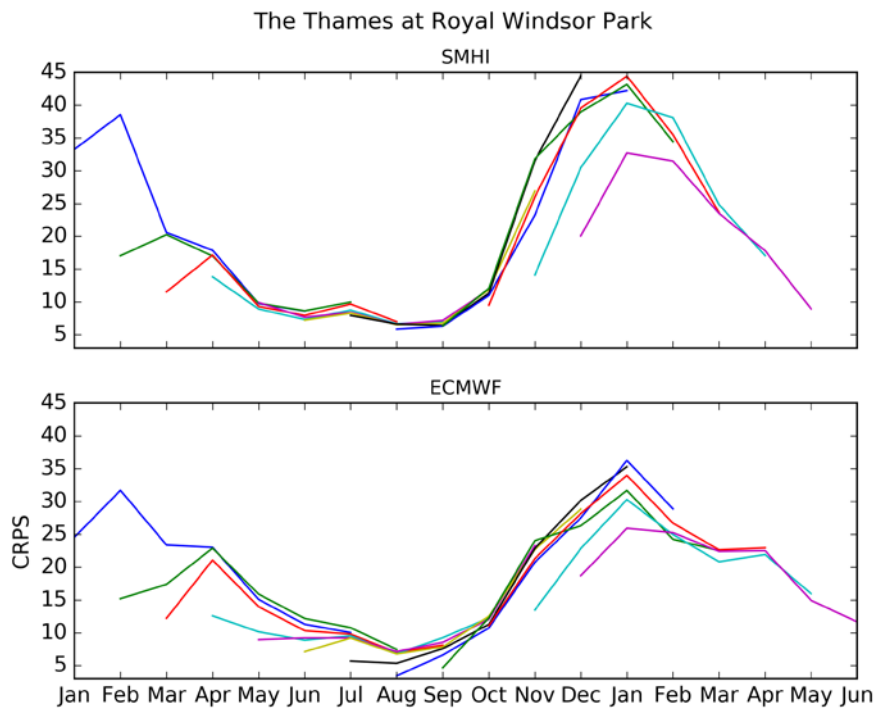


Figure 16 Same as Figure 4 but for the SMHI and the ECMWF forecasts only for the Thames at Royal Windsor Park.

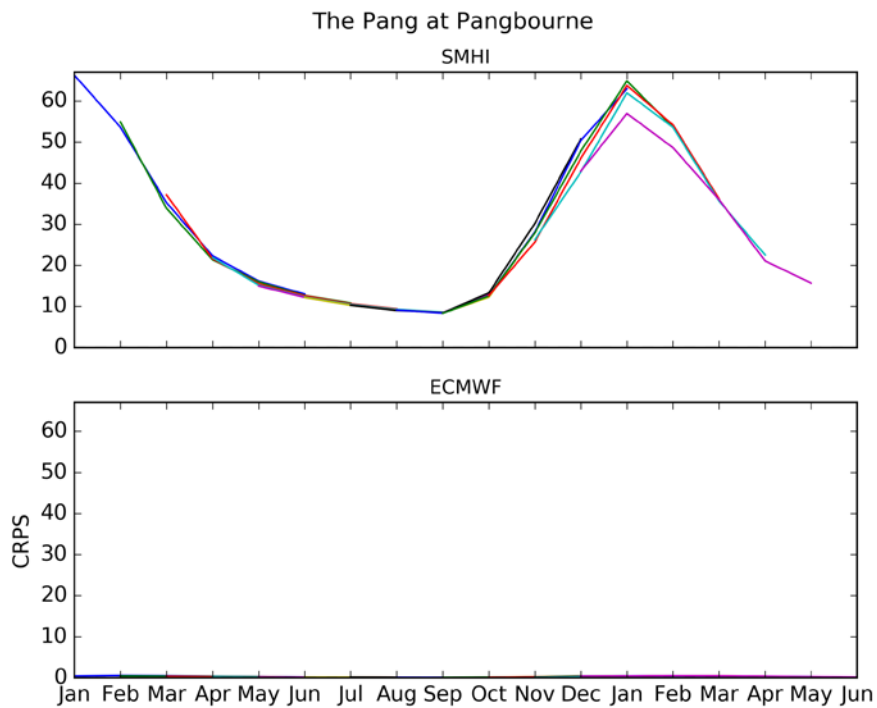


Figure 17 Same as Figure 4 but for the SMHI and the ECMWF forecasts only for the Pang at Panbourne.



In terms of the forecast bias (i.e., the ME) for both stations, the SMHI forecasts overestimate the November-March discharge (as seen for the Thames at Royal Windsor Park and the Pang at Pangbourne; Figures 18 and 19 respectively) and sometimes underestimate the April-May discharge (as seen for the Thames at Royal Windsor Park on Figure 18). A similar positive bias was described for stations of the Central European Rivers (Section 4.1.1) and could be here again due to a hydrological model error, where the model releases more water as river flow than is observed because it cannot store enough water as groundwater.

While there is almost no bias for the Pang at Pangbourne for the ECMWF forecasts (Figure 19), they underestimate the discharge from November-January and overestimate it more largely from February-June (increasingly with lead time) for the Thames at Royal Windsor Park (Figure 18). A similar bias pattern was observed for stations of the Central European Rivers and could be here again due to an overestimated percentage of precipitation falling as snow in the winter, leading to underestimated discharge in those months and a snowmelt compensation in spring.



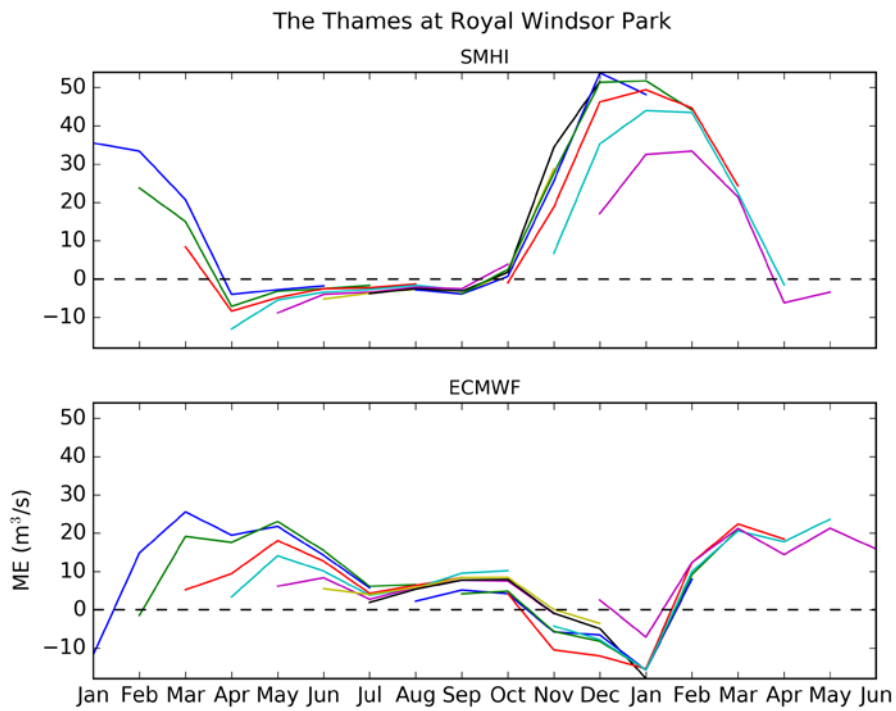


Figure 18 Same as Figure 8 but for the SMHI and the ECMWF forecasts only for the Thames at Royal Windsor Park.

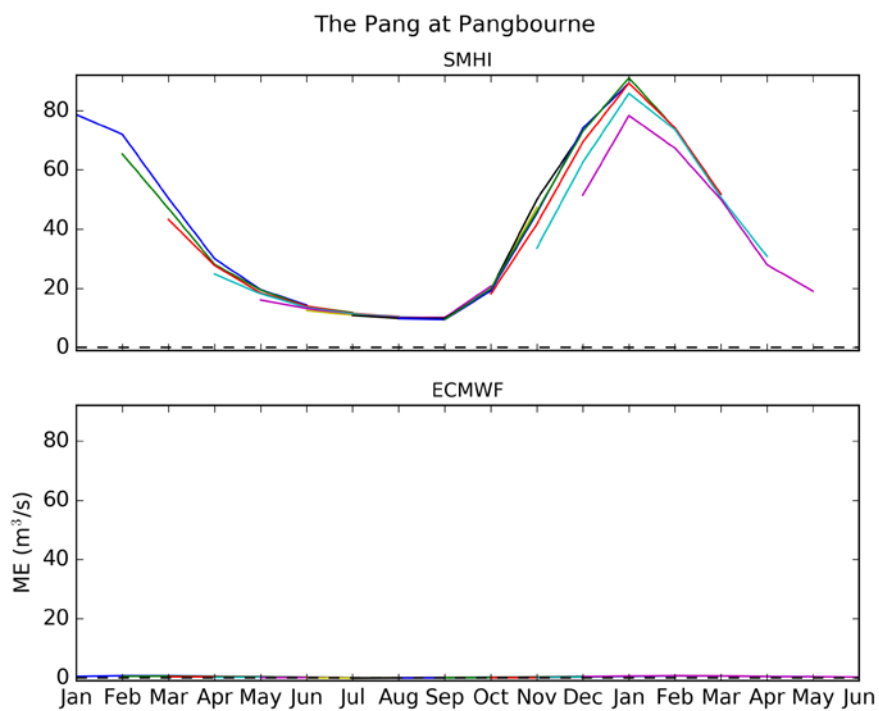


Figure 19 Same as Figure 8 but for the SMHI and the ECMWF forecasts only for the Pang at Panbourne.

In terms of reliability (i.e., CRPS reliability; see Figure 20 for an example at the Thames at Royal Windsor Park), the SMHI forecasts are overall less reliable than the ECMWF forecasts, especially for forecasts for the winter and the spring target months. The ECMWF forecasts are sometimes less reliable than the SMHI forecasts for the late summer or for the winter target months for a few stations. For both systems, the forecasts sometimes become more reliable with lead time, for a forecast made for the winter target months, which is a counter-intuitive behaviour.

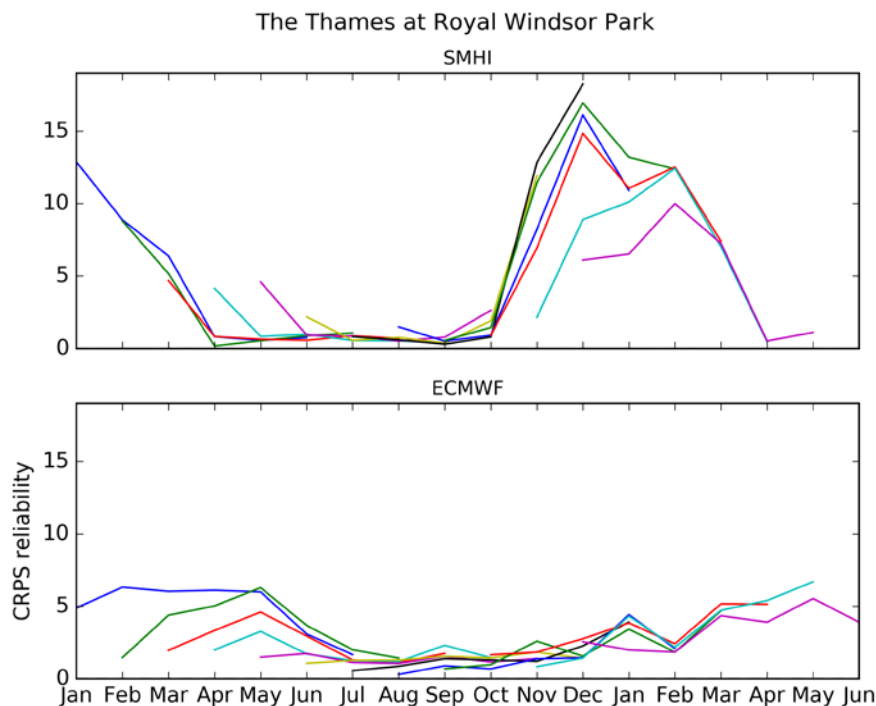


Figure 20 Same as Figure 12 but for the SMHI and the ECMWF forecasts only for the Thames at Royal Windsor Park.

In terms of the seasonal discharge forecasts skill, when compared to the observed discharge climatology (i.e., CRPSS\_CLI), for several stations the SMHI and the ECMWF seasonal discharge forecasts exhibit a positive skill for the first month of lead time, which then





decreases with increasing lead time. This can be observed on Figure 21 of the CRPSS\_CLI for the Thames at Royal Windsor Park for the SMHI and the ECMWF forecasts. The speed of decrease of the skill for both systems depends on the station and the event forecasted and can be negative for one month of lead time in some cases (not shown). For the Thames at Royal Windsor Park, the skill of the SMHI forecasts decreases the most from November-February, while the skill of the ECMWF forecasts decreases the most from March-July.

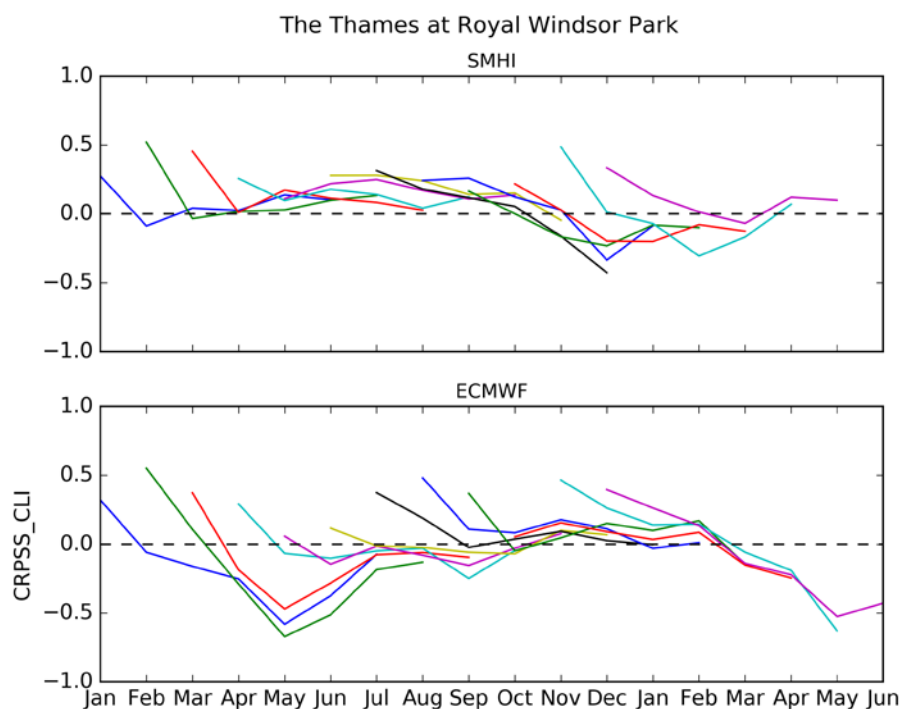


Figure 21 Same as Figure 14 but for the SMHI and the ECMWF forecasts only for the Thames at Royal Windsor Park.

The forecasts' accuracy for the lower and the upper terciles of the observed discharge is variable depending on the station and the target season. In general however, both the SMHI and the ECMWF forecasts show a similar accuracy (Brier score of 0.2 on average over all lead times and all target seasons). For several stations, the SMHI forecasts have a worst BS33 and BS66 for all target seasons and all lead times. However, the ECMWF forecasts are less accurate than the SMHI forecasts for the upper tercile for JJA and MAM target months for a few stations (not shown).



### 4.1.3 The Segura and Tagus River Basins

For stations of the Segura and Tagus River Basins, scores were calculated from the SMHI, the ECMWF and FW forecasting systems. From this set of stations, the SMHI forecasts are on average less accurate and sharp than the two other forecasting systems, especially for forecasts made for the winter and the spring. The ECMWF forecasts appear more accurate and sharp for forecasts made for the summer for all stations shared for this river basin. See Figure 22 as an example for the Tagus at Entrepenas.



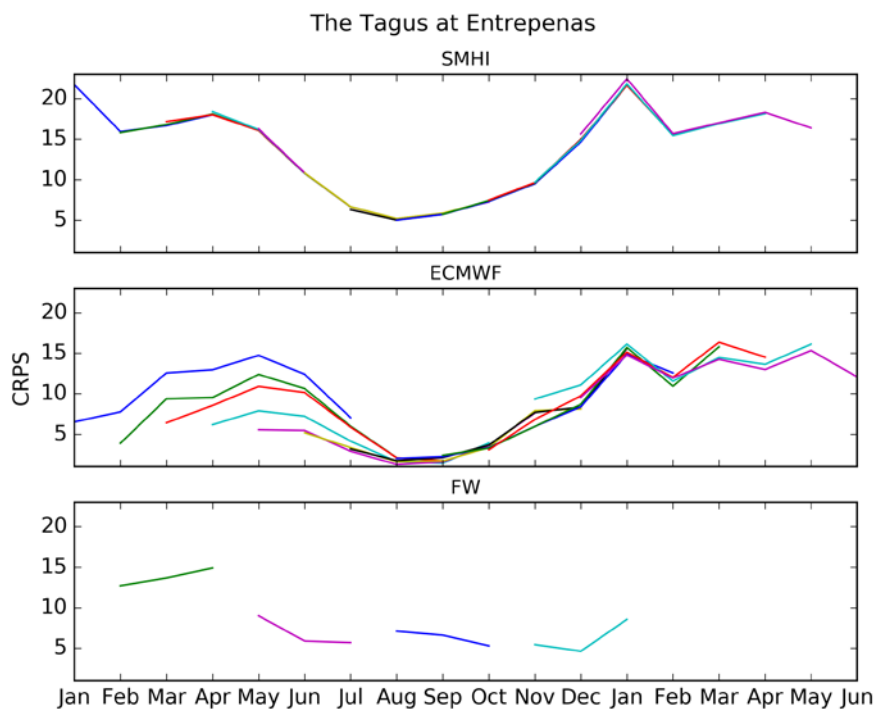


Figure 22 CRPS for the Tagus at Entrepenas for (top) the SMHI forecasts, (middle) the ECMWF forecasts and (bottom) the FW forecasts. The CRPS is given for each forecast initialisation date (on the first of each month for the SMHI and ECMWF forecasts and on the first of January, April, July and October for the FW forecasts; different colours) and for 6 months of lead time (for the SMHI forecasts), 7 months of lead time (for the ECMWF forecasts) or 3 months of lead time (for the FW forecasts).

Figures 23 and 24 show the forecast biases (i.e., the ME) for the Tagus at Entrepenas and the Segura at Cenajo, respectively. For these stations, the SMHI forecasts either underestimate or overestimate the observed discharge, more largely for the spring and the winter. The ECMWF forecasts have large biases for the winter and the spring as well, either positive or negative depending on the station. The summer biases are however the closest to zero for the ECMWF forecasts. The FW forecasts display large positive biases from February-April for the two stations on the Tagus River (see Figure 23 as an example for the Tagus at Entrepenas) and small negative biases throughout the whole year for the two stations on the Segura River (see Figure 24 as an example for the Segura at Cenajo).



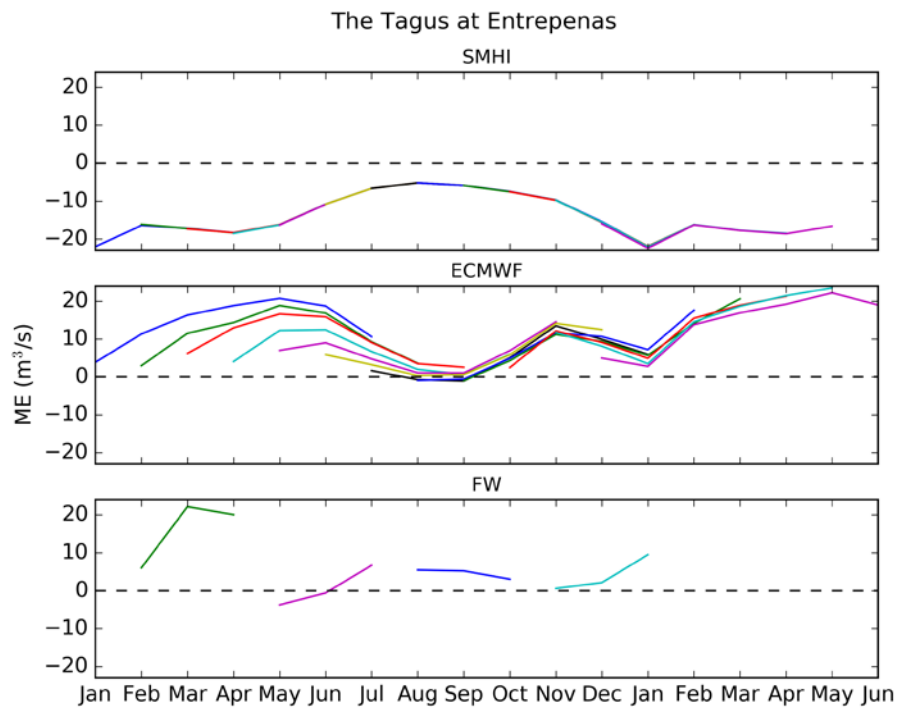


Figure 23 ME for the Tagus at Entrepenas for (top) the SMHI forecasts, (middle) the ECMWF forecasts and (bottom) the FW forecasts. The ME is given for each forecast initialisation date (on the first of each month for the SMHI and ECMWF forecasts and on the first of January, April, July and October for the FW forecasts; different colours) and for 6 months of lead time (for the SMHI forecasts), 7 months of lead time (for the ECMWF forecasts) or 3 months of lead time (for the FW forecasts).



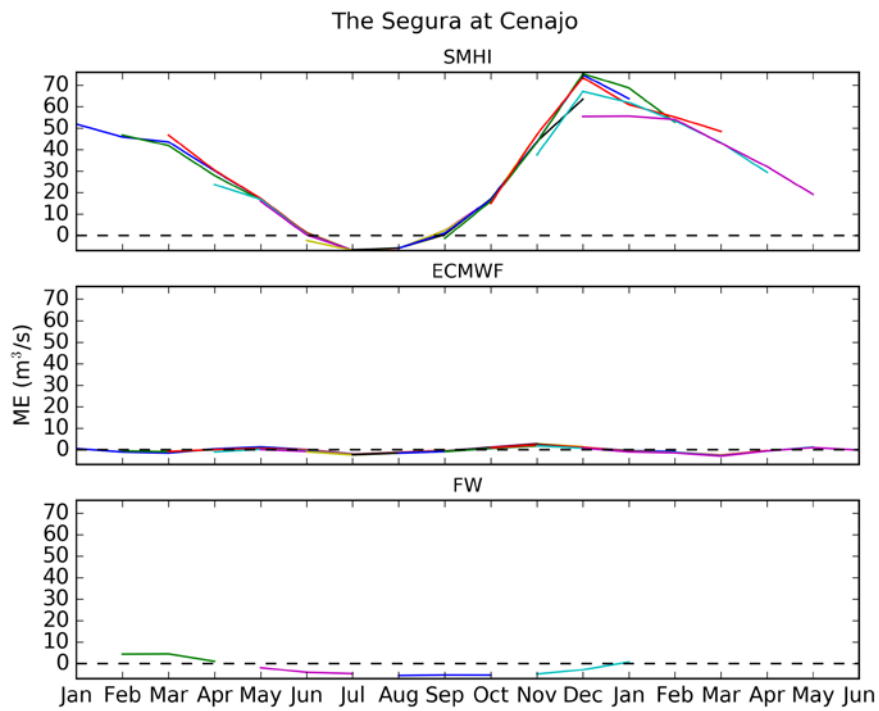


Figure 24 Same as Figure 23 but for the Segura at Cenajo.

The SMHI appears less reliable than the two other forecasts for all stations of the Segura and Tagus River Basins, especially for the winter and the spring (see Figure 25 as an example for the Tagus at Entrepenas).



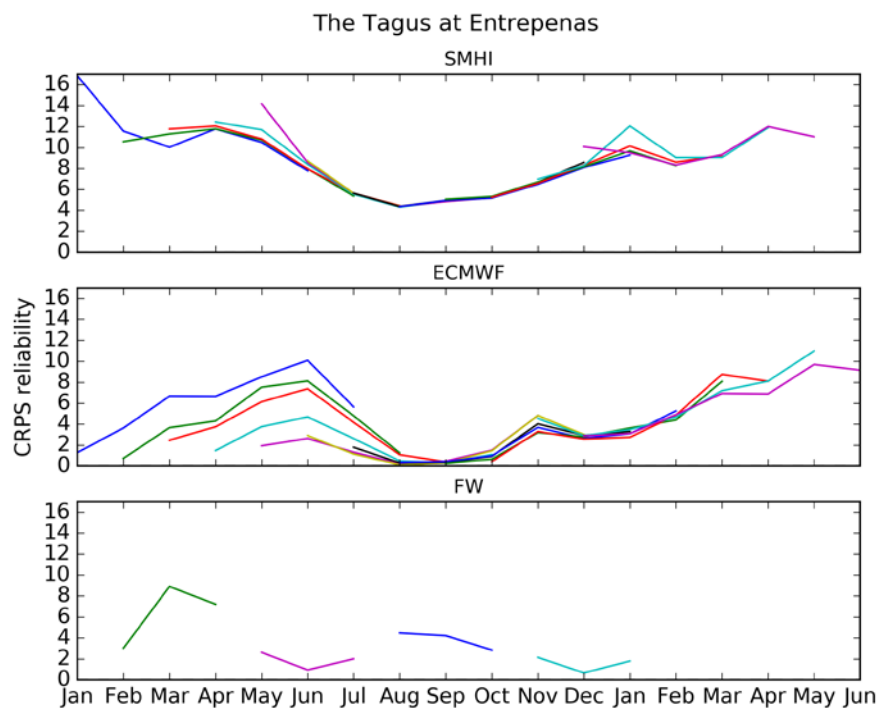


Figure 25 CRPS reliability for the Tagus at Entrepenas for (top) the SMHI forecasts, (middle) the ECMWF forecasts and (bottom) the FW forecasts. The CRPS reliability is given for each forecast initialisation date (on the first of each month for the SMHI and ECMWF forecasts and on the first of January, April, July and October for the FW forecasts; different colours) and for 6 months of lead time (for the SMHI forecasts), 7 months of lead time (for the ECMWF forecasts) or 3 months of lead time (for the FW forecasts).

In terms of the seasonal discharge forecasts skill, when compared to the observed discharge climatology (i.e., the CRPSS\_CLI), the SMHI, ECMWF and FW forecasts appear less skilful for the summer. The SMHI forecasts are also less skilful than the ECMWF and the FW forecasts. Both of these results can be seen on Figure 26 of the CRPSS\_CLI for the Tagus at Entrepenas.



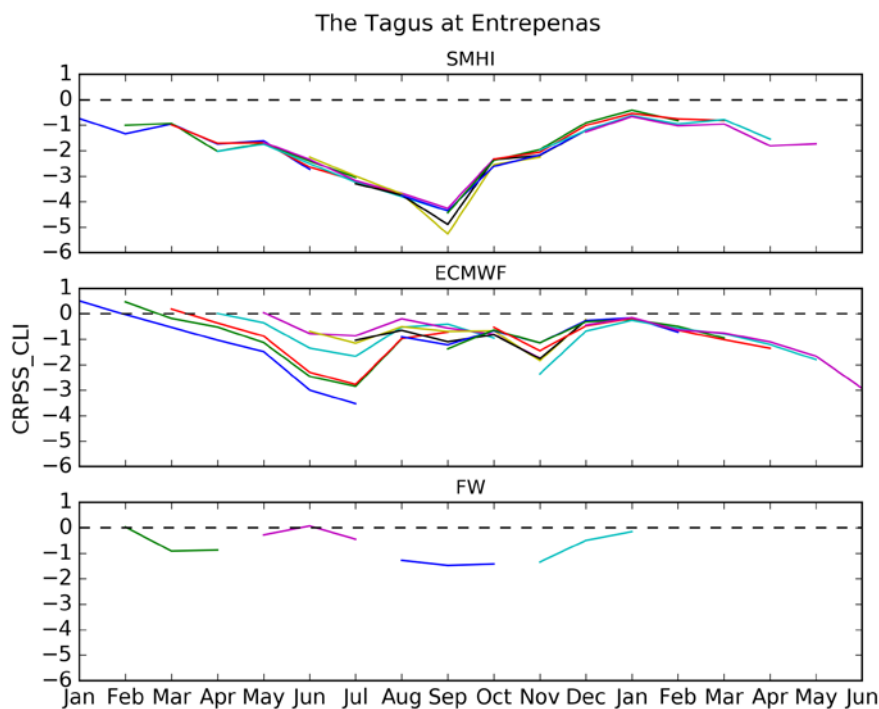


Figure 26 CRPSS of the seasonal discharge forecast against the observed discharge climatology for the Tagus at Entrepénas for (top) the SMHI forecasts, (middle) the ECMWF forecasts and (bottom) the FW forecasts. The CRPSS is given for each forecast initialisation date (on the first of each month for the SMHI and ECMWF forecasts and on the first of January, April, July and October for the FW forecasts; different colours) and for 6 months of lead time (for the SMHI forecasts), 7 months of lead time (for the ECMWF forecasts) or 3 months of lead time (for the FW forecasts).

#### 4.1.4 The Jucar River Basin

The analysis that will be performed in following sectoral work packages (i.e., WP8-Hydroelectricity and WP11-Agriculture), as well as in WP13-Sectoral integration, must be performed using the entire river basin domain, and integrating all the relevant elements of the water resources system. This requires producing forecasts for streamflows in several sites. The reliability of the forecasts and the statistical consistency for time correlations and cross correlation between sites are crucial factors to foster the use of the forecasts in real management of the water resources system. Otherwise, the impacts of droughts would be underestimated.



Since the Jucar River Basin is strongly anthropized, all forecasts and comparisons must be done in terms of natural flows (i.e., flows that would happen if man would not produce changes due to storage and releases from reservoirs, pumping from aquifers, and diversion and return flows from consumptive uses). Natural flows provide a consistent baseline in order to compare the performance of different programmes of measures in planning and management of the basin.

Therefore, we performed a comparison between E-HYPE results and the historical data in five different points or sub-basins of the Jucar River Basin. Four of them are inflows to the main reservoirs (Alarcon, Contreras, Molinar, Tous) and the fifth is located in Sueca, at the lower part of the basin. All of these stations are crucial from the point of view of water management.

In Figure 27, the comparison between the average monthly flows in the five mentioned locations produced by the SMHI-E-HYPE model and the historical re-naturalized flows at the same locations is depicted. As it can be seen, flows produced by E-HYPE in all sites are almost zero in the summer, while the historical values are much higher. This can be explained by the important natural regulation due to aquifers upstream and in the middle section of the basin. It seems that the E-HYPE model is not able to capture this important characteristic of the basin.

On the same figure, the average monthly flows produced by the hydrological model EVALHID, which is currently used by the UPV for the Jucar River Basin, are also depicted. Flows in the summer produced by the EVALHID model are much closer to the historical values for all stations.



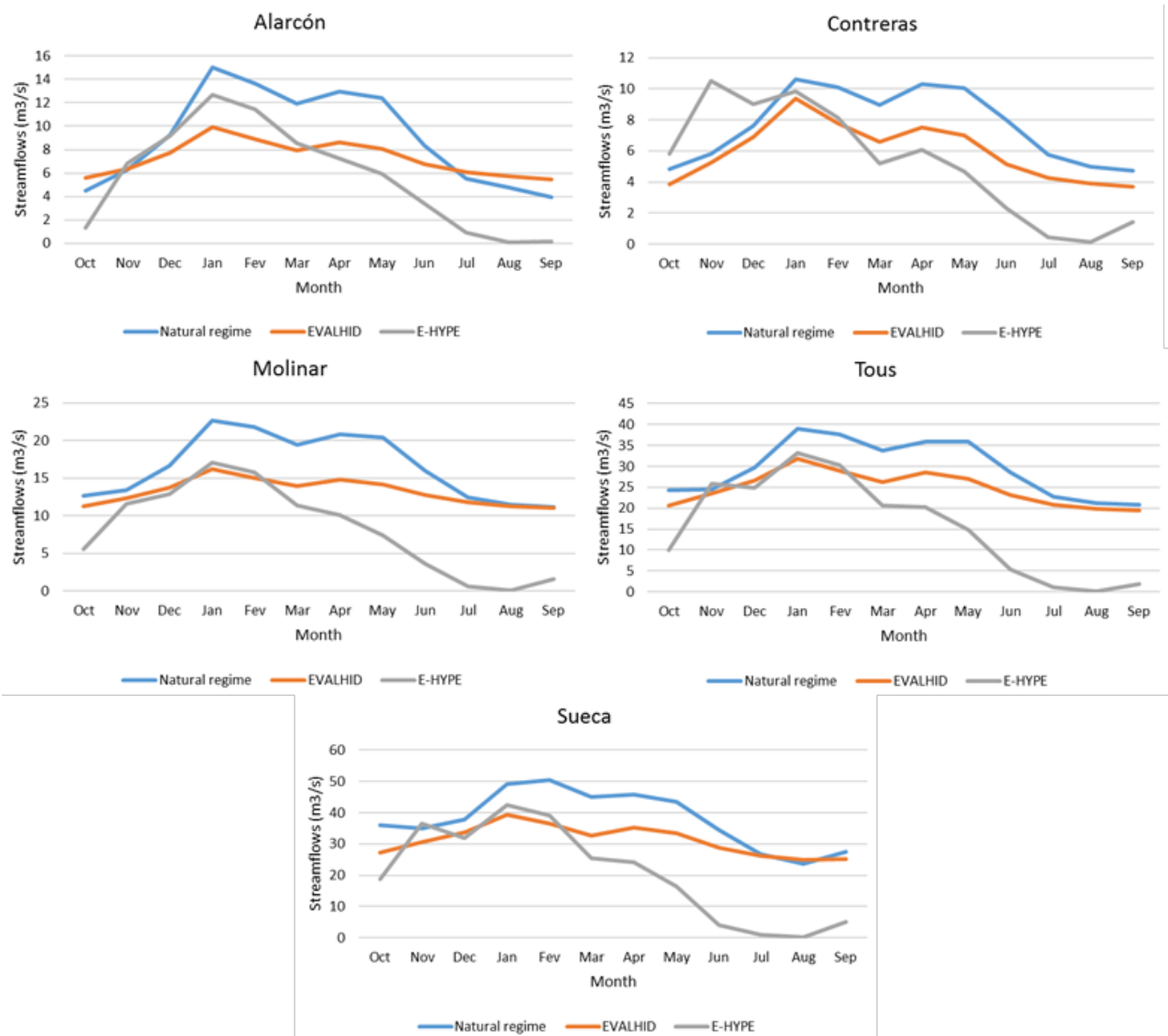


Figure 27 Comparison between streamflows from SMHI Pan-European data (E-HYPE), historical data as naturalized river flows and data from our hydrological model (EVALHID) in the five main sub-basins of Júcar River Basin: Alarcón, Contreras, Molinar, Tous and Sueca.

This essential mismatch between the E-HYPE results and observed values cannot be overcome by any bias correction, since in the summer months rainfall is almost negligible. This is only feasible by means of a conceptual modification of the model and recalibration in order to capture the real behaviour of the basin by the model. This will be discussed in the following months of the IMPREX project.



For this deliverable, forecasts produced by the EVALHID hydrological model forced with ECMWF meteorological data as input (i.e., precipitation and mean temperature) is compared to the ECMWF forecasts.

Figure 28 displays the CRPS obtained from the UPV forecasts for all five stations of the Jucar River Basin. From this figure, it appears that the forecast performance varies depending on the selected station, but the forecasts are on average more accurate and sharp in the spring and summer. The largest errors can be found in the winter months.

Figure 29 displays the CRPS for the ECMWF forecasts for the Jucar at Alarcon and at Tous. Results for these stations show a different behaviour of the ECMWF forecasts. For the Jucar at Alarcon, the largest errors are observed for the winter, similarly to what was observed for the UPV forecasts. For the Jucar at Tous however, the largest errors are situated in the summer.



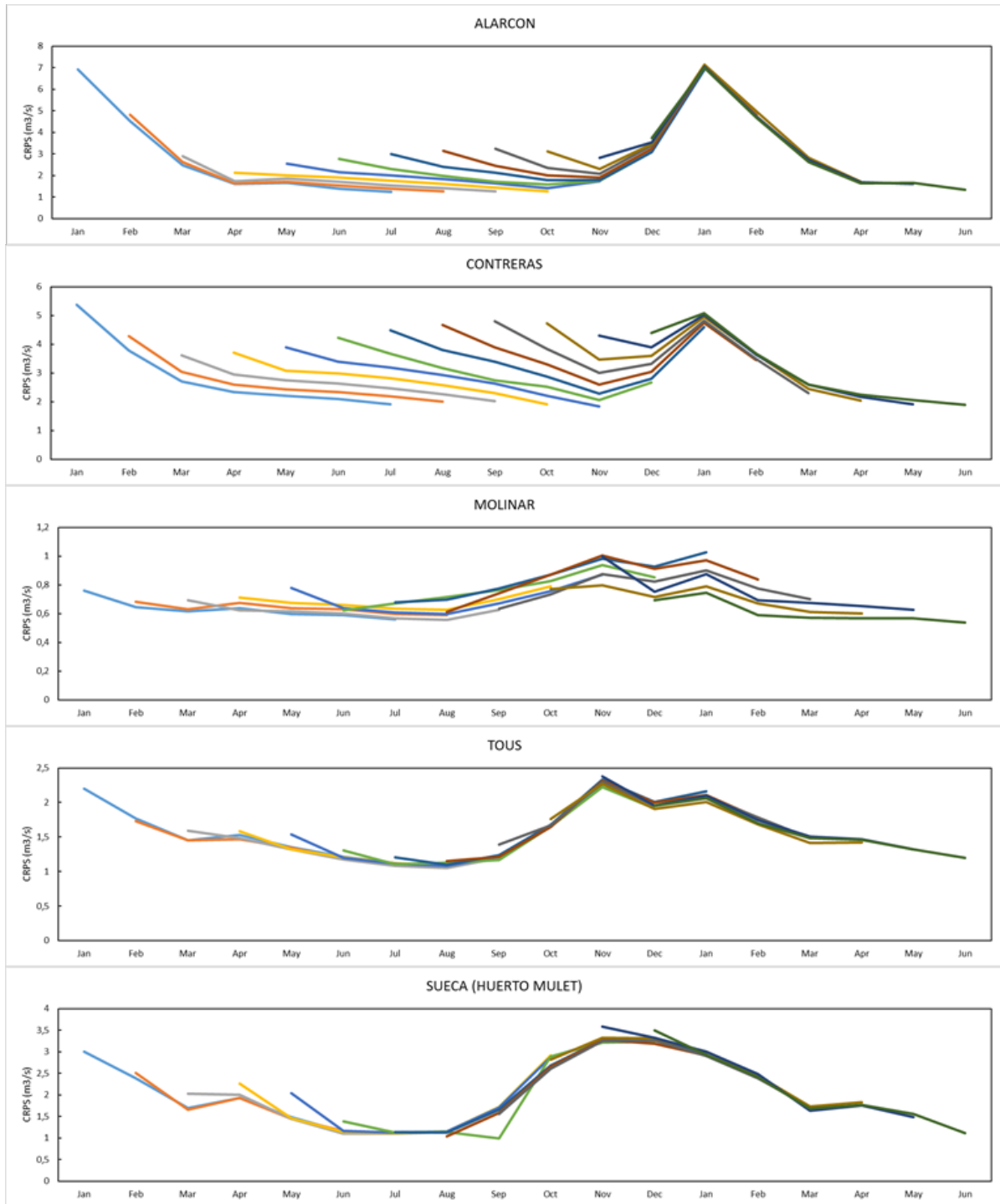
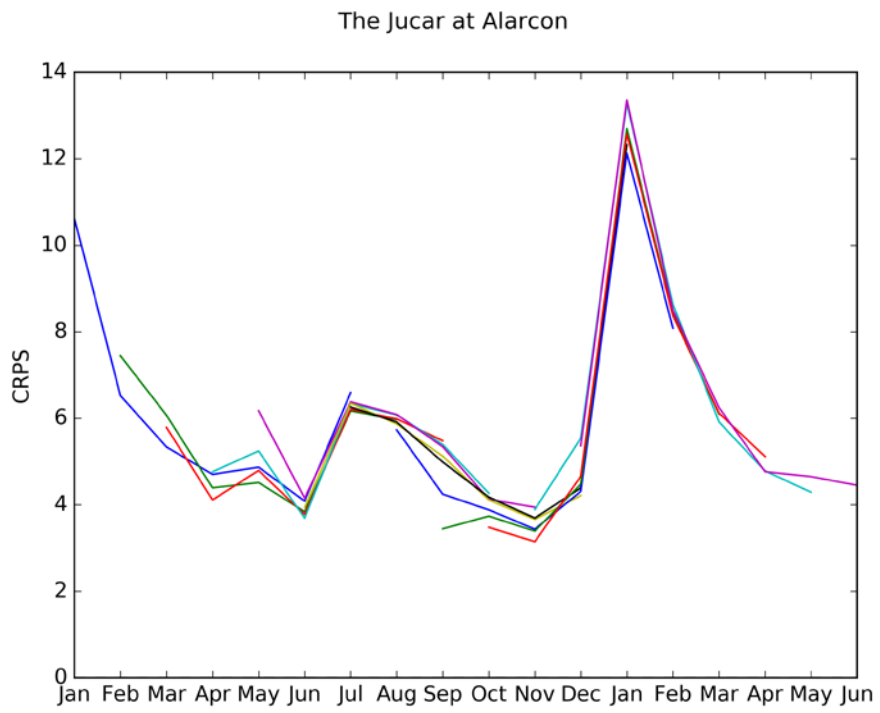


Figure 28 CRPS for the Jucar River at Alarcon, Contreras, Molinar, Tous and Sueca for the UPV forecasts. The CRPS is given for each forecast initialisation date (on the first of each month, different colours) and for 7 months of lead time.





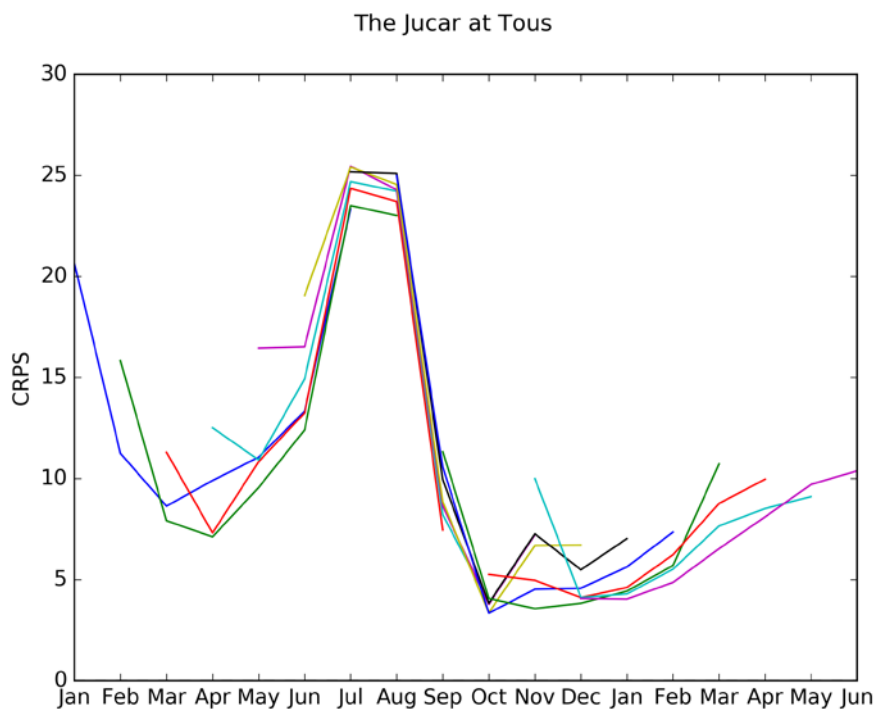


Figure 29 CRPS for (top) the Jucar at Alarcon and (bottom) the Jucar at Tous for the ECMWF forecasts. The CRPS is given for each forecast initialisation date (on the first of each month, different colours) and for 7 months of lead time.

Regarding to the UPV forecasts biases, different behaviours can be seen depending on the selected station (see Figure 30). For the Alarcon and Contreras stations, bias is positive all year except for January when it reaches negative values. This could be due to the fact that those two stations are situated in the mountainous headwaters of the river, where the faster discharge generating processes are likely misrepresented by the model and/or the precipitation is underestimated for this time of the year at those stations. The Molinar and Sueca stations display a slight positive bias all year long, while the Tous presents a negative bias all year.

For the ECMWF forecasts (see Figure 31), the biases are similar to the UPV forecasts biases for the Jucar at Alarcon, which could be due to the same model misrepresentation and/or precipitation underestimation. For the Jucar at Tous, the ECMWF forecasts present slightly different and much larger biases than the UPV forecasts, with negative biases in the summer and positive biases the rest of the year. This hints towards an underestimation of the groundwater discharge by the ECMWF forecasts for this station.



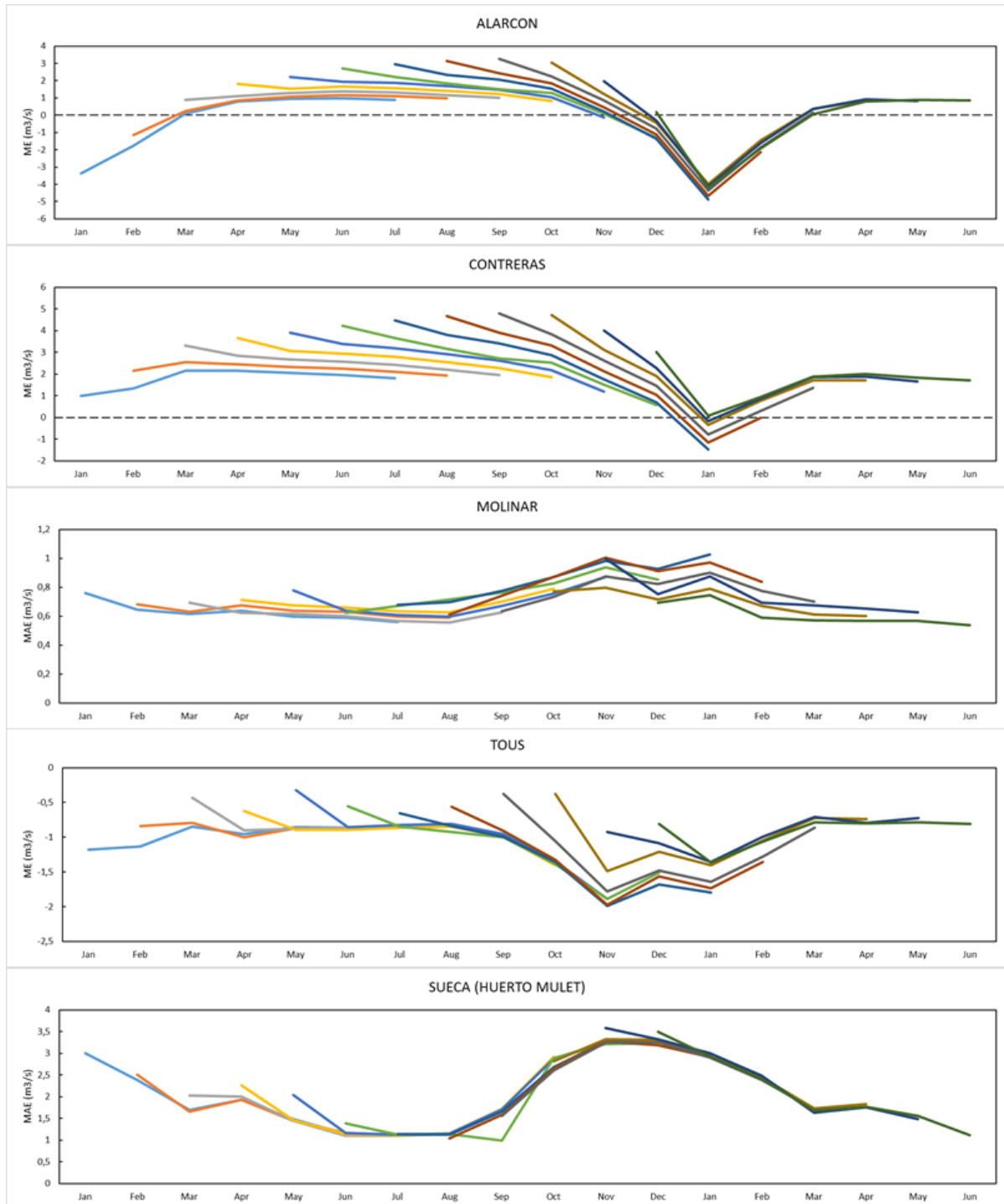
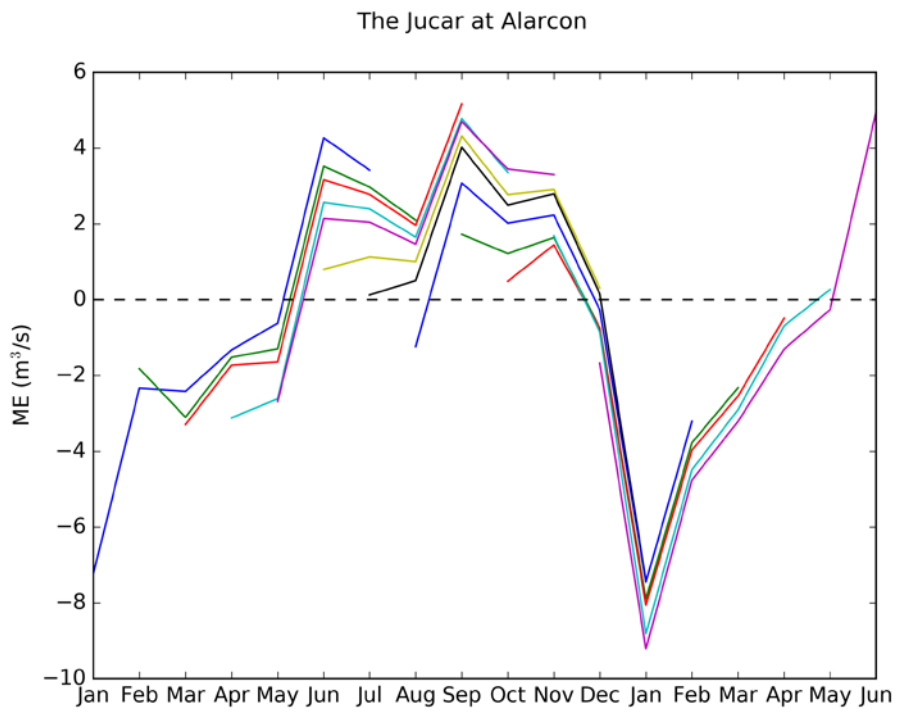


Figure 30 ME for the Jucar River at Alarcon, Contreras, Molinar, Tous and Sueca for the UPV forecasts. The ME is given for each forecast initialisation date (on the first of each month, different colours) and for 7 months of lead time.





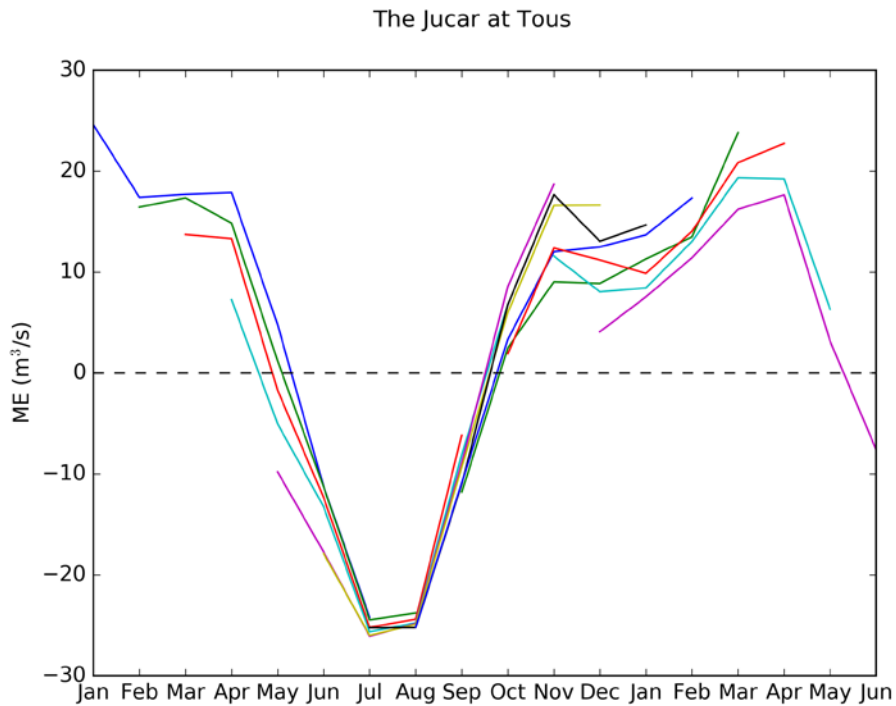


Figure 31 ME for the Jucar River at Alarcon and Tous for the ECMWF forecasts. The ME is given for each forecast initialisation date (on the first of each month, different colours) and for 7 months of lead time.

#### 4.1.5 Swedish Rivers

For stations on the Swedish Rivers, scores were calculated from the SMHI and the ECMWF forecasting systems. From this set of stations, the SMHI and the ECMWF forecasts appear equally accurate and sharp, with larger errors from May-September for all four stations shared. This can be seen on Figure 32, which displays the CRPS for the Vindelaelven at Granaker for both systems.



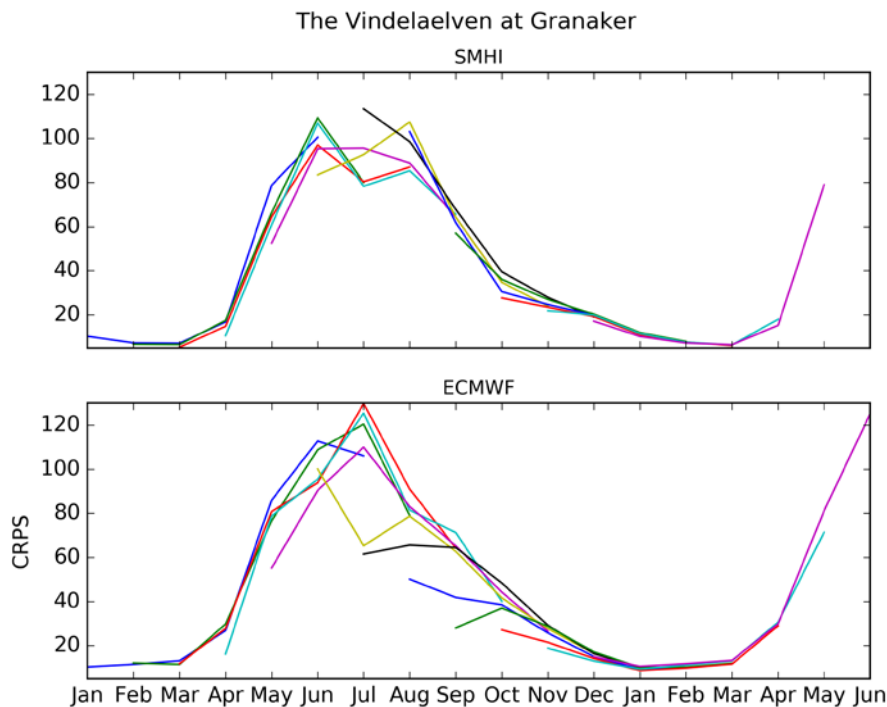


Figure 32 Same as Figure 16 but for the Vindelaelven at Granaker.

Figure 33 displays the bias (i.e., the ME) for the Vindelaelven at Granaker for both systems. On this figure, the SMHI forecasts appear to underestimate both May and July-September observed discharges, while they overestimate the June observed discharge. The ECMWF forecasts underestimate the May observed discharge and overestimate largely the June-August observed discharge. This last characteristic of the ECMWF forecasts is however only seen for forecasts made in May or earlier. For forecasts made in June or after, the June-August observed discharge is underestimated.

These behaviours of the SMHI and the ECMWF forecasts were observed for the other shared stations for Swedish Rivers. For the SMHI forecasts, this could be due to a large underestimation of groundwater storage and recharge in the winter, subsequently leading to underestimated flows in the summer. For the ECMWF forecasts, the biases could be due to a delayed snowmelt process in the model, either due to model errors or to biased seasonal temperature forecasts input into the model.



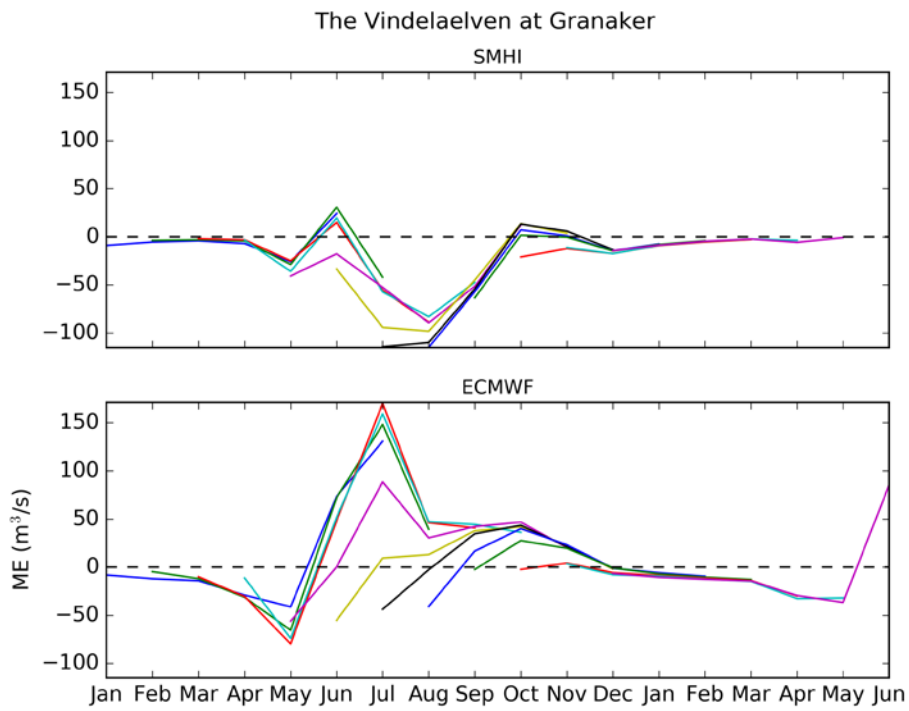


Figure 33 Same as Figure 18 but for the Vindelaelven at Granaker.

For both systems, the reliability is the worst during from June-August (see Figure 34), approximately when the largest CRPS errors were observed (see Figure 32).



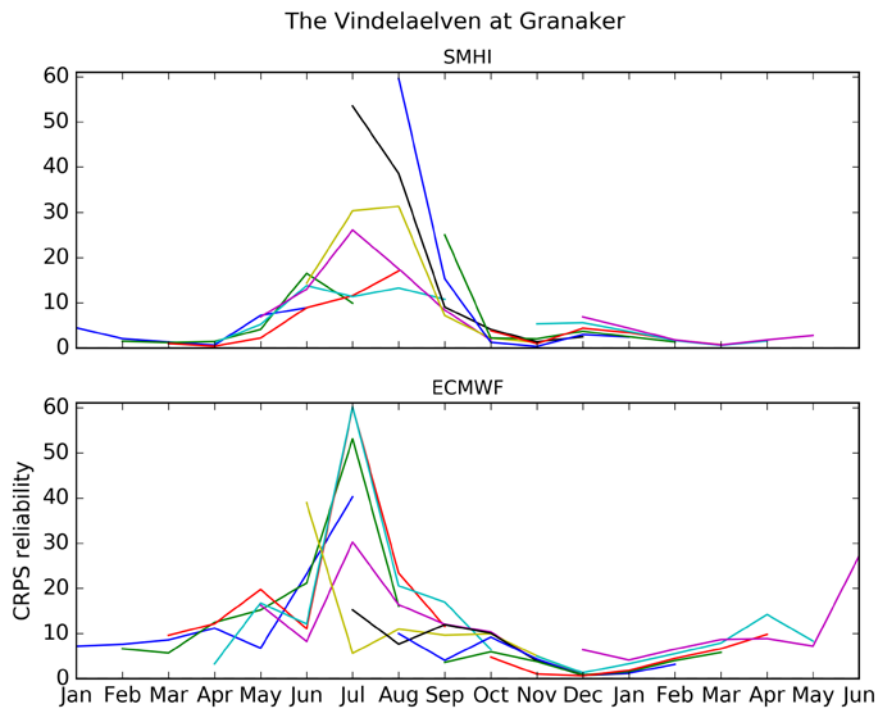


Figure 34 Same as Figure 20 but for the Vindelaelven at Granaker.

In terms of the seasonal discharge forecasts skill, when compared to the observed discharge climatology (i.e., the CRPSS\_CLI), the ECMWF forecasts appear less skilful from February-April and in July (see Figure 35 as an example of this general behaviour for the Vindelaelven at Granaker). The skill of the SMHI forecasts depends given the station looked at, but they are generally more skilful than the ECMWF forecasts.



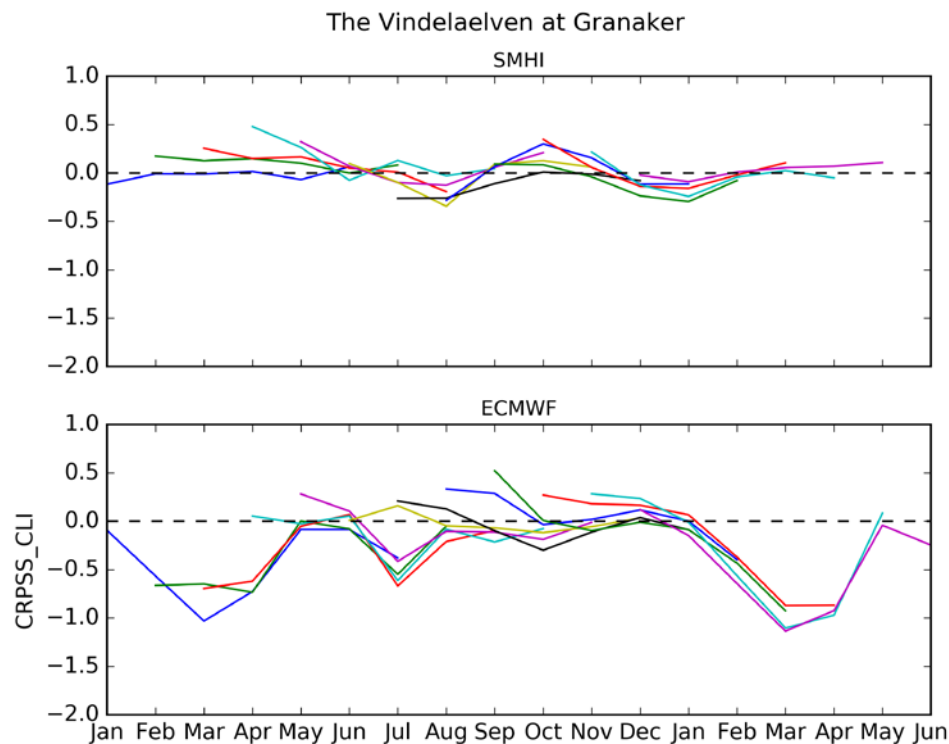


Figure 35 Same as Figure 21 but for the Vindelaelven at Granaker.

The forecasts' accuracy for the lower and the upper terciles of the observed discharge is variable depending on the station and the target season. In general however, both the SMHI and the ECMWF forecasts show a similar accuracy (Brier score of 0.2-0.3 on average over all lead times and all target seasons). For several stations, the ECMWF forecasts have a worst BS33 for DJF for all lead times (not shown). Both systems exhibit a very good accuracy (BS66 close to 0) for the upper tercile for forecasts made for MAM at all lead times (not shown).

#### 4.2 The EPB sensitivity analysis

Figure 36 shows maps of the dominant predictability source (IHC or SCF), the predictability source for which the skill elasticity is highest and which could therefore lead to higher seasonal discharge forecast skill after being improved. The skill elasticities were derived from forecasts produced by the ECMWF seasonal hydrological forecasting system, using the CRPSS calculated against the observed climatology. The results are shown for 74 regions





across Europe, as these regions are the same as the ones used for the seasonal outlook in EFAS. The maps were made for each forecast initialisation date (on the first of each month; each row) and for seven months of lead time. However, only the first three months of lead time (each column) are shown here as the impact of initialisation tends to disappear for lead times exceeding 3 months for most regions in Europe.

From the maps one can see that on average, for the first month of lead time, improving the IHC would lead to a higher discharge forecasting skill. As lead time increases, the relative importance of IHC to SCF decreases and improving the SCF becomes more important to improve the discharge forecasting skill. There are however temporal and spatial variabilities.

For the first month of lead time, the density of regions for which the IHC are relatively more important than the SCF is higher for forecasts starting from May to July, with the largest density in June. This is probably because from May to July, rainfall is low in most parts of Europe, leading to groundwater dominated discharges for most European basins.

For most regions in Scandinavia, the IHC appear to dominate the uncertainty for forecasts started in the winter, with a signal that persists until three months of lead time (and further, not shown). This is maybe due to precipitation falling as snow during those months in these regions, leading to a more groundwater based discharge. Furthermore, a good knowledge of the antecedent snow content will lead to a high skill in spring, when discharge is snowmelt driven in those regions. This is however not the case for windward Scandinavia, where the discharge is mostly sensitive to the SCF. This could be due to weather systems raining out on Scandinavia's western part, leading to a rainfall dominated discharge. Moreover, the ground memory is very low in this part of Scandinavia.

Over the Iberian Peninsula, the IHC dominate the uncertainty for forecast generated in summer (June to September), a signal which persists until three months of lead time. The reason for this pattern is the very dry climate over the Iberian Peninsula during the summer months, leading to a mainly groundwater dominated discharge with long memory over several months.

In central Europe, the eastern side appears to be more IHC dependent for the first month of lead time than the western part. This is probably mostly due to weather systems raining out on central Europe's west coast. The IHC importance in Eastern central Europe could also be due to snowmelt drive discharge in spring.



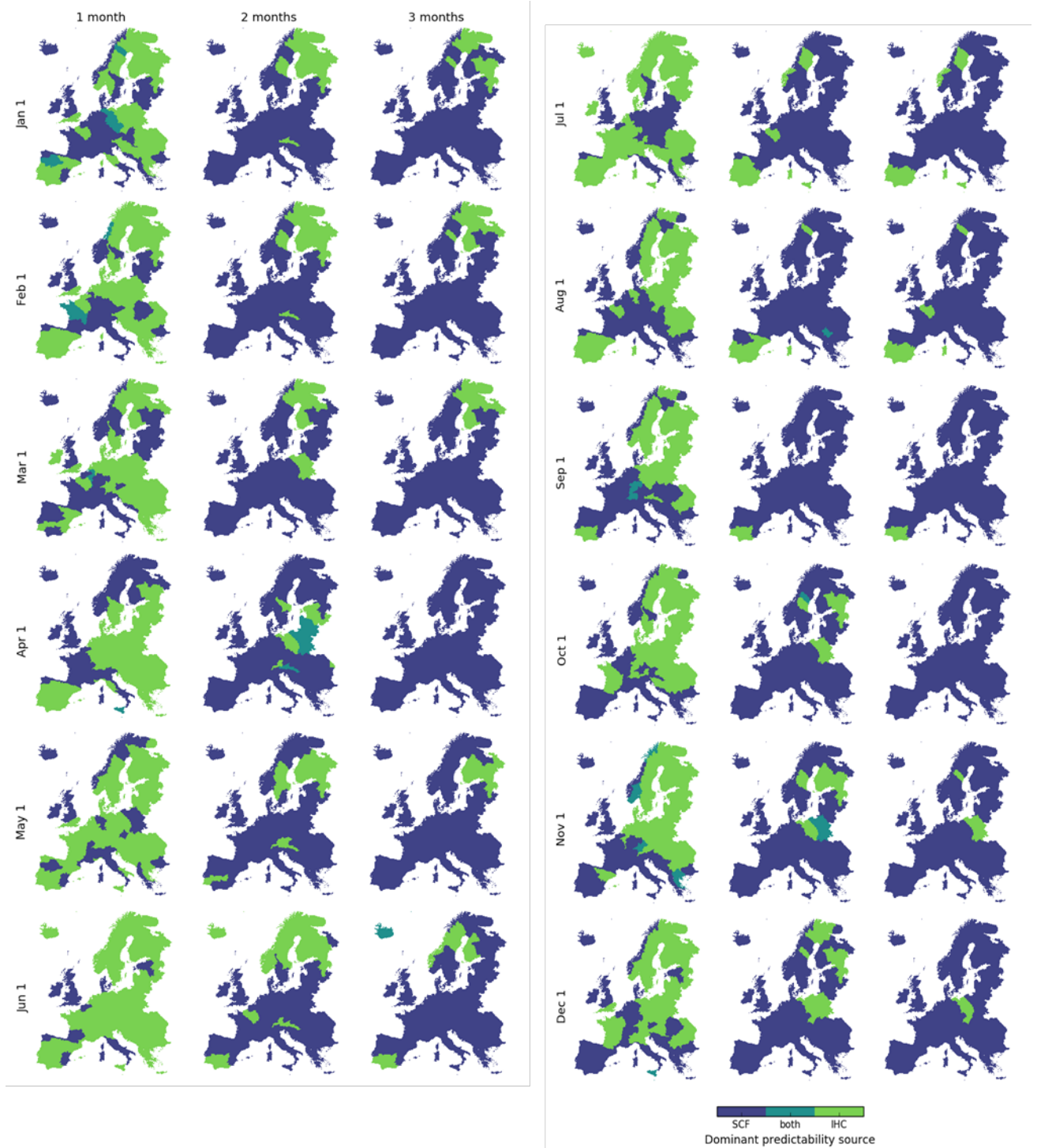


Figure 36 Maps of the dominant predictability source for each forecast initialisation date and the first three months of lead time for the EFAS regions across Europe. Blue [green] colours signify that the SCF [IHC] form the dominant source of predictability.





Figures 37 to 42 display the skill elasticities obtained for several EFAS regions (from the ECMWF forecasts) and for the BfG stations falling in each of those regions (from the BfG forecasts). Results are shown for all forecast initialisation dates and for the first and second months of lead time. The seasonal discharge forecasting skill elasticity to SCF ( $E_{SCF_i}$  in blue) and the seasonal discharge forecasting skill elasticity to IHC ( $E_{IHC_i}$  in green) indicate the potential to improve the seasonal discharge forecasting skill as a result of improving the quality of those respective predictability sources. When one skill elasticity is larger than the other, it implies that this predictability source has the largest potential to improve the seasonal discharge forecasting skill (for that specific station or region, lead time and forecasting initialisation date) once improved. These figures allow a comparison of the sensitivities of the ECMWF and the BfG seasonal discharge forecasts to the IHC and the SCF. Overall, one can see that the skill elasticities obtained for both the EFAS regions and the BfG stations from the two different forecasts are very similar. There are however slight differences, such as the larger relative importance of the IHC for the forecasts made in the spring for the EFAS region of Figure 37, compared to the corresponding station (The Inn at Passau Ingling). These differences between the skill elasticities for the EFAS regions and the BfG stations could be due to differences between the two systems for which the sensitivity analysis was performed as well as the scale (regional or at a station) at which the analysis was made.



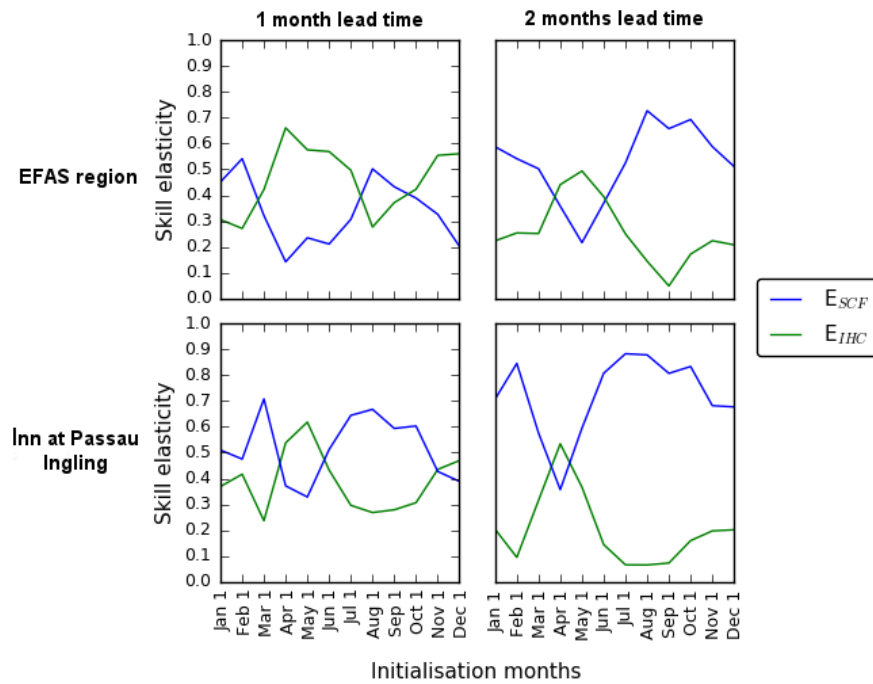


Figure 37 Skill elasticities for (left) the first and (right) the second month of lead time, for (top) the EFAS region and (bottom) the corresponding BfG station for the Inn at Passau Ingling. Skill elasticities are shown for each forecast initialisation month.

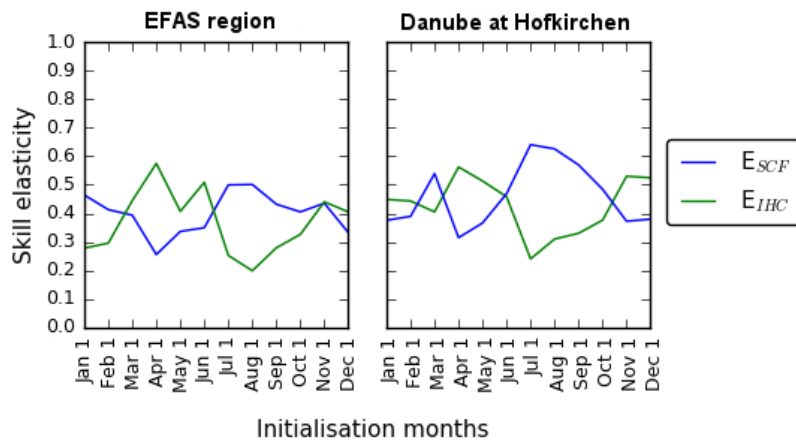


Figure 38 Skill elasticities for (left) the first and (right) the second month of lead time, for (top) the EFAS region and (bottom) the corresponding BfG station for the Danube at Hofkirchen. Skill elasticities are shown for each forecast initialisation month.



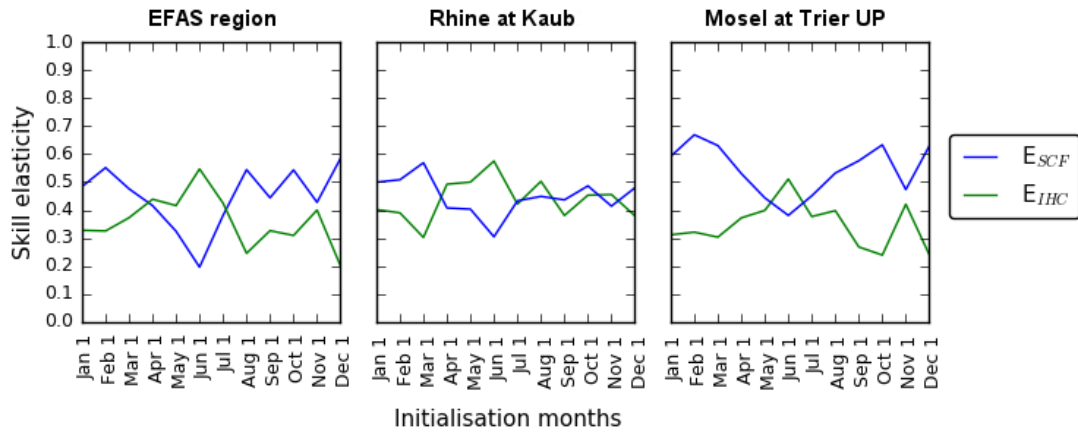


Figure 39 Skill elasticities for (left) the first and (right) the second month of lead time, for (top) the EFAS region and (bottom) the corresponding BfG stations for the Rhine at Kaub and the Mosel at Trier UP. Skill elasticities are shown for each forecast initialisation month.

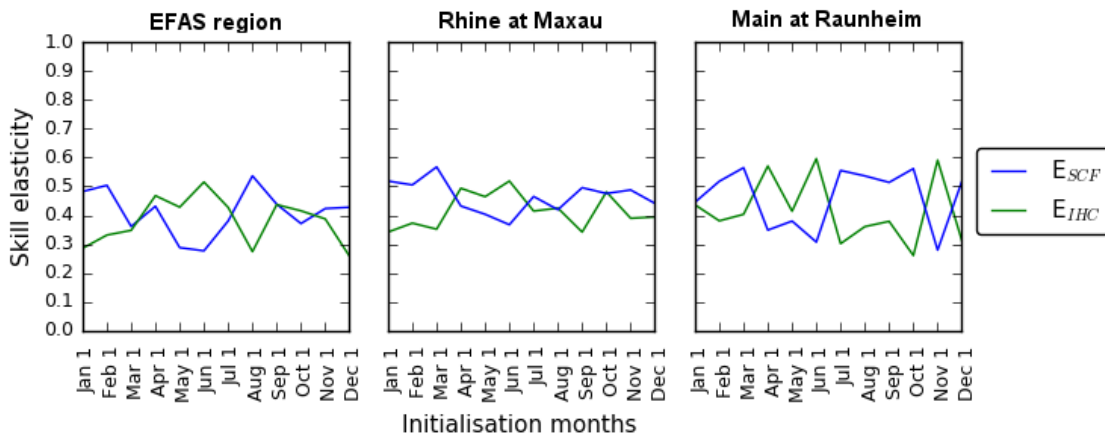


Figure 40 Skill elasticities for (left) the first and (right) the second month of lead time, for (top) the EFAS region and (bottom) the corresponding BfG stations for the Rhine at Maxau and the Main at Raunheim. Skill elasticities are shown for each forecast initialisation month.



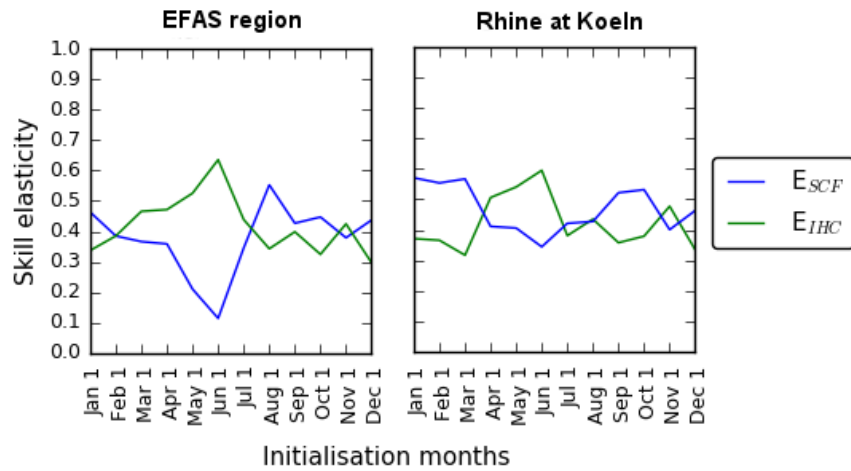


Figure 41 Skill elasticities for (left) the first and (right) the second month of lead time, for (top) the EFAS region and (bottom) the corresponding BfG station for the Rhine at Koeln. Skill elasticities are shown for each forecast initialisation month.

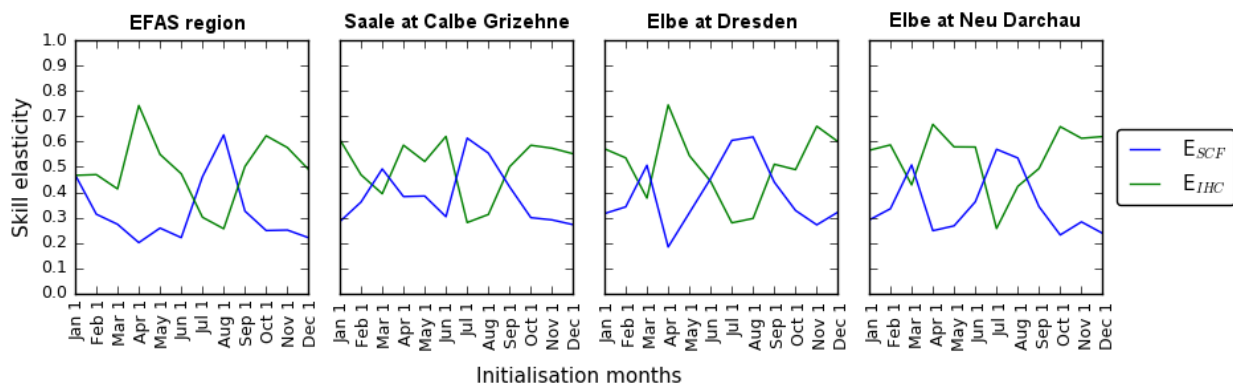


Figure 42 Skill elasticities for (left) the first and (right) the second month of lead time, for (top) the EFAS region and (bottom) the corresponding BfG stations for the Saale at Calbe Grizehne, the Elbe at Dresden and the Elbe at Neu Darchau. Skill elasticities are shown for each forecast initialisation month.

### 4.3 Comparative analysis

For spatial interpretation of hydrological skill, we investigated potential relationships between predictive skill and physiographic-hydrological-climatic characteristics; hence allowing to identify the key controls of poor/good model skill. First the 15 descriptors (see





Table 3) were analysed for inter-dependence, and one of the highly inter-dependent descriptors was omitted to avoid potential artefacts in the CART regression analysis. Consequently a set of nine significant descriptors was statistically identified for application in the CART analysis, which further allowed us to estimate the descriptors' importance.

Figure 43 shows the ranking of nine descriptors (ranked by importance, with number 1 being the most important descriptor) for all months and lead months. Results show that the dominant descriptors resulting in poor/good model performance are the FlowID (describing the hydrological behaviour of the basin), elevation and remaining bias in temperature (BiasTemp). It is generally expected that remaining biases in temperature will have an impact on the form of precipitation (rainfall or snowfall) during the cold months, and the processes (i.e. changing from (to) snow accumulation to (from) melting). For example, this occurs in northern Europe for April where the mean average temperatures for April is close to 0°C and hence small deviations in the meteorological forecasts will affect the basin response. Elevation (Elev.) is also an important factor. It is expected that the meteorological forecasts are reliable in predicting the climatological variability in highly elevated basins, which are usually snow dominated. Consequently the hydrological regime can be better described in comparison to a rain-fed basin. The basin's hydrological behaviour (FlowID) seems to be the most important descriptor with basins of similar river flow properties achieving similar skill. It is known that river systems experience processes with high memory in comparison to the natural phenomena occurring in the atmosphere. Hence it is expected that hydrological variables (i.e. discharge, runoff, soil moisture) can have higher predictability than meteorological variables (i.e. precipitation, temperature). However, this cannot be linearly translated since the precipitation-discharge process is also not linear, and therefore different systems are expected to respond differently to the meteorological signal.



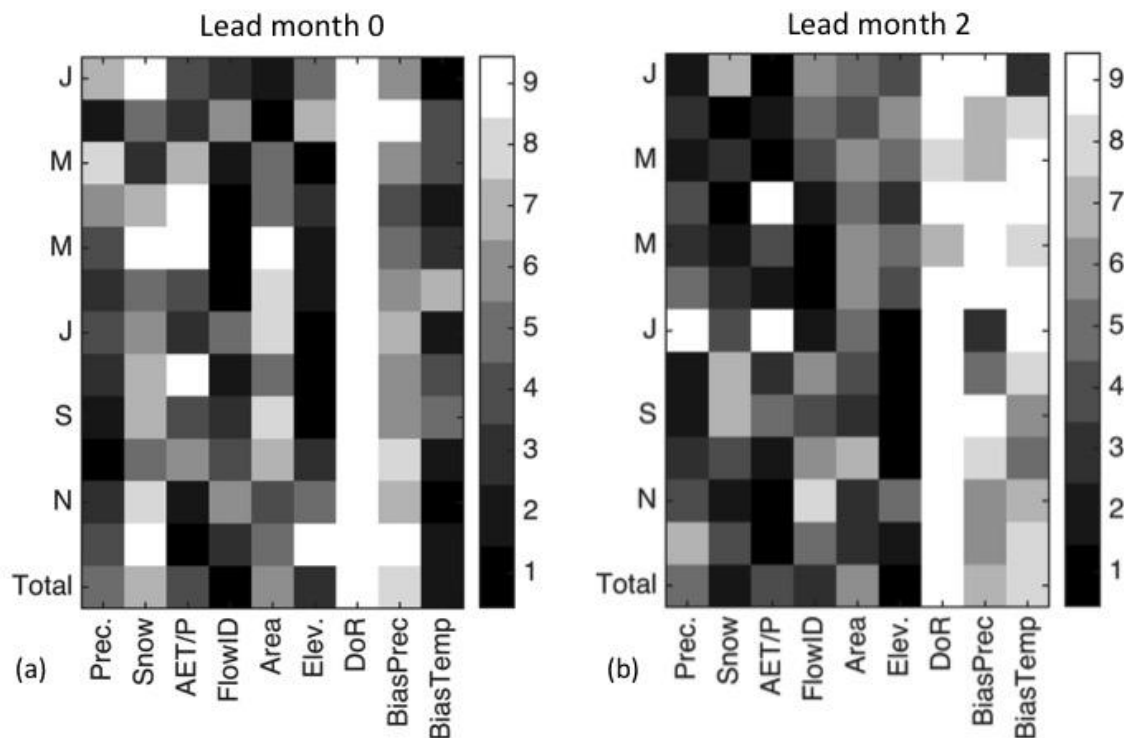


Figure 43 Importance ranking of key descriptors that influence the hydrological forecasting skill over Europe for all months and in lead month: (a) 0, and (b) 2.

To get a better understanding of the basin characteristics that are characterised by a good/poor skill, Figure 44 shows the 11 spatially variable clusters, their distribution of flow signatures, and the distribution of skill in each cluster group. Similarity in catchment behaviour for each class was interpreted and dominant flow generating processes could be distinguished.

Results give a clear separation between basins with poor and good skill. Basins in cluster 5 achieve the highest skill. These basins are characterised by high ranges of baseflow (BFI), low monthly variability (intra-annual variability) (DPar), and high values of low and medium flows ( $q_{95}$  and  $q_{70}$ ). These are properties of basins where short-memory precipitation is aggregated and converted into long-memory discharge. Similar behaviour have the basins in clusters 6, 7 and 9, however not to the distinct level of basins in cluster 5. Basins in cluster 8 and 10 are short-memory rivers characterised by flashy response and high seasonal





variability (DPar and CV). These basins are responding quite fast to the precipitation signal and with strong dynamics (RLD) whilst contribution from base flow is small (BFI). Basins that belong to clusters 1, 2 and 3 perform adequately and are generally characterised by the same flow signatures. These basins are mainly located in the Scandinavian region and also in the central Europe at highly elevated regions. They are distinct for their medium to high slope in their flow distribution (mFDC), which is an indicator of a regime driven by snowmelt.

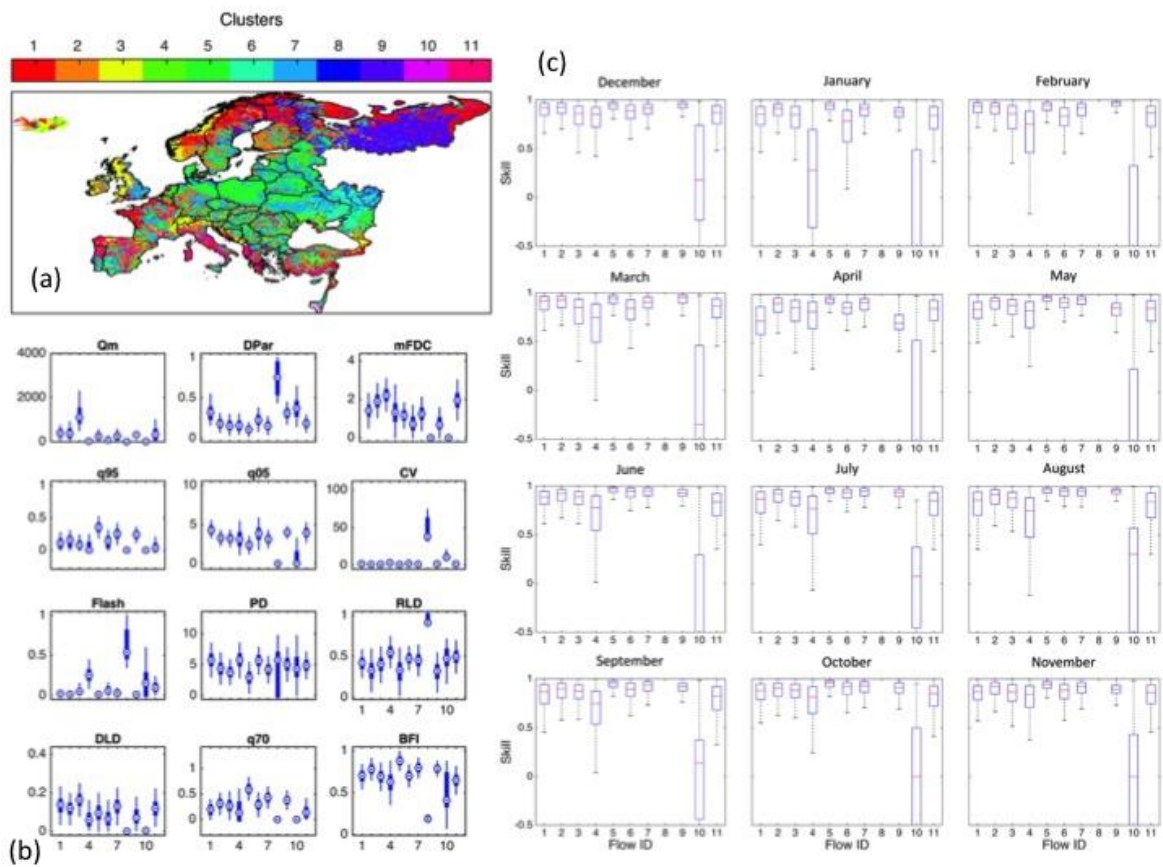


Figure 44 (a) Spatial distribution of hydrologically similar (clusters) basins over Europe, (b) distribution of flow signatures in each cluster group (see also Table 3), and (c) distribution of beta skill in each cluster group



## 5 Lessons learnt

The intercomparison of seasonal discharge quality from forecasting systems from the ECMWF, the SMHI, the BfG, the FW and the UPV done in a first part of this deliverable is a starting point for this larger task within the IMPREX project. Through this intercomparison, multiple scores of forecast quality were added to the scoreboard developed in WP4 (deliverable 4.1) by the partners of this deliverable for stations within each system's spatial boundaries.

Although the sample of stations for which the intercomparison was made was limited, this task has already revealed several major differences between the seasonal hydrological forecasting systems and their impacts on the relevant water sectors.

The BfG forecasting system overall mostly underestimates the observed discharge for stations shared for the Central European Rivers. This could be problematic for the navigation sector, who is most vulnerable to low flows in summer. These forecasts could potentially lead to an underestimation of the expected river flow in summer and consequently to an underestimation of the capacity of the river and a monetary loss.

The ECMWF forecasting system appears to almost systematically overestimate the spring flow and underestimate the winter flow for the stations shared for Central European Rivers and for the Thames River Basin. The underestimation of the winter discharge could be a problem for the flood protection sector, as it would not flag regions to watch for potential floods in the coming months. For the Segura and Tagus River Basins, the ECMWF forecasts are very accurate in summer. This could be highly beneficial for the agriculture sector in this region, which relies on accurate drought forecasts for the summer. However, the summer flow is highly biased (as well as the winter flow) in the Jucar River Basin, also in Spain. In Sweden, the ECMWF forecasts underestimate the May flow and overestimate the summer river flow. This could be problematic for the hydropower industry, for which there is a particular interest in forecasting the spring flow accurately.





The SMHI forecasting system overestimates the flow in winter and spring for the Central European Rivers and the Thames River Basin. This could be a problem for flood forecasting as it could indicate potential floods in the coming months when none actually occurs. The SMHI is also overall less accurate for the lower tercile of observed discharge for summer for a few Central European River stations. This could be a limitation for the navigation sector as the forecasts would not be able to capture accurately a low extreme event in the summer. The May and summer flow in Sweden appears underestimated by the SMHI forecasts, while the June discharge is overestimated. This could be an issue for the hydropower sector, which needs accurate forecasts especially in spring.

The FW forecasting system overestimates largely the early spring-spring flow for the Tagus River Basin and underestimates slightly the flow during all year for the Segura River Basin. Both biases could be challenging for the agricultural sector.

The UPV forecasts are overall greatly improved by using the EVALHID hydrological model compared to the E-HYPE model, especially in summer. There are however still some biases which need to be overcome before the forecasts can be used operationally for reservoir management purposes in the Jucar River Basin.

For most stations, after one to two months of lead time, using the observed flow climatology leads to more accurate and sharp forecasts than using seasonal hydrological forecasts. This shows that there are still model and meteorological forecast biases which need to be overcome in order to gain a real valuable additional from using seasonal hydrological forecasts operationally for many applications of the water sector.

These results are a starting point, to which it will be possible to add more results along the course of the project. Indeed, as the project proceeds, anyone will be able to upload additional scores, scores for different stations or from a new or modified system to the scoreboard. The latter will enable us to monitor and visualise progresses made throughout the IMPREX project, such as improvements in the seasonal discharge forecast quality as a result of improving the seasonal meteorological forecast quality. Towards this goal, it is in our plans to expand on the work done in this deliverable by adding seasonal discharge forecasting scores from systems using different seasonal meteorological forecasts, such as GloSea5.



The intercomparison results are useful for the multi-modelling of task 4.3 of WP4. The multi-modelling approach could for example use weights for each forecasting system based on the forecasting systems' performances for a certain location, type of event, time of the year. Beyond this deliverable, the results of the intercomparison are valuable for the risk outlook, a deliverable of WP14 within IMPREX. The risk outlook will provide an overview of the hydrological 'risk' for Europe and it will also showcase examples of making hydrological information relevant at a local scale, focusing on selected IMPREX case studies. It is currently under development, so it is not yet fully known what will be included within the tool, but it is likely to show current hydrological status, climatology and seasonal forecasted anomalies as well as sector-specific indicators. An improved understanding of forecasting systems' strengths and weaknesses will enable IMPREX communicate this information in a comprehensive way, by adding information which will help the users know with what level of confidence each forecast can be used.

The EPB sensitivity analysis enabled to highlight which component of the forecast system should be improved in order to improve the seasonal discharge forecasting skill for all forecast initialisation dates and lead time for regions in Europe and individual Central European River stations. These results should be used as an indication of where to concentrate resources in order to obtain the largest improvements in the seasonal discharge forecasting skill. Where the analysis indicated the IHC to be the largest contributors to the errors in seasonal discharge forecasts, data assimilation methods could be used. Where the SCF were highlighted to be the largest contributors to seasonal discharge errors, the SCF used to force the hydrological models should be improved.

Finally, from the comparative analysis of the hydrological skill we spotted the strengths and weaknesses of ensemble seasonal forecasts from ECMWF System 4. We identified links between forecasting skill and different physiographic and hydro-climatic characteristics. CART showed that skill is dependent on the basin's hydrological regime. Elevation and remaining bias in temperature were also identified to be important aspects (dependence of





response at mountainous basins to temperature). The skill seems to be limited for relatively flashy basins experiencing strong flow dynamics over the year (less memory in the system).



## 6 References

- Arnal, L., A. Wood, E. Stephens, H. Cloke, and F. Pappenberger, 2017: An Efficient Approach for Estimating Streamflow Forecast Skill Elasticity. *J. Hydrometeor.* doi:10.1175/JHM-D-16-0259.1, in press.
- Arribas, A., et al., 2010: The GloSea4 Ensemble Prediction System for Seasonal Forecasting. *Monthly Weather Review*, 139, 6, 1891–1910, doi:10.1175/2010MWR3615.1.
- Berendrecht, W.L., A.H. Weerts, A.A. Veldhuizen, T. Kroon, 2011: An operational drought forecasting system using coupled models for groundwater, surface water and unsaturated zone. IAHS-AISH Publication, Volume 341, 2011, Pages 3-8. 7th International Conference on Calibration and Reliability in Groundwater Modeling: managing groundwater and the environment, ModelCARE 2009, Wuhan, China, September 20-23, 2009.
- Bierkens, M. F. P., and L. P. H. van Beek, 2009: Seasonal Predictability of European Discharge: NAO and Hydrological Response Time. *Journal of Hydrometeorology*, 10, 4, 953–68, doi:10.1175/2009JHM1034.1.
- Blöschl, G., M. Sivapalan, T. Wagener, A. Viglione, and H. Savenije: Runoff prediction in ungauged basins. Synthesis across processes, places and scales, Cambridge University Press, Cambridge, UK, 2013.
- cawcr: Forecast verification, available at <http://cawcr.gov.au/projects/verification/>, last access: 6th January 2017, 2015.
- Church, J. E., 1935: Principles of Snow Surveying as Applied to Forecasting Stream Flow. Vol. 51. 2. *Journal of Agricultural Research*.
- Day, Gerald N., 1985: Extended Streamflow Forecasting Using NWSRFS. *Journal of Water Resources Planning and Management*, 111, 2, 157–70, doi:10.1061/(ASCE)0733-9496(1985)111:2(157).
- Easey, J., C. Prudhomme, and D. M. Hannah, 2006: Seasonal Forecasting of River Flows: A Review of the State-of-the-Art. *IAHS Publication*, 308, 158-162.





Goddard, L., W. E. Baethgen, H. Bhojwani, and A. W. Robertson, 2014: The International Research Institute for Climate & Society: Why, What and How. *Earth Perspectives*, 1, 1, doi:10.1186/2194-6434-1-10.

Gupta, H. V., C. Perrin, G. Blöschl, A. Montanari, R. Kumar, M. Clark, and V. Andréassian, 2014: Large-sample hydrology: a need to balance depth with breadth, *Hydrol. Earth Syst. Sci.*, 18, 2, 463–477, doi:10.5194/hess-18-463-2014.

Helms, D., S. E. Phillips, and P. F. Reich, 2008: The History of Snow Survey and Water Supply Forecasting: Interviews with US Department of Agriculture Pioneers. 8. US Department of Agriculture, Natural Resources Conservation Service, Resource Economics and Social Sciences Division.

Herrera, S., J. Fernández, and J.M. Gutiérrez, 2016: Update of the Spain02 gridded observational dataset for EURO-CORDEX evaluation: assessing the effect of the interpolation methodology. *Int. J. Climatol.*, 36: 900–908. doi:10.1002/joc.4391.

Hersbach, H., 2000: Decomposition of the Continuous Ranked Probability Score for Ensemble Prediction Systems. *Weather and Forecasting*, 15, 5, 559–70, doi:10.1175/1520-0434(2000)015<0559:DOTCRP>2.0.CO;2.

Klein, B., and D. Meissner, 2016: Vulnerability of Inland Waterway Transport and Waterway Management on Hydro-meteorological Extremes. EU Horizon2020 IMPREX Deliverable 9.1. <http://www.imprex.eu/system/files/generated/files/resource/d9-1-imprex-v1.pdf>.

Pagano, T. C., and D. C. Garen, 2005: Integration of Climate Information and Forecasts into Western US Water Supply Forecasts. *Climate Variations, Climate Change, and Water Resources Engineering*, 86–103.

Pechlivanidis, I. G., and B. Arheimer, 2015: Large-scale hydrological modelling by using modified PUB recommendations: the India-HYPE case. *Hydrol. Earth Syst. Sci.*, 19, 4559–4579, doi:10.5194/hess-19-4559-2015.

Saltelli, A., S. Tarantola, F. Campolongo, and M. Ratto, 2004: Sensitivity Analysis in Practice: A Guide to Assessing Scientific Models. John Wiley & Sons.

Saltelli, A., M. Ratto, T. Andres, F. Campolongo, J. Cariboni, D. Gatelli, M. Saisana, and S. Tarantola, 2008: Global Sensitivity Analysis: The Primer. John Wiley & Sons.



Schaake, J. C., 1978: The National Weather Service Extended Streamflow Prediction Techniques: Description and Applications during 1977. In 3rd Annual Climate Diagnostics Workshop.

Twedt, T. M., J. C. Schaake Jr, and E. L. Peck., 1977: National Weather Service Extended Streamflow Prediction [USA]. In Proceedings Western Snow Conference.

Wang, E., Y. Zhang, J. Luo, F. H. S. Chiew, and Q. J. Wang, 2011: Monthly and Seasonal Streamflow Forecasts Using Rainfall-Runoff Modeling and Historical Weather Data. *Water Resources Research*, 47, 5, W05516, doi:10.1029/2010WR009922.

Wood, A. W., and D. P. Lettenmaier, 2003: Comparing Hydrologic Forecast Uncertainty due to Initial Condition Error versus Climate Forecast Error. In EGS-AGU-EUG Joint Assembly, 1:8162. <http://adsabs.harvard.edu/abs/2003EAEJA.....8162W>.

Wood, A. W., and D. P. Lettenmaier, 2006: A Test Bed for New Seasonal Hydrologic Forecasting Approaches in the Western United States. *Bulletin of the American Meteorological Society*, 87, 12, 1699, doi:10.1175/BAMS-87-12-1699.

Wood, A. W., and Dennis P. Lettenmaier, 2008: An Ensemble Approach for Attribution of Hydrologic Prediction Uncertainty. *Geophysical Research Letters*, 35, 14, doi:10.1029/2008GL034648.

Wood, A. W., T. Hopson, A. Newman, L. Brekke, J. Arnold, and M. Clark, 2016: Quantifying Streamflow Forecast Skill Elasticity to Initial Condition and Climate Prediction Skill. *Journal of Hydrometeorology*, 17, 2, 651–68, doi:10.1175/JHM-D-14-0213.1.





## 7 Annex A – Tabulated overview on hydrological model features

Table 4 Tabulated overview on hydrological model features of SPHY

<b>1. General Information</b>	
Model name	SPHY ( <b>S</b> patial <b>P</b> rocesses in <b>H</b> ydrology)
Version	V2.1
Author(s) / First publication	Terink et al. (2015a)
Contact person	Wilco Terink (w.terink@futurewater.nl)
Institute	FutureWater
Website	<a href="http://www.sphy.nl/">http://www.sphy.nl/</a>
General modelling objectives	Calculation of river basins water balance
Domain of applicability (catchment types and climate conditions)	The SPHY model has been applied and tested in various studies ranging from real-time soil moisture predictions in flat lands, to operational reservoir inflow forecasting applications in mountainous catchments, irrigation scenarios in the Nile Basin, and detailed climate change impact studies in the snow- and glacier-melt dominated the Himalayan region.
<b>2. Model</b>	



description	
Model type (empirical, conceptual, physically based)	Conceptual/Physically-based model
Continuous or event-based	Continuous
Possible running time steps	24h
Spatial discretization (lumped, semidistributed, distributed)	Spatially distributed leaky bucket type
Short description of model structure detailing main function (evaporation, soil moisture accounting,	SPHY is grid-based and cell values represent averages over a cell, but sub-grid variability is taken into account. A cell can be glacier-free, partially glaciated, or completely covered by glaciers. The cell fraction not covered by glaciers consists of either land covered with snow or land that is free of snow. Land that is free of snow can consist of vegetation, bare soil, or open water. In order to distinct between land cover types at sub-grid level, SPHY calculates and stores the state variables as grid-cell averages. Sub-





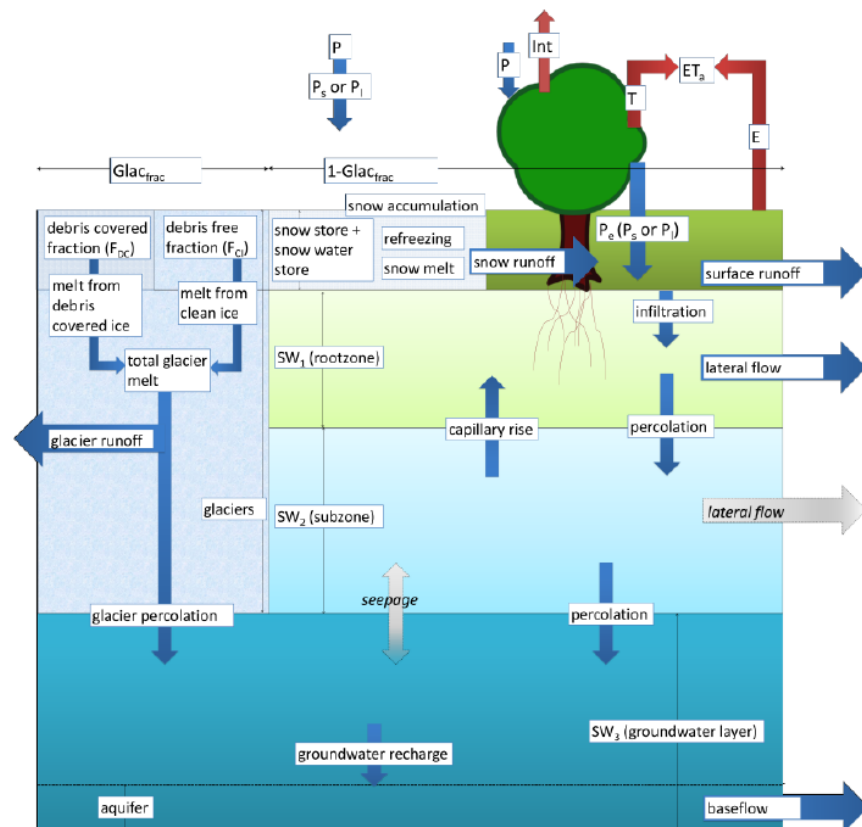
groundwater, routing, snowmelt, etc.)	<p>grid variability is mainly determined by the fractional vegetation coverage, which affects processes such as interception, effective precipitation, and potential evapotranspiration.</p> <p>The land compartment is divided in two upper soil stores and a third groundwater store, with their corresponding drainage components: surface runoff, lateral flow and base flow. SPHY simulates for each cell precipitation in the form of rain or snow, depending on the temperature. Any precipitation that falls on land surface can be intercepted by vegetation and in part or in whole evaporated. The snow storage is updated with snow accumulation and/or snow melt. A part of the liquid precipitation is transformed in surface runoff, whereas the remainder infiltrates into the soil. The resulting soil moisture is subject to evapotranspiration, depending on the soil properties and fractional vegetation cover, while the remainder contributes in the long-term to river discharge by means of lateral flow from the first soil layer, and base flow from the groundwater reservoir.</p> <p>Melting of glacier ice contributes to the river discharge by means of a slow and fast component, being (i) percolation to the groundwater reservoir that eventually becomes base flow, and (ii) direct runoff. The cell-specific runoff, which becomes available for routing, is the sum of surface runoff, lateral flow, base flow, snow melt and glacier melt.</p> <p>If no lakes are present, then the user can choose for a simple flow accumulation routing scheme: for each cell the accumulated amount of material that flows out of the cell into its neighbouring downstream cell is calculated. This accumulated amount is the amount of material in the cell itself plus the amount of material in upstream cells of the cell. For each cell, the following procedure is</p>
---	---



performed: using the local drain direction network, the catchment of a cell is determined which is made up the cell itself and all cells that drain to the cell. If lakes are present, then the fractional accumulation flux routing scheme is used: depending on the actual lake storage, a fraction of that storage becomes available for routing and is extracted from the lake, while the remaining part becomes the updated actual lake storage. The flux available for routing is routed in the same way as in the simple flow accumulation routing scheme.

SPHY enables the user to turn on/off any of the six available modules that are not required: glaciers, snow, groundwater, dynamic vegetation, simple routing, and lake/reservoir routing.

Scheme of model structure





	Source: Terink et al. (2015a)
<b>3. Model parameters</b>	
Distribution of model parameters (yes/no)	Yes
Number of free parameters	Numerous free parameters (Terink et al. (2015a))
Procedure of model parameter estimation (measurement, manual or automatic algorithm, etc.)	<ul style="list-style-type: none"> <li>- Calibration for each sub basin possible</li> <li>- An automatic calibration routine does not belong to the model itself.</li> <li>- For setting-up the model data on streamflows are not necessary. However, to undertake a proper calibration and validation procedure flow data are required. The model could also be calibrated using actual evapotranspiration, soil moisture contents, or snow coverage.</li> </ul>
<b>4. Model inputs / Model outputs</b>	
List and characteristics of input variables (type, time step,	As input SPHY requires data on state variables as well as dynamic variables. For the state variables the most relevant are: Digital Elevation Model (DEM), land use type, glacier cover, reservoirs and soil characteristics. The main dynamic variables are climate data such as precipitation, temperature, reference evapotranspiration.



spatial resolution, etc.)	Since SPHY is grid-based optimal use of remote sensing data and global data sources can be made. For example, the Normalized Difference Vegetation Index (NDVI) can be used to determine the Leaf Area Index (LAI) in order to estimate the growth-stage of land cover.
List and characteristics of output variables (type, time step, spatial resolution, etc.)	The SPHY model provides a wealth of output data that can be selected based on the preference of the user. Spatial output can be presented as maps of all the hydrological processes. Maps often displayed as output include actual evapotranspiration, runoff generation (separated by its contributors), and groundwater recharge. These maps can be generated on daily base, but most users prefer to get those at monthly or annual aggregated time periods. Time-series can be generated for each location in the study area. Time-series often used are stream flow under current and future conditions, actual evapotranspiration and recharge to the groundwater.
<b>5. Examples of previous model applications</b>	
Catchments, objectives, etc.  Results of existing comparisons with other models	A number of evaluations and applications are documented at the website.





6. List of selected references	
	<ul style="list-style-type: none"> <li>● Terink, W., S. Khanal. 2016. SPHY: Spatial Processes in Hydrology. Advanced training: input data, sensitivity analysis, model calibration, and scenario analyses. FutureWater Report 159.</li> <li>● Terink, W., A.F. Lutz, G.W.H. Simons, W.W. Immerzeel, P. Droogers. 2015a. SPHY v2.0: Spatial Processes in Hydrology. Geoscientific Model Development, 8, 2009-2034, doi:10.5194/gmd-8-2009-201</li> <li>● Terink, W., A.F. Lutz, W.W. Immerzeel. 2015b. SPHY v2.0: Spatial Processes in Hydrology. Model theory, installation, and data preparation. FutureWater report 142.</li> <li>● Terink, W., A.F. Lutz, W.W. Immerzeel. 2015c. SPHY: Spatial Processes in Hydrology. Graphical User-Interfaces (GUIs). FutureWater report 144.</li> <li>● Terink, W., A.F. Lutz, G.W.H. Simons, W.W. Immerzeel. 2015d. SPHY: Spatial Processes in Hydrology. Case-studies for training. FutureWater report 143.</li> </ul>

Table 5 Tabulated overview on hydrological model features of HYPE

1. General Information	
Model name	HYPE ( <b>H</b> ydrological <b>P</b> redictions for the <b>E</b> nvironment)
Version	v4.13



Author(s) / First publication	Lindström et al. (2010)
Contact person	Charlotta Pers (charlotta.pers@smhi.se) Ilias Pechlivanidis (ilias.pechlivanidis@smhi.se)
Institute	Swedish Meteorological and Hydrological Institute
Website	<a href="http://hypecode.smhi.se">http://hypecode.smhi.se</a>
General modelling objectives	Calculation/prediction of river basin responses (water quantity and quality)
Domain of applicability (catchment types and climate conditions)	The HYPE model has been applied and tested in different scales, various domains and hydro-climatic conditions. See <a href="http://hypeweb.smhi.se">http://hypeweb.smhi.se</a>
<b>2. Model description</b>	
Model type (empirical, conceptual, physically based)	Conceptual/Process-based model
Continuous or	Continuous





event-based	
Possible running time steps	Daily (also hourly for national operational services)
Spatial discretization (lumped, semidistributed, distributed)	Spatially distributed at the sub-basin scale. Sub-basin resolution depends on the application. In Europe, this is 215 km <sup>2</sup> .
Short description of model structure detailing main function (evaporation, soil moisture accounting, groundwater, routing, snowmelt, etc.)	HYPE is most often run at a daily time step and simulates the water flow paths in soil for hydrological response units (HRUs), which are defined by gridded soil and land- use classes and can be divided in up to three layers with a fluctuating groundwater table. The HRUs are further aggregated into sub-basins based on topography. Elevation is also used to get temperature variations within a sub-basin to influence the snowmelt and storage as well as evapotranspiration. Glaciers have a variable surface and volume, while lakes are defined as classes with specified areas and variable volume. Lakes receive runoff from the local catchment and, if located in the sub-basin outlet, also the river flow from upstream sub- basins. On glaciers and lakes, precipitation falls directly on the surface and water evaporates at the potential rate. Each lake has a defined depth below an outflow threshold. The outflow from lakes is determined by a general rating curve unless a specific one is given or if the lake is regulated. Regulated lakes and man-made reservoirs are treated equally but a simple regulation rule can be used, in which the outflow is constant or follows a



seasonal function (as it is often the case with hydropower) for water levels above the threshold. A rating curve for the spillways can be used when the reservoir is full.

### Irrigation

Irrigation is simulated based on crop water demands calculated either with the FAO-56 crop coefficient method (Allen et al., 1998) or relative to a reference flooding level for sub-merged crops (e.g. rice). The demands are withdrawn from rivers, lakes, reservoirs, and/or groundwater within and/or external to the sub-basin where the demands originated and are constrained by the water available at these sources. After subtraction of conveyance losses, the withdrawn water is applied as additional infiltration to the irrigated soils. The agriculture and irrigation data sets (see Table 1) are used to define irrigated area, crop types, growing seasons, crop coefficients, irrigation methods and efficiencies, and irrigation sources. The irrigation parameters regulating water demand and abstraction are usually manually calibrated using discharge stations in irrigation-dominated areas.

River discharge is routed between the sub-basins along the river network and may also pass sub-basins, flow laterally in the soil between sub-basins or interact with a deeper groundwater aquifer in the model.





<p>Scheme of model structure</p>	<p>Source: Hundecha et al. (2016)</p>
<p><b>3. Model parameters</b></p>	
<p>Distribution of model parameters (yes/no)</p>	<p>Yes</p>
<p>Number of free parameters</p>	<p>Numerous free parameters (Lindström et al. (2010))</p>
<p>Procedure of model parameter estimation (measurement, manual or automatic algorithm, etc.)</p>	<p>Many of the parameters are linked to physiographic characteristics in the landscape, such as soil type and depth (soil dependent parameters) or vegetation (land-use-dependent parameters), while others are assumed to be general to the entire domain (general parameters) or specific to a defined region or river (regional parameters). Parameters for each HRU are calibrated for representative gauged basins and then transferred to similar HRUs, which are gridded at a higher resolution than the sub-basins across the whole domain to</p>



	<p>account for spatial variability in soil and land use. Using the distributed HRU approach in the multi-basin concept is thus one part of the regionalisation method for parameter values.</p> <p>Some other parameters, however, are either estimated from literature values and from previous modelling experiences (a priori values) or identified in the (automatic or manual) calibration procedure.</p> <p>Slightly different methods for regionalisation of parameter values have been used when setting up the different HYPE model applications, depending on access to gauging stations, additional data sources, and expert knowledge.</p> <p>An automatic calibration routine based on the differential-evolution Markov-chain (DE-MC) algorithm has also been used.</p> <p>The model parameters can also be constrained using evapotranspiration or snow information.</p>
<p><b>4. Model inputs / Model outputs</b></p>	
<p>List and characteristics of input variables</p>	<p>As input HYPE requires data on: Digital Elevation Model (DEM), land use type, glacier cover, reservoirs, irrigation, and soil characteristics. Depending on the application information about crop and vegetation, bifurcations of the river network,</p>





<p>(type, time step, spatial resolution, etc.)</p>	<p>point sources and water extraction, floodplains and regional aquifers can be used.</p> <p>The main dynamic variables are climate data such as precipitation and temperature. Other observations can also be used for different purposes:</p> <p><a href="http://www.smhi.net/hype/wiki/doku.php?id=start:hype_file_reference#observation_data_files">http://www.smhi.net/hype/wiki/doku.php?id=start:hype_file_reference#observation_data_files</a></p>
<p>List and characteristics of output variables (type, time step, spatial resolution, etc.)</p>	<p>A list of output variables can be found in:</p> <p><a href="http://www.smhi.net/hype/wiki/doku.php?id=start:hype_file_reference:info.txt:variables">http://www.smhi.net/hype/wiki/doku.php?id=start:hype_file_reference:info.txt:variables</a></p> <p>The exported time-step depends on the user, i.e. daily, weekly, monthly, and annual.</p> <p>The variables are exported for the basin outlet or represent basin averages.</p>
<p><b>5. Examples of previous model applications</b></p>	<p style="background-color: #cccccc; height: 100px;"></p>
<p>Catchments, objectives, etc.</p> <p>Results of existing comparisons with other models</p>	<p>A number of evaluations and applications are documented at the website.</p>
<p><b>6. List of selected references</b></p>	<p style="background-color: #cccccc; height: 70px;"></p>
	<ul style="list-style-type: none"> <li>● Andersson, J.C.M., Pechlivanidis, I.G., Gustafsson, D., Donnelly, C., and Arheimer, B., 2015. Key factors for im-</li> </ul>



proving large-scale hydrological model performance. *European Water* 49:77-88.

- Donnelly, C, Andersson, J.C.M. and Arheimer, B., 2016. Using flow signatures and catchment similarities to evaluate a multi-basin model (E-HYPE) across Europe. *Hydr. Sciences Journal* 61(2):255-273, doi: 10.1080/02626667.2015.1027710
- Hundecha, Y., Arheimer, B., Donnelly, C., Pechlivanidis, I., 2016. A regional parameter estimation scheme for a pan-European multi-basin model. *Journal of Hydrology: Regional Studies*, Volume 6, June 2016, Pages 90-111. doi:10.1016/j.ejrh.2016.04.002
- Lindström, G., Pers, C.P., Rosberg, R., Strömqvist, J., and Arheimer, B., 2010. Development and test of the HYPE (Hydrological Predictions for the Environment) model – A water quality model for different spatial scales. *Hydrology Research* 41.3-4:295-319.
- Pechlivanidis, I. G. and Arheimer, B., 2015. Large-scale hydrological modelling by using modified PUB recommendations: the India-HYPE case, *Hydrol. Earth Syst. Sci.*, 19, 4559-4579, doi:10.5194/hess-19-4559-2015.
- Strömqvist, J., Arheimer, B., Dahné, J., Donnelly, C. and Lindström, G., 2012. Water and nutrient predictions in ungauged basins – Set-up and evaluation of a model at the national scale. *Hydrological Sciences Journal* 57(2):229-247.





Table 6 Tabulated overview on hydrological model features of LARSIM

<b>1. General Information</b>	
Model name	LARSIM (Large Area Runoff Simulation Model)
Version	LARSIM Revision 968 (neue Formate)
Author(s) / First publication	Ludwig & Bremicker (2006)
Contact person	LARSIM development community <a href="http://www.larsim.info">http://www.larsim.info</a>
Institute	LARSIM development community <a href="http://www.larsim.info">http://www.larsim.info</a>
Website	<a href="http://www.larsim.info">http://www.larsim.info</a>
General modelling objectives	Continuous simulation of runoff processes in catchments and river networks
Domain of applicability (catchment types and climate conditions)	Largely applied by forecasting centers in Germany, Austria, Luxembourg, Switzerland and the French regions of Alsace and Lorraine, Central Europe
<b>2. Model description</b>	
Model type (empirical, conceptual,	Deterministic conceptual model



physically based)	
Continuous or event-based	Continuous
Possible running time steps	Hourly, daily
Spatial discretization (lumped, semidistributed, distributed)	Distributed
Short description of model structure detailing main function (evaporation, soil moisture accounting, groundwater, routing, snowmelt, etc.)	<p>The main components of the model are routines for interception, evapotranspiration, snow accumulation, compaction and melt, soil water retention, storage and lateral water transport, as well as flood-routing in channels and retention in lakes.</p> <p>Spatial units are grid-based subareas or subareas according to hydrologic subcatchments. Hydrological processes are modelled for each single land use category or alternatively for each land use soil type category in a subarea (Hydrological response unit HRU). HRUs can be further subdivided in elevation zones for snow simulation.</p> <p>Different process descriptions could be selected to model snow</p>





	<p>processes and evaporation. Here the configuration used in this study is described.</p> <p><b>Snow Routine:</b></p> <p>Precipitation is divided into rainfall and snowfall using a threshold temperature. On days with temperatures below the threshold, precipitation is supposed to be snow. The consideration of a transition from rain to snow over a temperature interval is possible. Based on a degree-day approach snow melt is computed. Water retention, snow compaction, meltwater outflow is calculated after the snow compaction approach of Bertle. Snow processes could be simulated separately for different elevation zones in the subarea.</p> <p><b>Soil Routine:</b></p> <p>The routine mainly controls runoff formation. To simulate the soil storage the Xinanjiang-model is used. Soil water content is calculated by the water balance equation, taking into account the precipitation supply, withdrawal of water through evapotranspiration as well as runoff formation. In the configuration applied here three runoff components are considered: runoff formation on saturated areas towards direct runoff storage, water release from soil storage through lateral drainage towards interflow storage and water release through vertical percolation towards groundwater storage. Saturated areas which control the direct runoff are derived from the soil water storage via the soil-moisture-saturated areas function. Actual evapotranspiration is computed from potential evapotranspiration as a function of soil moisture.</p> <p><b>Runoff Generation Routine:</b></p> <p>Runoff concentration from direct runoff storage, interflow storage and groundwater storage of the subareas are calculated by a</p>
--	---



	<p>single linear storage model. The combination of the outflows of these storages results in the total outflow of the subarea.</p> <p><b>Routing Procedure:</b></p> <p>The translation and the retention in the channel are calculated in dependency of the channel geometry and the friction of the channel.</p> <p><b>Lake and Reservoir:</b></p> <p>Storage effects including operation of dams, lakes and reservoirs can be simulated using different approaches depending on the available data.</p>
--	---





<p>Scheme of model structure</p>	<p style="text-align: center;">Source: Demuth and Rademacher (2016)</p>
<p><b>3. Model parameters</b></p>	
<p>Distribution of model parameters (yes/no)</p>	<p>Yes</p>
<p>Number of free parameters</p>	<p>Numerous free parameters (Ludwig &amp; Bremicker 2006)</p>
<p>Procedure of</p>	<p>- Calibration for each subarea is possible, generally several</p>



model parameter estimation (measurement, manual or automatic algorithm, etc.)	subareas are combined and calibrated together - An automatic calibration routine for some parameters is available
<b>4. Model inputs / Model outputs</b>	
List and characteristics of input variables (type, time step, spatial resolution, etc.)	Depending on the considered process descriptions for potential evapotranspiration and modelling of snow processes different input data sets are required. In the configuration used here daily precipitation, temperature and global radiation are required as input data.
List and characteristics of output variables (type, time step, spatial resolution, etc.)	Numerous possible output variables (Ludwig & Bremicker 2006) e.g. total computed outflow, actual evaporation, soil moisture,... Depending on the variable output is available for subareas, HRUs, combination of several connected subareas, and defined output nodes (e.g. gauges)
<b>5. Examples of previous model applications</b>	





<p>Catchments, objectives, etc.</p> <p>Results of existing comparisons with other models</p>	<p>Operational forecast model, climate change analysis, water balance, water temperature. Applications and publications are documented at the website <a href="http://www.larsim.info">www.larsim.info</a>. Mesoscale application for the River Rhine (Ebel et al. 2000).</p>
<p><b>6. List of selected references</b></p>	
	<ul style="list-style-type: none"> <li>● Bremicker, M., M. C. Casper &amp; I. Haag (2011): Extrapolationsfähigkeit des Wasserhaushaltsmodells LARSIM auf extreme Abflüsse am Beispiel der Schwarzen Pockau. KW Korrespondenz Wasserwirtschaft 4(8), 445-451</li> <li>● Demuth, N. &amp; S. Rademacher (2016): Chapter 5 - Flood Forecasting in Germany — Challenges of a Federal Structure and Transboundary Cooperation A2 - Adams, Thomas E. In: T. C. Pagano (Ed.): Flood Forecasting. Academic Press, Boston, 125-151</li> <li>● Ebel, M., K. Ludwig &amp; K. G. Richter (2000): Mesoskalige Modellierung des Wasserhaushaltes im Rheineinzugsgebiet mit LARSIM. Hydrologie und Wasserbewirtschaftung 6, 308-312</li> <li>● Haag, I. &amp; A. Luce (2008): The integrated water balance and water temperature model LARSIM-WT. Hydrological Processes 22(7), 1046-1056</li> <li>● Ludwig, K. &amp; M. Bremicker (2006): The Water Balance Model LARSIM –Design, Content and Applications. 22. C. Leibundgut, S. Demuth and J. Lange (Eds), Freiburger Schriften zur Hydrologie, Institut für Hydrologie, Universität</li> </ul>



	Freiburg im Breisgau, Freiburg, 141 pp.
--	---

Table 7 Tabulated overview on hydrological model features of LISFLOOD

<b>1. General Information</b>	
Model name	LISFLOOD
Version	NA
Author(s) / First publication	De Roo et al. (2000)
Contact person	A.P.J. De Roo
Institute	Joint Research Centre, Space Applications Institute, AIS Unit Environment and Natural Hazards, TP 950, 21020 Ispra (Va), Italy
Website	<a href="https://ec.europa.eu/jrc/en/publication/eur-scientific-and-technical-research-reports/lisflood-distributed-water-balance-and-flood-simulation-model-revised-user-manual-2013">https://ec.europa.eu/jrc/en/publication/eur-scientific-and-technical-research-reports/lisflood-distributed-water-balance-and-flood-simulation-model-revised-user-manual-2013</a>
General modelling objectives	To produce a tool that can be used in large and trans-national catchments for a variety of applications, including: <ul style="list-style-type: none"> <li>• Flood forecasting</li> <li>• Assessing the effects of river regulation measures</li> </ul>





	<ul style="list-style-type: none"> <li>Assessing the effects of land-use change</li> <li>Assessing the effects of climate change</li> </ul>
Domain of applicability (catchment types and climate conditions)	The LISFLOOD model has been developed for European catchments. It was designed to make the best possible use of several existing databases that contain pan-European information on soils (King et al., 1997; Wösten et al., 1999), land cover (CEC, 1993), topography (Hiederer & de Roo, 2003) and meteorology (Rijks et al., 1998).
<b>2. Model description</b>	
Model type (empirical, conceptual, physically based)	Conceptual/Physically-based model
Continuous or event-based	Continuous
Possible running time steps	24h
Spatial discretization (lumped, semidistributed, distributed)	Spatially distributed
Short description	The figure below gives an overview of the structure of the

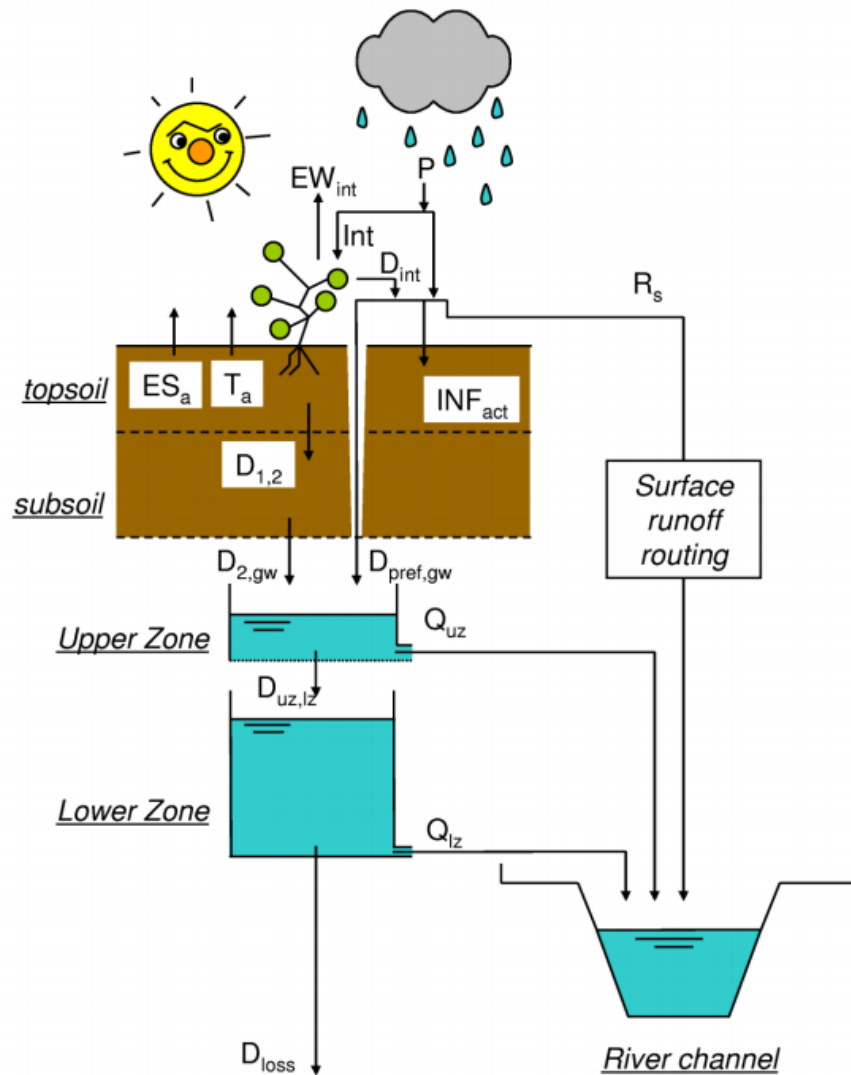


<p>of model structure detailing main function (evaporation, soil moisture accounting, groundwater, routing, snowmelt, etc.)</p>	<p>LISFLOOD model. Basically, the model is made up of the following components:</p> <ul style="list-style-type: none"> <li>• a 2-layer soil water balance sub-model</li> <li>• sub-models for the simulation of groundwater and subsurface flow (using 2 parallel interconnected linear reservoirs)</li> <li>• a sub-model for the routing of surface runoff to the nearest river channel</li> <li>• a sub-model for the routing of channel flow (not shown in the Figure)</li> </ul> <p>The processes that are simulated by the model include snow melt (not shown in the figure), infiltration, interception of rainfall, leaf drainage, evaporation and water uptake by vegetation, surface runoff, preferential flow (bypass of soil layer), exchange of soil moisture between the two soil layers and drainage to the groundwater, sub-surface and groundwater flow, and flow through river channels.</p>
---	--





Scheme of model structure



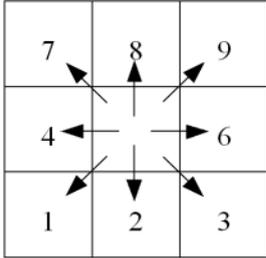
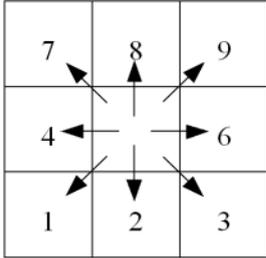
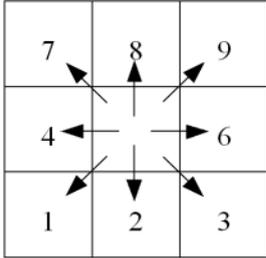
Overview of the LISFLOOD model.  $P$  = precipitation;  $Int$  = interception;  $EW_{int}$  = evaporation of intercepted water;  $D_{int}$  = leaf drainage;  $ES_a$  = evaporation from soil surface;  $T_a$  = transpiration (water uptake by plant roots);  $INF_{act}$  = infiltration;  $R_s$  = surface runoff;  $D_{1,2}$  = drainage from top- to subsoil;  $D_{2,gw}$  = drainage from subsoil to upper groundwater zone;  $D_{pref,gw}$  = preferential flow to upper groundwater zone;  $D_{uz,lz}$  = drainage from upper- to lower groundwater zone;  $Q_{uz}$  = outflow from upper groundwater zone;  $Q_{lz}$  = outflow from lower groundwater zone;  $D_{loss}$  = loss from lower



	<b>groundwater zone. Note that snowmelt is not included in the Figure (even though it is simulated by the model).</b>
<b>3. Model parameters</b>	
Distribution of model parameters (yes/no)	Yes
Number of free parameters	Numerous free parameters ( <a href="http://publications.jrc.ec.europa.eu/repository/bitstream/JRC78917/lisflood_2013_online.pdf">http://publications.jrc.ec.europa.eu/repository/bitstream/JRC78917/lisflood_2013_online.pdf</a> ).
Procedure of model parameter estimation (measurement, manual or automatic algorithm, etc.)	"A calibration exercise completed in 2013 (Zajac et al., 2013) produced Europe wide parameter maps based on the estimation of parameter values for 693 catchments. Estimation was carried out using the Standard Particle Swarm 2011 (SPSO-2011) algorithm (Zambrano-Bigiarini and Rojas, 2013) and a root mean squared error criteria. For 659 of these a set of 9 parameters that control snowmelt, infiltration, preferential bypass flow through the soil matrix, percolation to the lower ground water zone, percolation to deeper groundwater zones, residence times in the soil and subsurface reservoirs and river routing, were estimated by calibrating the model against historical records of river discharge. For the remaining 34 catchments the option to represent





	reservoirs was used requiring the calibration of four additional parameters related to reservoir operation; though neglecting the calibration of the deepest groundwater store resulted in 12 calibration parameters for these catchments." (Smith et al., 2016)																																				
4. Model inputs / Model outputs																																					
List and characteristics of input variables (type, time step, spatial resolution, etc.)	<table border="1"> <thead> <tr> <th colspan="4" data-bbox="450 719 1350 775"><i>Table A12.1 LISFLOOD input maps (continued on next pages)</i></th> </tr> <tr> <th colspan="4" data-bbox="450 775 1350 797">GENERAL</th> </tr> <tr> <th data-bbox="450 797 619 819">Map</th> <th data-bbox="619 797 794 819">Default name<sup>15</sup></th> <th data-bbox="794 797 992 819">Units, range</th> <th data-bbox="992 797 1350 819">Description</th> </tr> </thead> <tbody> <tr> <td data-bbox="450 819 619 875">MaskMap</td> <td data-bbox="619 819 794 875">area.map</td> <td data-bbox="794 819 992 875">Unit: - Range: 0 or 1</td> <td data-bbox="992 819 1350 875">Boolean map that defines model boundaries</td> </tr> <tr> <th colspan="4" data-bbox="450 875 1350 898">TOPOGRAPHY</th> </tr> <tr> <th data-bbox="450 898 619 920">Map</th> <th data-bbox="619 898 794 920">Default name</th> <th data-bbox="794 898 992 920">Units, range</th> <th data-bbox="992 898 1350 920">Description</th> </tr> <tr> <td data-bbox="450 920 619 1491">Ldd</td> <td data-bbox="619 920 794 1491">ldd.map</td> <td data-bbox="794 920 992 1491">U.: flow directions R.: <math>1 \leq \text{map} \leq 9</math></td> <td data-bbox="992 920 1350 1491">local drain direction map (with value 1-9); this file contains flow directions from each cell to its steepest downslope neighbour. Ldd directions are coded according to the following diagram:  This resembles the numeric key pad of your PC's keyboard, except for the value 5, which defines a cell without local drain direction (pit). The pit cell at the end of the path is the outlet point of a catchment.</td> </tr> <tr> <td data-bbox="450 1491 619 1536">Grad</td> <td data-bbox="619 1491 794 1536">gradient.map</td> <td data-bbox="794 1491 992 1536">U.: [m m<sup>-1</sup>] R.: map &gt; 0 !!!</td> <td data-bbox="992 1491 1350 1536">Slope gradient</td> </tr> <tr> <td data-bbox="450 1536 619 1592">Elevation Stdev</td> <td data-bbox="619 1536 794 1592">elvstd.map</td> <td data-bbox="794 1536 992 1592">U.: [m] R.: map ≥ 0</td> <td data-bbox="992 1536 1350 1592">Standard deviation of elevation</td> </tr> </tbody> </table>	<i>Table A12.1 LISFLOOD input maps (continued on next pages)</i>				GENERAL				Map	Default name <sup>15</sup>	Units, range	Description	MaskMap	area.map	Unit: - Range: 0 or 1	Boolean map that defines model boundaries	TOPOGRAPHY				Map	Default name	Units, range	Description	Ldd	ldd.map	U.: flow directions R.: $1 \leq \text{map} \leq 9$	local drain direction map (with value 1-9); this file contains flow directions from each cell to its steepest downslope neighbour. Ldd directions are coded according to the following diagram:  This resembles the numeric key pad of your PC's keyboard, except for the value 5, which defines a cell without local drain direction (pit). The pit cell at the end of the path is the outlet point of a catchment.	Grad	gradient.map	U.: [m m <sup>-1</sup> ] R.: map > 0 !!!	Slope gradient	Elevation Stdev	elvstd.map	U.: [m] R.: map ≥ 0	Standard deviation of elevation
<i>Table A12.1 LISFLOOD input maps (continued on next pages)</i>																																					
GENERAL																																					
Map	Default name <sup>15</sup>	Units, range	Description																																		
MaskMap	area.map	Unit: - Range: 0 or 1	Boolean map that defines model boundaries																																		
TOPOGRAPHY																																					
Map	Default name	Units, range	Description																																		
Ldd	ldd.map	U.: flow directions R.: $1 \leq \text{map} \leq 9$	local drain direction map (with value 1-9); this file contains flow directions from each cell to its steepest downslope neighbour. Ldd directions are coded according to the following diagram:  This resembles the numeric key pad of your PC's keyboard, except for the value 5, which defines a cell without local drain direction (pit). The pit cell at the end of the path is the outlet point of a catchment.																																		
Grad	gradient.map	U.: [m m <sup>-1</sup> ] R.: map > 0 !!!	Slope gradient																																		
Elevation Stdev	elvstd.map	U.: [m] R.: map ≥ 0	Standard deviation of elevation																																		



<b>Table A12.1 LISFLOOD input maps (continued from previous page)</b>			
<b>LAND USE - fraction maps</b>			
<b>Map</b>	<b>Default name</b>	<b>Units, range</b>	<b>Description</b>
Fraction of water	fracwater.map	U.: [-] R.: $0 \leq \text{map} \leq 1$	Fraction of inland water for each cell. Values range from 0 (no water at all) to 1 (pixel is 100% water)
Fraction of sealed surface	fracsealed.map	U.: [-] R.: $0 \leq \text{map} \leq 1$	Fraction of impermeable surface for each cell. Values range from 0 (100% permeable surface - no urban at all) to 1 (100% impermeable surface).
Fraction of forest	fracforest.map	U.: [-] R.: $0 \leq \text{map} \leq 1$	Forest fraction for each cell. Values range from 0 (no forest at all) to 1 (pixel is 100% forest)
Fraction of other land cover	fracother.map	U.: [] R.: $0 \leq \text{map} \leq 1$	Other (agricultural areas, non-forested natural area, pervious surface of urban areas) fraction for each cell.
<b>LAND COVER depending maps</b>			
<b>Map</b>	<b>Default name</b>	<b>Units, range</b>	<b>Description</b>
Crop coef. for forest	cropcoef_forest.map	U.: [-] R.: $0.8 \leq \text{map} \leq 1.2$	Crop coefficient for forest
Crop coef. for other	cropcoef_other.map	U.: [-] R.: $0.8 \leq \text{map} \leq 1.2$	Crop coefficient for other
Crop group number for forest	crgrnum_forest.map	U.: [-] R.: $1 \leq \text{map} \leq 5$	Crop group number for forest
Crop group number for other	crgrnum_other.map	U.: [-] R.: $1 \leq \text{map} \leq 5$	Crop group number for other
Manning for forest	mannings_forest.map	U.: [-] R.: $0.2 \leq \text{map} \leq 0.4$	Manning's roughness for forest
Manning for other	mannings_other.map	U.: [-] R.: $0.01 \leq \text{map} \leq 0.3$	Manning's roughness for other
Soil depth for forest for layer1	soildep1_forest.map	U.: [mm] R.: $\text{map} \geq 50$	Forest soil depth for soil layer 1 (rooting depth)
Soil depth for other for layer2	soildep1_other.map	U.: [mm] R.: $\text{map} \geq 50$	Other soil depth for soil layer 1 (rooting depth)
Soil depth for forest for layer2	soildep2_forest.map	U.: [mm] R.: $\text{map} \geq 50$	Forest soil depth for soil layer 2
Soil depth for other for layer2	soildep2_other.map	U.: [mm] R.: $\text{map} \geq 50$	Other soil depth for soil layer 2





<b>Table A12.1 LISFLOOD input maps (continued from previous page)</b>			
<b>SOIL HYDRAULIC PROPERTIES (depending on soil texture)</b>			
<b>Map</b>	<b>Default name</b>	<b>Units, range</b>	<b>Description</b>
ThetaSat1 for forest	thetas1_forest.map	U: [-] R: 0 < map < 1	Saturated volumetric soil moisture content layer 1
ThetaSat1 for other	thetas1_other.map	U: [-] R: 0 < map < 1	Saturated volumetric soil moisture content layer 1
ThetaSat2 for forest and other	thetas2.map	U: [-] R: 0 < map < 1	Saturated volumetric soil moisture content layer 2
ThetaRes1 for forest	thetar1_forest.map	U: [-] R: 0 < map < 1	Residual volumetric soil moisture content layer 1
ThetaRes1 for other	thetar1_other.map	U: [-] R: 0 < map < 1	Residual volumetric soil moisture content layer 1
ThetaRes2 for forest and other	thetar2.map	U: [-] R: 0 < map < 1	Residual volumetric soil moisture content layer 2
Lambda1 for forest	lambda1_forest.map	U: [-] R: 0 < map < 1	Pore size index ( $\lambda$ ) layer 1
Lambda1 for other	lambda1_other.map	U: [-] R: 0 < map < 1	Pore size index ( $\lambda$ ) layer 1
Lambda2 for forest and other	lambda2.map	U: [-] R: 0 < map < 1	Pore size index ( $\lambda$ ) layer 2
GenuAlpha1 for forest	alpha1_forest.map	U: [-] R: 0 < map < 1	Van Genuchten parameter $\alpha$ layer 1
GenuAlpha1 for other	alpha1_other.map	U: [-] R: 0 < map < 1	Van Genuchten parameter $\alpha$ layer 1
GenuAlpha2 for forest and other	alpha2.map	U: [-] R: 0 < map < 1	Van Genuchten parameter $\alpha$ layer 2
Sat1 for forest	ksat1_forest.map	U: [cm day <sup>-1</sup> ] R: 1 ≤ map ≤ 100	Saturated conductivity layer 1
Sat1 for other	ksat1_other.map	U: [cm day <sup>-1</sup> ] R: 1 ≤ map ≤ 100	Saturated conductivity layer 1
Sat2 for forest and other	ksat2.map	U: [cm day <sup>-1</sup> ] R: 1 ≤ map ≤ 100	Saturated conductivity layer 2



<b>Table A12.1 LISFLOOD input maps (continued from previous page)</b>			
<b>CHANNEL GEOMETRY</b>			
<b>Map</b>	<b>Default name</b>	<b>Units, range</b>	<b>Description</b>
Channels	chan.map	U: [-] R: 0 or 1	Map with Boolean 1 for all channel pixels, and Boolean 0 for all other pixels on MaskMap
ChanGrad	changrad.map	U: [m m <sup>-1</sup> ] R: map > 0 !!!	Channel gradient
ChanMan	chanman.map	U: [-] R: map > 0	Manning's roughness coefficient for channels
ChanLength	chanleng.map	U: [m] R: map > 0	Channel length (can exceed grid size, to account for meandering rivers)
ChanBottomWidth	chanbw.map	U: [m] R: map > 0	Channel bottom width
ChanSdXdY	chans.map	U: [m m <sup>-1</sup> ] R: map ≥ 0	Channel side slope <b>Important:</b> defined as horizontal divided by vertical distance (dx/dy); this may be confusing because slope is usually defined the other way round (i.e. dy/dx)!
ChanDepth Threshold	chanbnkf.map	U: [m] R: map > 0	Bankfull channel depth
<b>METEOROLOGICAL VARIABLES</b>			
<b>Map</b>	<b>Default prefix</b>	<b>Units, range</b>	<b>Description</b>
Precipitation Maps	pr	U: [mm day <sup>-1</sup> ] R: map ≥ 0	Precipitation rate
TavgMaps	ta	U: [°C] R: -50 ≤ map ≤ +50	Average <i>daily</i> temperature\
E0Maps	e	U: [mm day <sup>-1</sup> ] R: map ≥ 0	Daily potential evaporation rate, free water surface
ES0Maps	es	U: [mm day <sup>-1</sup> ] R: map ≥ 0	Daily potential evaporation rate, bare soil
ET0Maps	et	U: [mm day <sup>-1</sup> ] R: map ≥ 0	Daily potential evapotranspiration rate, reference crop
<b>DEVELOPMENT OF VEGETATION OVER TIME</b>			
<b>Map</b>	<b>Default prefix</b>	<b>Units, range</b>	<b>Description</b>
LAIMaps for forest	lai_forest	U: [m <sup>2</sup> m <sup>-2</sup> ] R: map ≥ 0	Pixel-average Leaf Area Index for forest
LAIMaps for other	lai_other	U: [m <sup>2</sup> m <sup>-2</sup> ] R: map ≥ 0	Pixel-average Leaf Area Index for other
<b>DEFINITION OF INPUT/OUTPUT TIMESERIES</b>			
<b>Map</b>	<b>Default name</b>	<b>Units, range</b>	<b>Description</b>
Gauges	outlets.map	U: [-] R: For each station an individual number	Nominal map with locations at which discharge timeseries are reported (usually correspond to gauging stations)
Sites	sites.map	U: [-] R: For each station an individual number	Nominal map with locations (individual pixels or areas) at which timeseries of intermediate state and rate variables are reported (soil moisture, infiltration, snow, etcetera)





	<i>Table A12.2 Optional maps that define grid size</i>			
	<b>Map</b>	<b>Default name</b>	<b>Units, range</b>	<b>Description</b>
	PixelLengthUser	pixleng.map	U.: [m] R.: map > 0	Map with pixel length
	PixelAreaUser	pixarea.map	U.: [m] R.: map > 0	Map with pixel area
	<i>Table A12.3 LISFLOOD input tables</i>			
	<b>LAND USE</b>			
	<b>Table</b>	<b>Default name</b>	<b>Description</b>	
	Day of the year -> LAI	LaiOfDay.txt	Lookup table: Day of the year -> LAI map	
List and characteristics of output variables (type, time step, spatial resolution, etc.)	<i>Table A13.1 LISFLOOD default output time series</i>			
	<b>RATE VARIABLES AT GAUGES</b>			
	<b>Description</b>	<b>Units</b>	<b>Settings variable</b>	<b>File name</b>
	<sup>1,2</sup> channel discharge	m <sup>3</sup> s <sup>-1</sup>	disTS	dis.tss
	<b>NUMERICAL CHECKS</b>			
	<b>Description</b>	<b>Units</b>		<b>File name</b>
	<sup>2</sup> cumulative mass balance error	m <sup>3</sup>	WaterMassBalanceTSS	mbError.tss
	<sup>2</sup> cumulative mass balance error, expressed as mm water slice (average over catchment)	mm	MassBalanceMM TSS	mbErrorMm.tss
	<sup>2</sup> number of sub-steps needed for channel routing	-	NoSubStepsChan	NoSubStepsChannel.tss
	<sup>2</sup> number of sub-steps needed for gravity-based soil moisture routine	-	StepsSoilTS	steps.tss
	<sup>1</sup> Output only if option 'InitLisflood' = 1 (pre-run)			
	<sup>2</sup> Output only if option 'InitLisflood' = 0			



<b>Table A13.2 LISFLOOD optional output time series (only 'InitLisflood' = 0) (continued on next pages)</b>			
<b>STATE VARIABLES AT SITES (option repStateSites)<sup>16</sup></b>			
Description	Units	Settings variable	Default name
depth of water on soil surface	mm	WaterDepthTS	wDepth.tss
depth of snow cover on soil surface (pixel-average) <sup>17</sup>	mm	SnowCoverTS	snowCover.tss
depth of interception storage	mm	CumInterceptionTS	cumInt.tss
soil moisture content upper layer	mm <sup>3</sup> / mm <sup>3</sup>	Theta1TS	thTop.tss
soil moisture content lower layer	mm <sup>3</sup> / mm <sup>3</sup>	Theta2TS	thSub.tss
storage in upper groundwater zone	mm	UZTS	uz.tss
storage in lower groundwater zone	mm	LZTS	lz.tss
number of days since last rain	days	DSLRTS	dslr.tss
frost index	°C days <sup>-1</sup>	FrostIndexTS	frost.tss
<b>Table A13.2 LISFLOOD optional output time series (continued from previous page)</b>			
<b>RATE VARIABLES AT SITES (option repRateSites)<sup>18</sup></b>			
Description	Units	Settings variable	Default name
rain (excluding snow)	mm/timestep	RainTS	rain.tss
snow <sup>19</sup>	mm/timestep	SnowTS	snow.tss
snow melt	mm/timestep	SnowmeltTS	snowMelt.tss
actual evaporation	mm/timestep	ESActTS	esAct.tss
actual transpiration	mm/timestep	TaTS	tAct.tss
rainfall interception	mm/timestep	InterceptionTS	interception.tss
evaporation of intercepted water	mm/timestep	EWIntTS	ewIntAct.tss
leaf drainage	mm/timestep	LeafDrainageTS	leafDrainage.tss
infiltration	mm/timestep	InfiltrationTS	infiltration.tss
preferential (bypass) flow	mm/timestep	PrefFlowTS	prefFlow.tss
percolation upper to lower soil layer	mm/timestep	PercolationTS	dTopToSub.tss
percolation lower soil layer to subsoil	mm/timestep	SeepSubToGWTS	dSubToUz.tss
surface runoff	mm/timestep	SurfaceRunoffTS	surfaceRunoff.tss
outflow from upper zone	mm/timestep	UZOutflowTS	qUz.tss
outflow from lower zone	mm/timestep	LZOutflowTS	qLz.tss
total runoff	mm/timestep	TotalRunoffTS	totalRunoff.tss
percolation from upper to lower zone	mm/timestep	GwPercUZLZTS	percUZLZ.tss
loss from lower zone	mm/timestep	GwLossTS	loss.tss





<b>TIME SERIES, AVERAGE UPSTREAM OF GAUGES</b>				
<b>METEOROLOGICAL INPUT VARIABLES (option repMeteoUpsGauges)</b>				
Description	Units	Settings variable	Default name	
precipitation	mm/timestep	PrecipitationAvUpsTS	precipUps.tss	
potential reference evapotranspiration	mm/timestep	ETRefAvUpsTS	etUps.tss	
potential evaporation from soil	mm/timestep	ESRefAvUpsTS	esUps.tss	
potential open water evaporation	mm/timestep	EWRefAvUpsTS	ewUps.tss	
average daily temperature	°C	TavgAvUpsTS	tAvgUps.tss	
<i>Table A13.2 LISFLOOD optional output time series (continued from previous page)</i>				
<b>STATE VARIABLES (option repStateUpsGauges)</b>				
Description	Units	Settings variable	Default name	
depth of water on soil surface	mm	WaterDepthAvUpsTS	wdepthUps.tss	
depth of snow cover on	mm	SnowCoverAvUpsTS	snowCoverUps.tss	
depth of interception storage	mm	CumInterceptionAvUpsTS	cumInterceptionUps.tss	
soil moisture upper layer	mm <sup>3</sup> / mm <sup>3</sup>	Theta1AvUpsTS	thTopUps.tss	
soil moisture lower layer	mm <sup>3</sup> / mm <sup>3</sup>	Theta2AvUpsTS	thSubUps.tss	
groundwater upper zone	mm	UZAvUpsTS	uzUps.tss	
groundwater lower zone	mm	LZAvUpsTS	lzUps.tss	
number of days since last rain	Days	DSLRAvUpsTS	dslrUps.tss	
frost index	°C days <sup>-1</sup>	FrostIndexAvUpsTS	frostUps.tss	
<i>Table A13.2 LISFLOOD optional output time series (continued from previous page)</i>				
<b>RATE VARIABLES (option repRateUpsGauges)</b>				
Description	Units	Settings variable	Default name	
rain (excluding snow)	mm/timestep	RainAvUpsTS	rainUps.tss	
snow <sup>20</sup>	mm/timestep	SnowAvUpsTS	snowUps.tss	
snow melt	mm/timestep	SnowmeltAvUpsTS	snowMeltUps.tss	
actual evaporation	mm/timestep	ESActAvUpsTS	esActUps.tss	
actual transpiration	mm/timestep	TaAvUpsTS	tActUps.tss	
rainfall interception	mm/timestep	InterceptionAvUpsTS	interceptionUps.tss	
evaporation of intercepted water	mm/timestep	EWIntAvUpsTS	ewIntActUps.tss	
leaf drainage	mm/timestep	LeafDrainageAvUpsTS	leafDrainageUps.tss	
infiltration	mm/timestep	InfiltrationAvUpsTS	infiltrationUps.tss	
preferential (bypass) flow	mm/timestep	PrefFlowAvUpsTS	prefFlowUps.tss	
percolation upper to lower soil layer	mm/timestep	PercolationAvUpsTS	dTopToSubUps.tss	
percolation lower soil layer to subsoil	mm/timestep	SeepSubToGWAvUpsTS	dSubToUzUps.tss	
surface runoff	mm/timestep	SurfaceRunoffAvUpsTS	surfaceRunoffUps.tss	
outflow from upper zone	mm/timestep	UZOutflowAvUpsTS	qUzUps.tss	
outflow from lower zone	mm/timestep	LZOutflowAvUpsTS	qLzUps.tss	
total runoff	mm/timestep	TotalRunoffAvUpsTS	totalRunoffUps.tss	
percolation upper to lower zone	mm/timestep	GwPercUZLZAvUpsTS	percUZLZUps.tss	
loss from lower zone	mm/timestep	GwLossTS	lossUps.tss	
<b>WATER LEVEL IN CHANNEL (option repWaterLevelTs)</b>				
Description	Units	Settings variable	Default name	
water level in channel	m (above channel bottom)	WaterLevelTS	waterLevel.tss	
<b>OUTPUT RELATED TO LOWER ZONE INITIALISATION</b>				
Description	Option		Settings variable	Default name
average inflow into lower zone	repLZAvInflowSites	mm day <sup>-1</sup>	LZAvInflowTS	lzAvIn.tss
average inflow into lower zone	repLZAvInflowUpsGauges	mm day <sup>-1</sup>	LZAvInflowAvUpsTS	lzAvInUps.tss



<b>Table A13.3 LISFLOOD default output maps</b>			
<b>AVERAGE RECHARGE MAP (for lower groundwater zone) (option InitLisflood)</b>			
Description	Units	File name	Domain
<sup>1</sup> average inflow to lower zone	mm day <sup>-1</sup>	lzavin.map	other fraction
<sup>1</sup> average inflow to lower zone (forest)	mm day <sup>-1</sup>	lzavin_forest.map	forest fraction
<b>INITIAL CONDITION MAPS at defined time steps<sup>21</sup> (option repStateMaps)</b>			
Description	Units	File name <sup>22</sup>	Domain
<sup>2</sup> waterdepth	mm	wdepth00.xxx	whole pixel
<sup>2</sup> channel cross-sectional area	m <sup>2</sup>	chcro000.xxx	channel
<sup>2</sup> days since last rain variable	days	dslr0000.xxx	other pixel
<sup>2</sup> snow cover zone A <sup>23</sup>	mm	scova000.xxx	snow zone A (1/3 <sup>rd</sup> pixel)
<sup>2</sup> snow cover zone B	mm	scovb000.xxx	snow zone B (1/3 <sup>rd</sup> pixel)
<sup>2</sup> snow cover zone C	mm	scovc000.xxx	snow zone C (1/3 <sup>rd</sup> pixel)
<sup>2</sup> frost index	°C days <sup>-1</sup>	frost000.xxx	other pixel
<sup>2</sup> cumulative interception	mm	cumi0000.xxx	other pixel
<sup>2</sup> soil moisture upper layer	mm <sup>3</sup> /mm <sup>3</sup>	thtop000.xxx	other fraction
<sup>2</sup> soil moisture lower layer	mm <sup>3</sup> /mm <sup>3</sup>	thsub000.xxx	other fraction
<sup>2</sup> water in lower zone	mm	lz000000.xxx	other fraction
<sup>2</sup> water in upper zone	mm	uz000000.xxx	other fraction
<sup>2</sup> days since last rain variable (forest)	days	dslF0000.xxx	forest pixel
<sup>2</sup> cumulative interception (forest)	mm	cumF0000.xxx	forest pixel
<sup>2</sup> soil moisture upper layer (forest)	mm <sup>3</sup> /mm <sup>3</sup>	thFt0000.xxx	forest fraction
<sup>2</sup> soil moisture lower layer (forest)	mm <sup>3</sup> /mm <sup>3</sup>	thFs0000.xxx	forest fraction
<sup>2</sup> water in lower zone (forest)	mm	lzF00000.xxx	forest fraction
<sup>2</sup> water in upper zone (forest)	mm	uzF00000.xxx	forest fraction
<sup>2</sup> water in depression storage (sealed)	mm	cseal000.xxx	sealed fraction
<sup>1</sup> Output only if option 'InitLisflood' = 1 (pre-run)			
<sup>2</sup> Output only if option 'InitLisflood' = 0			





<b>Table A13.4 LISFLOOD optional output maps (only 'InitLisflood' = 0) (continued on next page)</b>				
<b>DISCHARGE AND WATER LEVEL</b>				
Description	Option	Units	Settings variable	Prefix
discharge	repDischargeMaps	m <sup>3</sup> s <sup>-1</sup>	DischargeMaps	dis
water level	repWaterLevelMaps	m (above channel bottom)	WaterLevelMaps	wl
<b>METEOROLOGICAL INPUT VARIABLES</b>				
Description	Option		Settings variable	Prefix
precipitation	repPrecipitationMaps	mm	PrecipitationMaps	pr
potential reference evapotranspiration	repETRefMaps	mm	ETRefMaps	et
potential evaporation from soil	repESRefMaps	mm	ESRefMaps	es
potential open water evaporation	repEWRefMaps	mm	EWRefMaps	ew
average daily temperature	repTavgMaps	mm	TavgMaps	tav
<b>STATE VARIABLES<sup>24</sup></b>				
Description	Option		Settings variable	Prefix
depth of water on soil surface	repWaterDepthMaps	mm	WaterDepthMaps	wdep
channel cross-sectional area	repChanCrossSectionMaps	m <sup>2</sup>	ChanCrossSectionMaps	chcro
depth of snow cover on soil surface	repSnowCoverMaps	mm	SnowCoverMaps	scov
depth of interception storage	repCumInterceptionMaps	mm	CumInterceptionMaps CumInterceptionForestMaps	cumi cumF
soil moisture content upper layer	repTheta1Maps	mm <sup>3</sup> / mm <sup>3</sup>	Theta1Maps Theta1ForestMaps	thtop thFt
soil moisture content lower layer	repTheta2Maps	mm <sup>3</sup> / mm <sup>3</sup>	Theta2Maps Theta2ForestMaps	thsub thFs
storage in upper groundwater zone	repUZMaps	mm	UZMaps UZForestMaps	uz uzF
storage in lower groundwater zone	repLZMaps	mm	LZMaps LZForestMaps	lz lzF
number of days since last rain	repDSLRLMaps	days	DSLRLMaps DSLRLForestMaps	dslr dslF
frost index	repFrostIndexMaps	°C days <sup>-1</sup>	FrostIndexMaps	frost
<b>RATE VARIABLES<sup>25</sup></b>				
Description	Option		Settings variable	Prefix
rain (excluding snow)	repRainMaps	mm/timestep	RainMaps	rain
snow <sup>26</sup>	repSnowMaps	mm/timestep	SnowMaps	snow
snow melt	repSnowMeltMaps	mm/timestep	SnowMeltMaps	smelt
actual evaporation	repESActMaps	mm/timestep	ESActMaps	esact
actual transpiration	repTaMaps	mm/timestep	TaMaps	tact
rainfall interception	repInterceptionMaps	mm/timestep	InterceptionMaps	int
evaporation of intercepted water	repEWIntMaps	mm/timestep	EWIntMaps	ewint
leaf drainage	repLeafDrainageMaps	mm/timestep	LeafDrainageMaps	ldra
infiltration	repInfiltrationMaps	mm/timestep	InfiltrationMaps	inf
<b>Table 12.4 LISFLOOD optional output maps (continued from previous page)</b>				
preferential (bypass) flow	repPrefFlowMaps	mm/timestep	PrefFlowMaps	pflow
percolation upper to lower soil layer	repPercolationMaps	mm/timestep	PercolationMaps	to2su
percolation lower soil layer to subsoil	repSeepSubToGWMaps	mm/timestep	SeepSubToGWMaps	su2gw
surface runoff	repSurfaceRunoffMaps	mm/timestep	SurfaceRunoffMaps	srun
outflow from upper zone	repUZOutflowMaps	mm/timestep	UZOutflowMaps	quz
outflow from lower zone	repLZOutflowMaps	mm/timestep	LZOutflowMaps	qlz
total runoff	repTotalRunoffMaps	mm/timestep	TotalRunoffMaps	trun
percolation upper to lower zone	repGwPercUZLZMaps	mm/timestep	GwPercUZLZMaps	uz2lz
loss from lower zone	repGwLossMaps	mm/timestep	GwLossMaps	loss
<b>5. Examples of previous model applications</b>				



<p>Catchments, objectives, etc.</p> <p>Results of existing comparisons with other models</p>	
<p><b>6. List of selected references</b></p>	
	<ul style="list-style-type: none"> <li>● De Roo, A. P. J., C. G. Wesseling, and W. P. A. Van Deursen, 2000: Physically Based River Basin Modelling within a GIS: The LISFLOOD Model. <i>Hydrological Processes</i>, <b>14</b>, 11-12, 1981–92. doi:10.1002/1099-1085(20000815/30)14:11/12&lt;1981::AID-HYP49&gt;3.0.CO;2-F.</li> <li>● "LISFLOOD - Distributed Water Balance and Flood Simulation Model - Revised User Manual 2013 - EU Science Hub - European Commission." 2013. EU Science Hub. October 14. <a href="https://ec.europa.eu/jrc/en/publication/eur-scientific-and-technical-research-reports/lisflood-distributed-water-balance-and-flood-simulation-model-revised-user-manual-2013">https://ec.europa.eu/jrc/en/publication/eur-scientific-and-technical-research-reports/lisflood-distributed-water-balance-and-flood-simulation-model-revised-user-manual-2013</a>.</li> <li>● Smith, Paul, Florian Pappenberger, Fredrik Wetterhall, Jutta Thielen, Blazej Krzeminski, Peter Salamon, Davide Muraro, Milan Kalas, and Calum Baugh. 2016. On the Operational Implementation of the European Flood Awareness System (EFAS). European Centre for Medium-Range Weather Fore-</li> </ul>





	<p>casts.</p> <p><a href="http://www.ecmwf.int/sites/default/files/elibrary/2016/16337-operational-implementation-european-flood-awareness-system-efas.pdf">http://www.ecmwf.int/sites/default/files/elibrary/2016/16337-operational-implementation-european-flood-awareness-system-efas.pdf</a>.</p> <ul style="list-style-type: none"><li>● Bódis, K., 2009. Development of a data set for continental hydrologic modelling.</li><li>● De Roo, A., Thielen, J., Gouweleeuw, B., 2003. LISFLOOD, a Distributed WaterBalance, Flood Simulation, and Flood Inundation Model, User Manual version 1.2. Internal report, Joint Research Center of the European Communities, Ispra, Italy, 74 pp.</li><li>● Hock, R., 2003. Temperature index melt modelling in mountain areas. <i>Journal of Hydrology</i>, 282(1-4), 104–115.</li><li>● Van Der Knijff, J., De Roo, A., 2006. LISFLOOD – Distributed Water Balance and Flood Simulation Model, User Manual. EUR 22166 EN, Office for Official Publications of the European Communities, Luxembourg, 88 pp.</li><li>● Van der Knijff, J., 2008. LISVAP– Evaporation Pre-Processor for the LISFLOOD Water Balance and Flood Simulation Model, Revised User Manual. EUR 22639 EN/2, Office for Official Publications of the European Communities, Luxembourg, 31 pp.</li><li>● Van Der Knijff, J., De Roo, A., 2008. LISFLOOD – Distributed Water Balance and Flood Simulation Model, Revised User Manual. EUR 22166 EN/2, Office for Official Publications of the European Communities, Luxembourg, 109 pp.</li><li>● Van der Knijff, J. M., Younis, J. and de Roo, A. P. J.: LISFLOOD: A GIS-based distributed model for river basin scale water balance and flood simulation, <i>Int. J. Geogr. Inf. Sci.</i>, 24(2), 189–212, 2010.</li></ul>
--	--



Table 8 Tabulated overview on hydrological model features of wflow\_w3ra

<b>1. General Information</b>	
Model name	wflow_w3ra (World Wide Water Resources Analysis) + wflow_routing
Version	v1
Author(s) / First publication	Van Dijk et al. (2013)
Contact person	Albrecht Weerts (albrecht.weerts@deltares.nl) Jaap Schellekens (jaap.schellekens@deltares.nl)
Institute	Deltares
Website	<a href="https://github.com/openstreams/wflow">https://github.com/openstreams/wflow</a>
General modelling objectives	Calculation/prediction of hydrological water resources
Domain of applicability (catchment types and climate conditions)	The W3RA model has been applied on global scale
<b>2. Model description</b>	

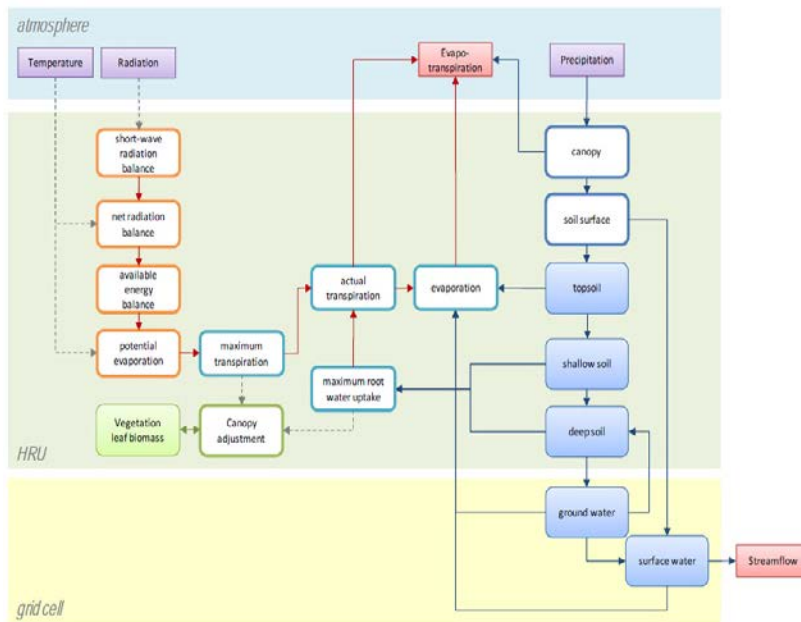




Model type (empirical, conceptual, physically based)	Conceptual/Process-based model
Continuous or event-based	Continuous
Possible running time steps	Daily (also hourly)
Spatial discretization (lumped, semidistributed, distributed)	Spatially distributed at the sub-basin scale. Sub-basin resolution depends on the application. In Europe, this is 215 km <sup>2</sup> .
Short description of model structure detailing main function (evaporation, soil moisture accounting, groundwater, routing, snowmelt, etc.)	<p style="text-align: center;"><b>World Wide Water Resources Assessment (W3RA)</b>  Rainfall-Runoff Model of the ANU  Based on the BoM Australian Water Resources Assessment (AWRA) model  Estimates water storage in three soil layers, shallow groundwater &amp; streams  Incorporates HBV-96 snow module  0.5° Resolution (~50 km) , Soon to be 5 km  River Network derived from NASA SRTM 90 m resolution digital elevation data and HydroSHEDS</p> <p style="text-align: center;"><b>wflow</b>  Deltares River Routing Model  Run at the resolutions of the Rainfall-Runoff Models</p> <p>from Emmerton et al. (2016)</p>



Scheme of model structure



Simplified conceptual diagram of the W3RA model structure. Shown are: the minimum dynamic inputs (atmosphere); aggregated water losses form the grid cell (evapotranspiration and streamflow); water fluxes and model states (tech report 3 AWRA-L).

<p><b>3. Model parameters</b></p>	
<p>Distribution of model parameters (yes/no)</p>	<p>Yes</p>
<p>Number of free parameters</p>	<p>Numerous free parameters (van Dijk et al, 2013 and references therein)</p>
<p>Procedure of model</p>	<p>Many of the parameters are linked to physiographic</p>





parameter estimation (measurement, manual or automatic algorithm, etc.)	characteristics in the landscape (see van Dijk et al. 2013 and references therein)
<b>4. Model inputs / Model outputs</b>	
List and characteristics of input variables (type, time step, spatial resolution, etc.)	The main dynamic variables are climate forcing data such as precipitation, temperature and potential evaporation. Other observations can also be used for different purposes.
List and characteristics of output variables (type, time step, spatial resolution, etc.)	The exported time-step depends on the user, i.e. hourly, daily. The variables (states and fluxes) can be exported for the whole grid or selected gauge locations .
<b>5. Examples of previous model applications</b>	



Catchments, objectives, etc. Results of existing comparisons with other models	Schellekens, J., Dutra, E., Martínez-de la Torre, A., Balsamo, G., van Dijk, A., Sperna Weiland, F., Minvielle, M., Calvet, J.-C., Decharme, B., Eisner, S., Fink, G., Flörke, M., Peßenteiner, S., van Beek, R., Polcher, J., Beck, H., Orth, R., Calton, B., Burke, S., Dorigo, W., and Weedon, G. P.: A global water resources ensemble of hydrological models: the earth2Observe Tier-1 dataset, <i>Earth Syst. Sci. Data Discuss.</i> , doi:10.5194/essd-2016-55, in review, 2016.
<b>6. List of selected references</b>	
	Van Dijk, Pea-Arancibia, J. L., Wood, E. F., Sheffield, J., & Beck, H. E. (2013). Global analysis of seasonal streamflow predictability using an ensemble prediction system and observations from 6192 small catchments worldwide. <i>Water Resources Research</i> , 49(5), 2729–2746. <a href="http://doi.org/10.1002/wrcr.20251">http://doi.org/10.1002/wrcr.20251</a>

Table 9 Tabulated overview on hydrological model features of wflow\_hbv

<b>1. General Information</b>	
Model name	wflow_hbv
Version	V1
Author(s) / First publication	Lindstrom et al. (1997), see also Rakovec et al. (2012, 2015)





Contact person	Albrecht Weerts (albrecht.weerts@deltares.nl)
Institute	Deltares
Website	<a href="https://github.com/openstreams/wflow">https://github.com/openstreams/wflow</a>
General modelling objectives	Calculation/prediction of hydrological water resources
Domain of applicability (catchment types and climate conditions)	wflow_hbv has been applied on catchment to global scale
<b>2. Model description</b>	
Model type (empirical, conceptual, physically based)	Conceptual/Process-based model
Continuous or event-based	Continuous
Possible running time steps	Hourly, daily
Spatial discretization (distributed)	spatially distributed, grid size determined by end user (grid size for Rhine 1.44 km <sup>2</sup> )



<p>Short description of model structure detailing main function (evaporation, soil moisture accounting, groundwater, routing, snowmelt, etc.)</p>	<p>The Hydrologiska Byrans Vattenbalansavdelning (HBV) model was introduced back in 1972 by the Swedish Meteorological and Hydrological Institute (SMHI). The HBV model is mainly used for runoff simulation and hydrological forecasting. The model is particularly useful for catchments where snow fall and snow melt are dominant factors, but application of the model is by no means restricted to these type of catchments.</p> <p>The wflow_hbv model is based on the HBV-96 model. However, the hydrological routing represent in HBV by a triangular function controlled by the MAXBAS parameter has been removed. Instead, the kinematic wave function is used to route the water downstream. All runoff that is generated in a cell in one of the HBV reservoirs is added to the kinematic wave reservoir at the end of a timestep. There is no connection between the different HBV cells within the model. Wherever possible all functions that describe the distribution of parameters within a subbasin have been removed as this is not needed in a distributed application/</p> <p>A catchment is divided into a number of grid cells. For each of the cells individually, daily runoff is computed through application of the HBV-96 of the HBV model. The use of the grid cells offers the possibility to turn the HBV modelling concept, which is originally lumped, into a distributed model.</p>
---	---





	<p>Adding lakes and reservoirs is also possible</p>
<p>Scheme of model structure</p>	<p>The diagram illustrates a hydrological model structure. On the left, a 3D grid-based catchment discretization is shown with a 'Grid cell' highlighted. On the right, a flowchart details the processes within a grid cell: Precipitation is either snowfall (if <math>T \leq 0^\circ C</math>) or rainfall (if <math>T &gt; 0^\circ C</math>). Snowfall leads to snow accumulation, which melts (if <math>T \geq 0^\circ C</math>) into soil moisture. Rainfall also contributes to soil moisture. Soil moisture is affected by actual evapotranspiration, seepage, and capillary rise. Direct runoff is generated from rainfall. Percolation moves water from the upper zone to the lower zone. Quick flow is generated from direct runoff and seepage, while base flow is generated from percolation. The final outputs are water level and surface runoff, modeled using a kinematic wave model.</p>
<p><b>3. Model parameters</b></p>	
<p>Distribution of model parameters (yes/no)</p>	<p>Yes</p>
<p>Number of free parameters</p>	<p>Numerous free parameters</p>
<p>Procedure of model parameter estimation (measurement, manual or automatic algorithm, etc.)</p>	<p>The parameter are obtained from lumped daily model calibrated using GLUE from upstream to downstream (ref)</p>
<p><b>4. Model inputs / Model outputs</b></p>	

<p>List and characteristics of input variables (type, time step, spatial resolution, etc.)</p>	<p>The main dynamic variables are climate forcing data such as precipitation, temperature and potential evaporation. For the daily model the other observations can also be used for different purposes (for instance DA using OpenDA).</p>
<p>List and characteristics of output variables (type, time step, spatial resolution, etc.)</p>	<p>The exported time-step depends on the user, i.e. hourly, daily. The variables (states and fluxes) can be exported for the whole grid or selected gauge locations .</p>
<p><b>5. Examples of previous model applications</b></p>	
<p>Catchments, objectives, etc. Results of existing comparisons with other models</p>	<p>Many (e.g. Rhine, Meuse etc)</p>
<p><b>6. List of selected references</b></p>	





- Lindstrom, G., Johansson, B., Persson, M., Gardelin, M., and Bergstrom, S.: Development and test of the distributed HBV-96 hydrological model, *J. Hydrol.*, 201, 272–288, 1997
- Rakovec, O., Weerts, A. H., Hazenberg, P., Torfs, P. J. J. F., and Uijlenhoet, R.: State updating of a distributed hydrological model with Ensemble Kalman Filtering: effects of updating frequency and observation network density on forecast accuracy, *Hydrol. Earth Syst. Sci.*, 16, 3435–3449, doi:10.5194/hess-16-3435-2012, 2012
- Operational aspects of asynchronous streamflow assimilation for improved flood forecasting, O. Rakovec, A. H. Weerts, J. Sumihar, and R. Uijlenhoet, *HESS*, 19(6), 2911-2924 doi:10.5194/hess-19-2911-2015.



